The ABC's of Cell Division: Regulation of Peptidoglycan Amidase Activity during Cytokinesis in Escherichia coli

Citation

Permanent link

Terms of Use

Share Your Story

Dissertation Advisor: Dr. Thomas G. Bernhardt   Desirée Choy Yang

The ABC's of Cell Division: Regulation of Peptidoglycan Amidase Activity During Cytokinesis in *Escherichia coli*

Abstract

The bacterial cell wall, composed of peptidoglycan (PG), is an essential component of the cell envelope. This macromolecular structure fortifies the cell membrane, determines cell shape, and helps prevent osmotic lysis. The synthesis and remodeling/recycling of this polymer is mediated by PG synthases and hydrolases, respectively. Proper control of the PG hydrolases is particularly important since misregulation of these enzymes can lead to lethal breaches in the cell wall. Surprisingly, however, the precise molecular mechanisms governing the activities of these enzymes remain poorly understood.

To help understand how PG hydrolases are regulated, I examined how their activity is controlled during cytokinesis in *Escherichia coli*. One important class of PG hydrolases necessary for cell division is the LytC-type amidases (AmiA, AmiB and AmiC). These enzymes require activation by the LytM factors EnvC and NlpD. My work focused on elucidating the mechanism by which the LytM factors activate the amidases. Using a genetic enrichment strategy, I isolated *amiB* misregulation mutants. Interestingly, the mutations mapped to a region of AmiB found only in cell separation amidases. Structural analysis of an AmiB ortholog indicates that this region corresponds to an alpha-helical domain that appears to occlude the active site. Thus, activation of the amidases by the LytM factors likely occurs via a conformational change that displaces the regulatory helix from the active site.

In addition to amidase regulation, I also investigated how the LytM activators are recruited to, and regulated at the site of division. Using genetic and biochemical approaches, I showed that EnvC is directly recruited to the division site by FtsEX, an ATP-binding transporter-like complex. Interestingly, ATPase-defective FtsEX derivatives can still recruit EnvC to the divisome, but fail to promote cytokinesis. These results support a model where conformational changes induced by the ATPase activity of FtsE are directly and specifically transmitted to the amidases via FtsX and EnvC. This model is attractive because it provides a mechanism for converting the potentially dangerous activity of septal PG splitting into a discrete process which can be cycled on and off in coordination with the division process.

Table of Contents

Acknowledgements

First and foremost, I would like to thank my PhD advisor Thomas (Tom) Bernhardt who graciously accepted me into his lab as a fifth year graduate student. I will be forever indebted to Tom for his generosity, kindness and most importantly his priceless mentorship. Tom's guidance and support over the past two years has been instrumental in building up both my scientific abilities and confidence. It has truly been an honor and tremendous privilege to work with Tom.

I am also sincerely grateful and fortunate to have a phenomenal dissertation advisory committee of Marcia Goldberg (chair), Eric Rubin and Matt Waldor, who consistently supported me through the highs and lows of graduate school and were pivotal in helping me to achieve the level of scientific training I desired.

Briefly, I would like to thank and acknowledge all the current and past members of the Bernhardt lab, who have been incredibly supportive and helpful during my time as a PhD student. I would like to particularly thank Nick Peters, a postdoc in the lab, who has been a beacon of support, both scientifically and personally. Monica Markovski, a fellow graduate student in the process of writing her own thesis, has been my bay-mate and Bernhardt lab comrade through the thick and thin. Prior to taking a job on the West Coast, Tsuyohsi Uehara was a talented instructor in the lab, whose scientific efforts set the foundation for my thesis work. Hongbaek Cho, Mary-Jane Tsang Mui Ching and Ghee Chuan Lai were kind enough to read through my thesis and provide useful comments and edits. I would also like to thank David Rudner and members of his lab who have offered many insightful suggestions and thought-provoking questions at our joint-group meetings. It has been fun working in such a collaborative and stimulating lab environment.

I would also like to thank Marcia Goldberg (chair), Simon Dove, Michael Laub and David Rudner, for agreeing to be on my defense committee and taking the time out of their busy schedules to read this dissertation.

And lastly, I must thank my family and dear friends whose unwavering support and encouragements have made this entire PhD process possible. My parents Robert and Chong-Son (aka Desirée Sr.), instilled the strong work ethic and determination that has been essential to surviving grad school. And my sister Renée, has been the cornerstone that has kept me grounded and sane over the past few years.

This dissertation is dedicated to

my parents and sister

I could not have done this without you

Chapter 1

Introduction to the Gram-negative cell wall and peptidoglycan hydrolases

Chapter 1: Introduction to the Gram-negative cell wall and peptidoglycan hydrolases

Section 1.1: The Gram-negative bacterial cell envelope and peptidoglycan

In Gram-negative bacteria, like *Escherichia coli*, the cell envelope consists of three distinct layers: an inner membrane and an outer membrane separated by the periplasm (Figure 1.1). Within the periplasmic space lies the cell wall also known as the peptidoglycan (PG) layer. As the principal load-bearing component of the bacterial cell envelope, PG is a vital macromolecule, helping to maintain cell shape and structure as well as preventing osmotic lysis. PG, also referred to as murein, is a polysaccharide polymer made up of glycan strands consisting of repeating aminosugars *N*-acetyl-glucosamine (GlcNAc) and *N*-acetyl-muramic acid (MurNAc), that are linked by β-1,4-glycosidic bonds. These glycan strands are covalently cross-linked to each other via short stem peptides that are attached to the MurNAc sugars (Figure 1.1 and Figure 1.2). The resulting meshwork forms a continuous structure that encases the cell. Therefore, synthesis and remodeling of PG are essential for growth and division in all cell-wall containing bacteria (1).

In order for a bacterial cell to grow and divide, it must synthesize new PG and incorporate this material into the existing matrix. *De novo* biosynthesis of PG begins in the cytoplasm where the precursor molecules UDP-GlcNAc and UDP-MurNAc-L-Ala-γ-D-Glu-(L)-*meso*-diaminopimelic acid (DAP)-D-Ala-D-Ala (UDP-MurNAc-pentapeptide) are synthesized by a series of enzymatic reactions. UDP-MurNAc-pentapeptide is then transferred to the lipid carrier undecaprenol phosphate to form lipid I. Next, GlcNAc from UDP-GlcNAc is added to lipid I producing lipid II, which contains the basic monomeric unit of PG, the disaccharide-
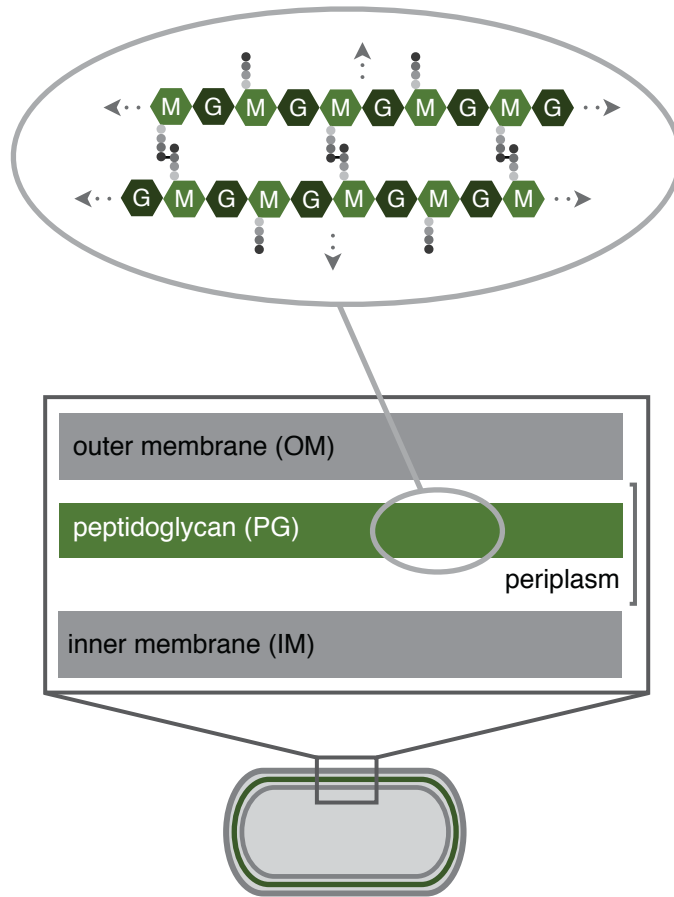
Figure 1.1. Schematic of the Gram-negative bacterial cell envelope. Diagram of a rod-shaped bacteria consisting of three distinct layers. The box contains a close-up diagram of the IM, inner membrane; OM, outer membrane and PG, peptidoglycan sandwiched in between. The oval contains a diagram of the PG chemical structure: M, *N*-acetyl-muramic acid; G, *N*-acetyl-glucosamine. Grey dots represent the attached peptides. The PG structure continues in all directions to envelop the cell (grey arrows). Adapted from (118).
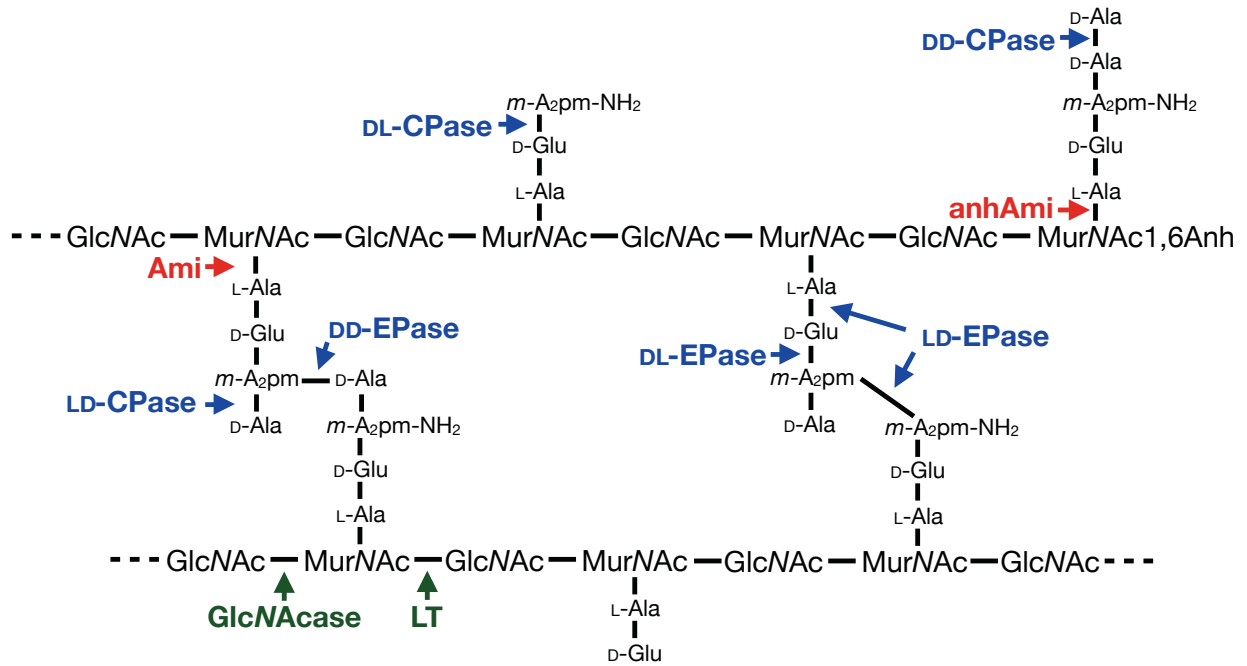
Figure 1.2. Structure of *E. coli* murein and sites of **glycan**, **amide** and **peptide** bond hydrolysis. Ami, amidase; EPase, endopeptidase; CPase, carboxypeptidase; Glc*N*Acase, *N*-acetylglucosaminidases; LT, lytic transglycosylase. Adapted from (13).

pentapeptide. Lipid II is then flipped across the inner membrane so that the disaccharide-pentapeptide moiety faces the periplasm. The identity of the flippase is currently controversial (2-4). In the periplasm, PG synthases with transglycosylase (TG) and transpeptidase (TP) activities polymerize lipid II into glycan strands and cross-link them into the existing PG meshwork via their short stem peptides (Figure 1.3) (1).

PG synthases (Table 1.1) are integral membrane proteins that are also known as the high-molecular weight (HMW) penicillin-binding proteins (PBPs) based on the ability of penicillin and other β-lactams to covalently bind and inhibit these enzymes (5). The HMW-PBPs are grouped into two distinct categories: class A and class B PBPs (5). There are three class A HMW-PBPs in *E. coli* (PBP1a, 1b and 1c) which are thought to be the primary PG synthases in the cell as they are bifunctional and possess domains for both TG and TP activity. Additionally, *E. coli* possesses a monofunctional transglycolase, MtgA, which can also catalyze the formation of glycan strands and is thought to act in concert with components of the cell division apparatus to incorporate PG subunits into the murein sacculus during division (6). In contrast to their bifunctional counterparts, the two class B PBPs in *E. coli* (PBP2 and PBP3) are monofunctional transpeptidases. Interestingly, depletion of PBP2 results in the formation of spherical cells that eventually lyse. Whereas inactivation of PBP3 causes cells to filament to death (7). These initial findings suggest that at least two modes of PG synthesis exist in rod-shaped bacteria, elongation requiring the activity of PBP2 and division necessitating PBP3 activity (7). Ultimately, these two systems must be carefully balanced in order to maintain proper cell shape (1, 8).
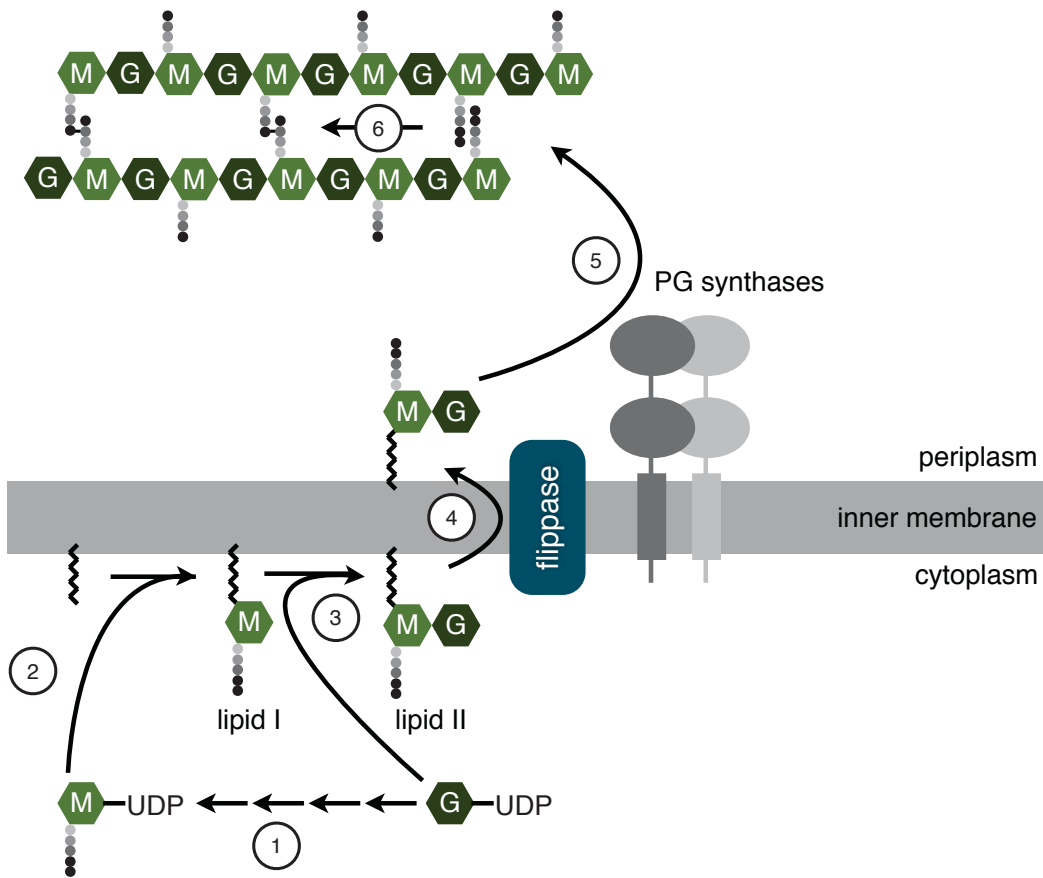
Figure 1.3. The steps of PG biosynthesis. ① UDP-GlcNAc is converted to UDP-MurNAc by several reaction steps represented here by multiple black arrows. ② UDP-MurNAc attached to a pentapeptide side chain is then anchored in the inner membrane, generating lipid I. ③ Attachment of GlcNAc to lipid I results in the formation of lipid II which can then be ④ flipped across the membrane and incorporated into the existing PG meshwork via ⑤ transglycosylation and ⑥ transpeptidation reactions.

Table 1.1. Peptidoglycan synthases in *E. coli.*

Enzyme	Gene	Localization
Transglycosylase/transpeptidase		
PBP1a	*ponA (mrcA)*	Inner membrane
PBP1b	*ponB (mrcB)*	Inner membrane
PBP1c	*pbpC*	Inner membrane
Transpeptidase		
PBP2	*pbpA (mrdA)*	Inner membrane
PBP3	*ftsI (pbpB)*	Inner membrane
Monofunctional glycosyltransferase		
MtgA	*mtgA*	Inner membrane

Table adapted from (1).

Section 1.2: Peptidoglycan hydrolases and their physiologic functions

In contrast to a relatively low number of PG synthases (Table 1.1), *E. coli* encodes many hydrolytic enzymes with the collective capability of cleaving every amide and glycosidic linkage in PG (Table 1.2, Figure 1.2) (1, 9). These PG hydrolases are also referred to as autolysins because elevated expression of these enzymes can result in cell lysis. In total, *E. coli* encodes over 30 factors known or predicted to possess PG hydrolase activity that are classified into 12 different protein families (Table 1.2) (9).

Peptidoglycan hydrolases and the bonds they cleave

As previously mentioned, PG is composed of two basic linkages that are broken by PG hydrolases: glycosidic and amide bonds (Figure 1.2). PG glycosidases are enzymes that cleave within the glycan strand of murein. β-*N*-acetylglucosaminidases specifically cleave the GlcNAc-(1→4)-MurNAc bond whereas *N*-acetylmuramidases, which encompass lysozymes and lytic transglycosylases (LT), break the MurNAc-(1→4)-GlcNAc linkage. *E. coli* possesses only one β-*N*-acetylglucosaminidase encoded by the *nagZ* gene (10). NagZ is not essential for cell viability, but its activity is required for cells to recycle PG. Its substrate is a cytoplasmic disaccharide intermediate of the recycling pathway (11, 12). The MurNAc-(1→4)-GlcNAc linkage can be hydrolyzed by two mechanisms: (1) hydrolysis of the glycosidic bond by lysozyme and related enzymes resulting in a terminal reducing MurNAc sugar, or (2) cleavage of the glycosidic bond by LTs resulting in an intramolecular transglycosylation reaction forming a 1,6-anhydro ring at the MurNAc sugar (13). There are seven LTs in *E. coli*, Slt70 (slt = soluble lytic transglycosylase) and MltA-F (mlt = membrane-bound lytic transglycosylase), which as

Table 1.2. Peptidoglycan hydrolases in *E. coli*.[a]

Enzyme	Gene	Localization	Substrate(s)
β-*N*-Acetylglucosaminidase			SC + PG
NagZ	*nagZ*	C	
Lytic transglycosylases			
Slt70	*slt*	P	PG
MltA	*mltA*	OM	SC + PG
MltB	*mltB*	OM	SC + PG
MltC	*mltC*	OM	PG
MltD	*mltD*	OM	PG
MltE	*mltE*	OM	SC + PG
MltF	*yfhD*	OM	PG
DD-Carboxypeptidases			
PBP4b	*yfeW*	CM	SC
PBP5	*dacA*	CM	SC + PG
PBP6	*dacC*	CM	SC
PBP6b	*dacD*	CM	PG
DD-Endopeptidases			
PBP7	*phpG*	P	PG
MepA	*mepA*	P	SC + PG
DD-Peptidases			
PBP4	*dacB*	P	SC + PG
AmpH	*ampH*	CM	SC + PG
LD-Carboxypeptidases			
LdcA	*ldcA*	C	SC
LD-Transpeptidases			
ErfK	*erfK*	P	PG
YbiS	*ybiS*	P	PG
YcbB	*ycbB*	P	PG
YcfS	*ycfS*	P	PG
YnhG	*ynhG*	P	PG
Endoamidase			
MpaA	*mpaA*	C	SC
MurNAc-L-Ala amidases			
AmiA	*amiA*	P	PG
AmiB	*amiB*	P	PG
AmiC	*amiC*	P	PG
AmiD	*amiD*	OM	SC + PG
AmpD	*ampD*	C	SC
L-Ala-D/L-Glu epimerase			
YcjG	*ycjG*	C	SC
D-Ala-D-Ala dipeptidase			
DdpX	*ddpX*	C	SC

[a] DD-peptidases show both DD-carboxypeptidase and DD-endopeptidase activities. C, cytoplasm; CM, cytoplasmic membrane; P, periplasm; OM, outer membrane; SC, soluble component (precursor, muropeptide, peptide or glycan chain); PG, isolated PG. Table adapted from (9).

indicated by their names, are either soluble or found associated with a membrane, respectively (reviewed in 9, 13). Deletion mutants lacking multiple LTs, including a sextuple mutant lacking six of the seven LTs (Slt70, MltA-E), are still viable, but grow in short chains. Surprisingly, only minor changes in the PG composition were observed for this mutant (14-16). Interestingly, however, attempts to knock-out all seven LTs have been unsuccessful, suggesting that LT activity is essential for cell growth (17).

The PG peptidases are enzymes that specifically break the amide bonds between the amino acids found in PG. These hydrolytic enzymes come in two basic flavors: carboxypeptidases, which remove the C-terminal residue from stem peptides, or endopeptidases that cleave within the peptide. The different designations of DD-, LD- or DL-peptidase refer to the stereochemistry of the bond cleaved by these enzymes (18). In *E. coli*, DD-endopeptidases (PBP4, 7 and MepA) cleave the D-Ala-*meso*-A$_2$pm cross-link formed by the transpeptidation reaction of the HMW-PBPs (5). Interestingly, since these enzymes recognize and break the same bonds that are made by the HMW-PBPs some of them bind and are inhibited by β-lactams and thus have been classified as low molecular weight (LMW) PBPs (5, 19). In fact, except for AmpC, all the LMW-PBPs (PBP4, 4b, 5, 6, 6b, 7/8, AmpC and AmpH) in *E. coli* possess peptidase activity (20). In addition to the LMW-PBPs there are number of penicillin-insensitive peptidases in *E. coli,* including MepA, MpaA and DdpX (21-24). Finally, the *N*-acetylmuramyl-L-alanine amidases are responsible for cleaving the amide bond between the N-terminal L-alanine residue and the D-lactoyl moiety of MurNAc. *E. coli* possesses five known amidases: AmiA, AmiB, AmiC, AmiD and AmpD (25-27). Based on their amino acid sequences they can

be categorized into two distinct families, Pfam amidase_3 also known as LytC-type amidases

(AmiA, AmiB and AmiC) and the amidase_2 family (AmiD and AmpD) (13, 28).

The physiologic functions of peptidoglycan hydrolases

Like *E. coli,* most PG-containing bacteria encode a sizable array of PG hydrolases, with

several representatives from each family often being produced. Functional redundancy among

these PG hydrolase families has hampered efforts to determine their specific physiological

function(s) (13). However, the systematic deletion of multiple/all members in a particular PG

hydrolase family is one approach that has yielded some insight (reviewed in 9, 14, 25, 29-31).

These studies and deletion analyses in other organisms have implicated PG hydrolases in a

diverse array of biological processes, some of which are listed in Table 1.3, including PG

turnover, cell elongation in rod-shaped bacteria, cell division, cell shape determination, and

contact-dependent cell lysis (reviewed in 13).

One of the most important functions for PG hydrolases is thought to be "space-maker"

enzymes that break bonds in the PG meshwork to allow for the insertion of new material (13).

This is largely based on theoretical considerations, as attempts to identify essential PG

hydrolases required for cell wall growth have been unsuccessful. Nevertheless, it is clear that

PG hydrolysis is occurring during growth based on the observed release of PG degradation

products from growing cells (32-36). The best evidence of a cell wall expansion function for PG

hydrolases has come from studies in *Bacillus subtilis*. Elongation of the cell cylinder in rod-

shaped bacteria like *B. subtilis* and *E. coli* is directed by an actin-like cytoskeletal element called

Table 1.3. Examples of biological processes that employ peptidoglycan hydrolases.

Biological Function	Functional Description and Example PG Hydrolases
Functions in bacterial cell physiology	
Regulation of cell wall growth	Removal of excess of pentapeptides in new PG by DD-carboxypeptidases PBP5 (*E. coli*); PBP3 (*S. pneumoniae*)
PG turnover*	Release of soluble PG fragments from the sacculus during growth Lytic transglycosylases (*E. coli*)
Enlargement of the sacculus*	Breaking of bonds to allow expansion of the sacculus during growth Lytic transglycosylases (*E. coli*); LytE (*B. subtilis*)
Production of signaling molecules	Induction of β-lactamase by PG turnover products Lytic transglycosylases (*E. coli*)
Recycling of PG turnover products	Cleavage turnover products to allow reuse in PG synthesis AmpD, LdcA, NagZ (*E. coli*)
Cell division*	Cleavage of the septum during cell division in Gram-negative species AmiA, AmiB, AmiC (*E. coli*) Cleavage of the cross-wall after division in Gram-positive species Atl (*S. aureus*)
Cell wall shape*	Altered PG profiles can influence bacterial cell wall shape Csd1, Csd2, Csd3 (*H. pylori*)
Sporulation and germination	Cleavage of asymmetric septum SpoIID, SpoIIP (*B. subtilis*) Spore cortex maturation LytH (*B. subtilis*) Digestion of the mother cell PG to release the endospore LytC, CwlC, CwlH (*B. subtilis*) Digestion of the spore PG during germination SleB, CwlJ (*B. subtilis*)
Assembly of secretion systems	Specialized PG hydrolases (lytic transglycosylases) for localized PG degradation associated with type II, type III and type IV secretion systems VirB1 (*A. tumefaciens*); TraB (*E. coli* plasmid R721)
Pilus assembly (type IV)	Specialized PG hydrolases for pilus assembly PilT (*E. coli* EPEC strains)
Flagellum assembly	Specialized PG hydrolases for flagellum assembly FlgJ (*E. coli*)
Resuscitation of dormant cells	Stimulation of cell division to exit dormant state RpfA (*M. luteus*); Rpf proteins (*M. tuberculosis*)

Table 1.3 continued.

Biological Function	Functional Description and Example PG Hydrolases
Functions in bacterial cell physiology	
Contact-dependent cell lysis*	Secretion of autolysin effectors via type VI secretion Tse1, Tse3 (*P. aeruginosa*)
Autolysis in genetic transformation	Fratricide of *S. pneumoniae*: induced lysis (allolysis) of non-competent cells LytA, LytC (*S. pneumoniae*)
Developmental lysis	Lysis of cells during fruiting body formation in *M. xanthus* Cannibalism in *B. subtilis*
Lysis of prey cells	Secretion of PG hydrolases to digest peptidoglycan of prey cells Exoenzymes of *M. xanthus*
Lysis of non-immune cells	Plasmid-encoded bacteriocin/immunity factor Pesticin (*Y. pestis*)
Biofilm formation	PG hydrolases are required for initial attachment of cells to hydrophobic surfaces AtlE (*S. epidermidis*)
Pathogen-host interaction	Release PG fragments recognized by the host

* Refer to text for more details about these particular examples. Table adapted from (13).

MreB (37, 38). *B. subtilis* encodes three MreB orthologs, MreB, Mbl, and MreBH, all of which have been implicated in cell elongation and rod-shape determination (39-45). Interestingly, Errington and co-workers have detected an interaction between the LytE PG hydrolase and MreBH, suggesting a role for LytE in cell wall elongation (46). Accordingly, *lytE* and *mreBH* mutants display similar cell-wall-related defects (46). Given that LytE is exported and MreBH is a cytoplasmic protein, it remains unclear how the observed LytE-MreBH interaction might facilitate proper elongation, but it has been proposed that MreBH might guide the secretion of LytE to specific locations to coordinate PG hydrolysis with the insertion of new material. Importantly, it was subsequently discovered that inactivation of the related endopeptidase CwlO was synthetically lethal with the loss of LytE function (47, 48). The terminal phenotype of the LytE⁻ CwlO⁻ cells was the cessation of growth, strongly suggesting that these enzymes are the postulated "space-maker" enzymes for *B. subtilis* cell wall expansion.

The most clearly defined cellular function for PG hydrolases is their role in cell division. The septal cell wall material deposited by the cell division apparatus is initially shared between daughter cells and must be carefully split in order to complete cell division. The PG hydrolases required for proper cell division have been identified in a number of organisms. In some cases a single enzyme plays the primary role in cell separation, as is the case of Atl from *Staphyloccocus aureus* (49, 50). Inactivation of Atl alone leads to the formation of relatively large cell clusters that are unable to separate (51). In other organisms, several PG hydrolases appear to play redundant roles in the separation process. For example, the LytC-type amidases in *E. coli*, AmiA, AmiB, and AmiC, are required for cell separation, and only when all three proteins are inactivated is a significant cell chaining phenotype observed (14, 25, 52).

14

In addition to the activities of cell growth and division, recent work in *Helicobacter pylori* suggests that relaxation of PG cross-links by autolysins can promote helical shape (53). Helical shape is thought to be determined by three morphological features: cell elongation, curvature and twist (53). Predictions made using biophysical modeling first suggested that cell curvature and twist might be achieved by the local modification of PG cross-links along a helical path (54). The identification of four genes necessary for helical shape in *H. pylori, csd1-3* (csd = cell shape determinant) and *ccmA* (ccm = curved cell morphology), was the first piece of evidence to support such a model (53). Loss of these genes resulted in variable curved-rod morphologies and changes in the abundance of specific classes of cross-linked muropeptides (53). Interestingly Csd1, Csd2 and Csd3 possess LytM peptidase domains that may be endopeptidases and/or carboxypeptidases that directly hydrolyze PG (53). In accordance with this idea, expression of a predicted catalytically impaired Csd1 variant resulted in the same curved-rod phenotype observed with the null allele of *csd1* (53). These results support the model that localized changes in murein architecture by PG hydrolases can induce the helical shape characteristic of *H. pylori* (53).

Lastly, the functions most often associated with PG hydrolases is cell wall destruction and lysis induction (55). These enzymes are employed by phages to lyse their host for the release of progeny virions into the surrounding milieu. In addition, the developmental regulation of lytic PG hydrolases is also used by endospore forming bacteria to release mature spores from the mother cell at the end of the sporulation process. Finally, PG hydrolases produced by certain bacteria are used as weapons to destroy competing bacteria in the environment. Interestingly, a recent study by Mougous and colleagues described the use of a type VI secretion system (T6SS)

in *Pseudomonas aeruginosa* to transfer lytic amidases into the periplasm of other recipient

bacteria to lyse them (56).

Section 1.3: Regulation of the peptidoglycan hydrolases

While the functions of many PG hydrolases remain to be uncovered, the examples

described above clearly highlight that these enzymes have diverse roles in cells ranging from

promoting cell growth to cell destruction. To use PG hydrolases for constructive purposes, such

as cell elongation or cell division, bacterial cells must maintain tight control over the potentially

lethal hydrolytic activity of these enzymes. Although this has been appreciated for some time,

very little is known about the mechanisms responsible for PG hydrolase regulation. While the

details remain obscure, several general regulatory strategies have been described and/or

postulated over the years ranging from transcriptional to post-translational control mechanisms

to the chemical modification of the PG substrate. Examples of each of these regulatory strategies

are discussed in turn below.

Transcriptional control

The regulation of PG hydrolase gene expression has been most extensively studied in

Gram-positive bacteria (13). Generally speaking, PG hydrolases controlled at the transcriptional

level are governed by the same sigma factors that activate the biological process or physiological

state requiring these specific enzymes (13, 18). For example, in *B. subtilis,* one of the major

vegetative autolysin genes *lytC* (*cwlB*) is dependent on σ^A (the main housekeeping sigma factor)

and σ^D (the flagellar, motility and chemotaxis sigma factor), corresponding to the role LytC plays

during vegetative growth, cell division and motility (57-60). Moreover, PG hydrolases critical for spore-formation and germination are controlled by sporulation-specific sigma factors that spatiotemporally restrict the production of these enzymes to a specific stage during the sporulation process (61, 62).

Another major transcriptional regulator important for cell wall homeostasis is the two component-system (TCS) WalRK, which is highly conserved among low GC-containing Gram-positive bacteria and is one of the few essential TCS identified to date (63-74). The WalRK system has been most thoroughly studied in *B. subtilis*, *Staphylococcus aureus* and *Streptococcus pneumoniae* (47, 64, 67, 75). In these systems, phosphorylated WalR (WalR-P), the response regulator, activates expression of genes encoding cell separation PG hydrolases and represses the expression of their inhibitors (63). In *B. subtilis*, the sensor kinase WalK is recruited to the divisome and its kinase activity is stimulated by interactions with septal ring components (76, 77). Interestingly, the activation of WalK and its ability to phosphorylate WalR appears to require a functional division apparatus (76-78). Taken together, these findings suggest that the WalRK systems may adjust the levels of cellular PG hydrolase activity in response to changes in growth rate and division.

Post-translational control

In addition to controlling the expression of PG hydrolases, mechanisms must be in place to regulate the activity of these factors once they are produced. Several general regulatory strategies have been uncovered, but as described below, mechanistic detail is limited.

(a) Multi-enzyme complexes

For proper cell wall assembly, PG synthesis and hydrolysis must be precisely coordinated. Therefore, it was proposed some time ago that the formation of multi-enzyme complexes, containing both PG synthases and PG hydrolases, could serve to coordinate these activities (1, 79). Indeed, several PBP-PG hydrolase interactions have been detected in *E. coli* using affinity chromatography (80, 81). Also, as mentioned previously, the cell wall hydrolase LytE from *B. subtilis* has been found to interact with a component of the cell elongation machinery, MreBH (46). Supporting evidence for such complexes also comes from work in mycobacteria, where PG synthase PBP1 was shown to interact with the PG peptidase RipA (82). Although these multi-enzyme complexes are often invoked when discussing the coordination of PG synthesis and degradation, the functional significance of PG synthase-PG hydrolase complex formation remains unclear; the phenotypic consequence of defects in synthase-hydrolase complex formation has not yet been investigated in any organism. Also, in only one instance has a biochemical effect of a PG synthase on a PG hydrolase been observed *in vitro*; mycobacterial PBP1 inhibited an observed synergy between the peptidase RipA and another hydrolase RpfB (82). This result is actually counter to the expectation of the original multi-enzyme complex model in which it was proposed that PG hydrolases would likely only be active when in complex with PG synthases. Thus, while the multi-enzyme complex model for coordinating PG hydrolase activity with PG synthesis remains attractive, a great deal more needs to be learned in order to understand the role of these complexes in PG hydrolase regulation.

(b) Peptidoglycan hydrolase processing

In addition to possible regulation within multi-enzyme complexes, a handful of PG hydrolases are known to require proteolytic processing for activation (13). These enzymes are synthesized and secreted as latent proenzymes and must be processed for maturation (83-87). For example, the lysostaphin-type metalloendopeptidases are inactive in their full-length form and require processing to become active (84). Additionally, the major *S. aureus* autolysin Atl, which facilitates daughter cell separation, is produced as a proenzyme and undergoes proteolytic processing that generates two important extracellular PG hydrolases (85). However, it remains unclear whether or not this processing event is required for Atl regulation. Interestingly, in most cases the biologically relevant peptidases responsible for these maturation events are unknown, although there are some examples where the pertinent protease has been identified (88). Identifying these proteases and determining whether or not the processing event is itself regulated will be important for understanding how proteolytic maturation might control PG hydrolase activity and promote their activation at the right time and place in the cell.

(c) Subcellular localization of peptidoglycan hydrolases

An important strategy for the spatiotemporal regulation of PG hydrolase activity is the control of enzyme localization. This is typically accomplished by the production of PG hydrolases with accessory domains that target the factor to the desired location. For example, the *E. coli* amidases AmiB and AmiC possess N-terminal AMIN domains that target them to the septum to participate in the division process (89, 90). In most cases the mechanism of localization is not clear, although in several Gram-positive organisms, an antagonism between

19

the cell wall binding domains of certain PG hydrolases and polyanionic cell wall polymers, like wall teichoic acids (WTAs), has been implicated in controlling PG hydrolase localization (85). For example, Schlag and colleagues report that WTA prevents Atl from binding cell wall in *S. aureus*, thus reducing its overall susceptibility to Atl-mediated PG cleavage (85). Interestingly, WTA appears to be absent at the cross-wall region and local depletion is thought to result in the targeting of Atl to the equatorial surface ring where it can promote the separation of the daughter cells (85).

(d) Other mechanisms

In addition to protein-protein interactions and the control of protein localization, chemical modification of the PG layer or changes in its conformation as well as physiochemical properties are also thought to play a role in PG hydrolase regulation. Koch, *et al*. proposed that topographical features of the bacterial cell wall could influence its degradation, postulating that in Gram-positive bacteria the PG bonds residing on the outer-most layers would be more stressed and therefore easier to cleave by "smart" autolysins (79, 91). In addition to physical distortion of PG, the ionic composition of the cell wall milieu may also affect enzyme activity as cell wall turnover and autolysis in *B. subtilis* was reported to be salt dependent (92). The proton gradient of cellular membranes in Gram-positive bacteria has also been implicated in modulating autolysin activity, which was first prompted by early observations that disruption of the proton motive force lead to cell lysis (91, 93-95). It was hypothesized that protons excreted across the cytoplasmic membrane neutralize the negative charges in the cell wall and lower the relative pH, thus creating a pH gradient where the region closest to the membrane would be acidic enough to

inhibit autolysin activity (91, 93, 94). In support of this model, the cell wall of *B. subtilis* was shown to be acidified during respiration using pH-sensitive probes and other chemical sensing agents (94, 95). Acetylation and/or deacetylation of the PG layer can also affect its susceptibility to cleavage by PG hydrolases. For example, many Gram-negative bacteria O-acetylate the C-6 position of MurNAc and this blocks cell wall cleavage by LTs (96). However, it is not clear how the acetylation status itself might be regulated or whether acetylation or similar PG modifications are localized to specific subcellular regions to guide when and where PG hydrolases are capable of acting.

As highlighted above, our current understanding of PG hydrolase regulation is far from comprehensive. Most of the strategies identified thus far appear to point towards global regulatory mechanisms that help determine the overall level of PG hydrolase activity in the cell (i.e. by controlling their expression). Specific mechanisms that turn a particular hydrolase "on" or "off" as needed during the processes of cell growth or division have not been described. I therefore chose to investigate the regulation of PG hydrolases required for cell division in *E. coli* as a model system for PG hydrolase regulation. Below I will present an overview of the cell division process and review what was known about the regulation of the cell separation amidases in *E. coli* prior to the start of my thesis work.

**Section 1.4: The cell division complex**

For most bacteria, cell division begins with the formation of a multi-protein complex known as the septal ring or divisome which ultimately drives cytokinesis (97, 98). *E. coli*, a Gram-negative organism, must coordinate both the constriction and separation of all three

envelope layers simultaneously (Figure 1.1). Formation of the septal ring starts with the GTP-dependent polymerization of FtsZ, a tubulin homolog, into a ring-like structure also known as the Z-ring directly underneath the inner membrane, demarcating the future site of division (99). After formation of the Z-ring, FtsA and ZipA along with three non-essential factors ZapA, ZapB and ZapC are recruited and help to stabilize this highly dynamic structure (100-105). Once the Z-ring is formed, recruitment of other essential and non-essential downstream components occurs in an interdependent manner (Figure 1.4) (106-113). The assembly of the divisome happens in two stages, starting with the formation and stabilization of the Z-ring, which persists for about 20% of the cell cycle, followed by the simultaneous recruitment of FstQ-FtsN at about the time constriction is initiated (114).

During cytokinesis, the divisome must facilitate a number of different functions in a coordinated fashion. These activities include invagination and fission of the inner membrane, synthesis of the septal PG layer, splitting of this septal PG shared between daughter cells and finally invagination and fission of the outer membrane (98). Hydrolysis of the septal murein layer requires the activity of PG hydrolases. In *E. coli,* the specific autolysins required for this process have been identified and are discussed in more detail below.

Section 1.5: The cell division peptidoglycan hydrolases

In an effort to elucidate which murein hydrolases are the most critical for cell division, Heidrich and colleagues began constructing a series of mutants deleted for one or more PG hydrolase (14, 25). The results indicated that the three periplasmic, LytC-type *N*-acetylmuramyl-L-alanine amidases (AmiA, AmiB and AmiC) in *E. coli* are necessary for septal PG splitting

22
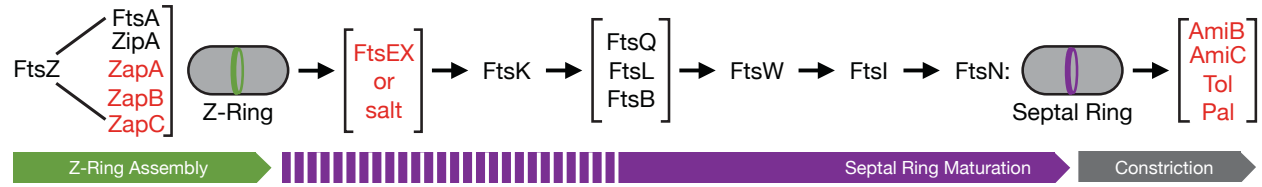
Figure 1.4. Dependency pathway for septal ring assembly. The dependency pathway for assembly of the cell division apparatus is shown. Factors in black are essential and those in red are non-essential. The three main phases of the division process are indicated below the dependency pathway.

during division. As previously mentioned, amidases are hydrolytic enzymes that cleave the stem

peptide from the glycan strands of PG and are thus capable of destroying peptide cross-links.

Heidrich and co-workers found that mutants lacking all three amidases formed extremely long

chains of cells that were unable to separate. Electron microscopy images of these cells showed

that constriction and fission of the cytoplasmic membrane had occurred, but there was no

evidence of any septal PG cleavage (14, 25, 31, 52). These results suggested that the amidases

might be recruited to the divisome to participate directly in the division process. The subcellular

localization of the amidases was therefore investigated using fluorescent protein fusions (90,

115). While both AmiB and AmiC were shown to localize to the septal ring using GFP fusions,

AmiA-GFP displayed a diffuse distribution pattern throughout the periplasm indicating that it is

not specifically recruited to the site of division (90). Accordingly, AmiA lacks the N-terminal

septal targeting domain present in both AmiB and AmiC (Figure 1.5) (89, 90). However,

although AmiA is not specifically recruited to the divisome, Δ*amiB*Δ*amiC* mutants do not

display a severe separation defect, implying that specific septal localization of the amidases is

not required for successful cell division (115, 117, 118).

In addition to the LytC-type amidases, *E. coli* possesses another set of factors recently

shown to be important for daughter cell separation, the LytM (lysostaphin)-domain containing

proteins (referred to as LytM factors for convenience) (119). LytM and lysostaphin are the best

characterized members of this family and are metalloendopeptidases that cleave the pentaglycine

cross-bridges found in staphylococcal PG (83, 84, 120). There are four LytM factors in *E. coli*

(EnvC, NlpD, YgeR and YebA) (Figure 1.5), but only EnvC and NlpD have been shown to

localize to the septal ring (119, 121). Mutants deleted of all four LytM factors form
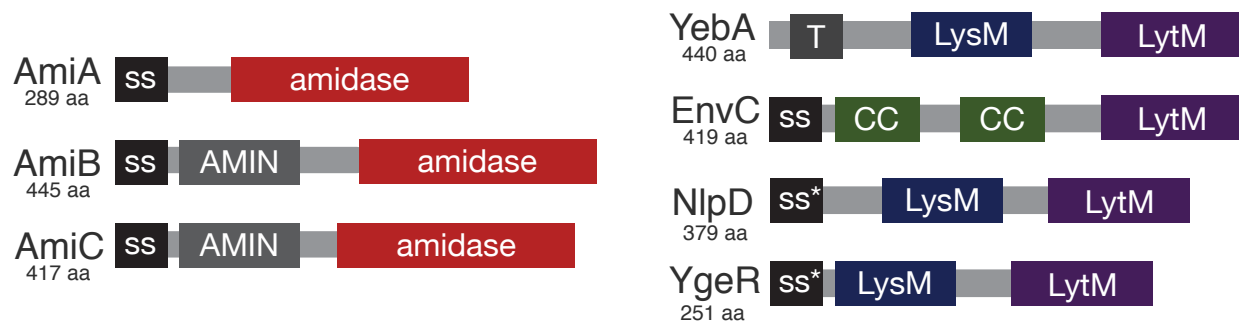
Figure 1.5. Predicted domain structure of the *E. coli* LytC-type amidases and LytM factors. Shown is a diagram depicting the predicted domain architecture of the three *E. coli* amidases (left) and four factors with identifiable LytM domains (right). Abbreviations: SS, signal sequence; SS*, lipoprotein signal sequence; AMIN, amidase N-terminal domain (89); amidase, amidase catalytic domain; T, transmembrane domain; LysM, LysM PG-binding domain (116), CC, coiled coil; LytM, LytM domain.

long chains of cells that are connected by a layer of unsplit septal PG, reminiscent of the triple

amidase mutants (119). It was subsequently shown that the LytM factors are actually activators

of the LytC-type amidases (118). By themselves, the amidases display relatively weak PG

hydrolase activity *in vitro*. Interestingly, however, the LytM factors were shown to be activators

of amidase activity (118). EnvC specifically activates AmiA and AmiB, while NlpD activates

only AmiC (118). Although it is unclear what the remaining two LytM factors do, it is apparent

that YebA and YgeR play a minor role if any during cell division (119). In total, AmiA, AmiB

and AmiC along with their cognate LytM activating factors, EnvC and NlpD, constitute two

partially redundant septal PG splitting pathways in *E. coli* (Figure 1.6). These studies shed

important light on the control of PG hydrolase activation at the division site of *E. coli*. The goal

of my thesis work has been to address two outstanding questions: (i) what components of the

septal ring might control the ability of the LytM factors to activate the amidases? and (ii) how are

the amidases activated by the LytM factors?

Section 1.6: Dissertation overview

Chapter 2 describes the efforts made in identifying the regulatory components governing

the ability of EnvC to activate AmiA and AmiB. Results from a previous synthetic lethal screen

in the lab indicated a possible genetic interaction between FtsEX and EnvC (122). FtsEX, a

putative ABC transporter, had been identified as a component of the divisome a number of years

ago, but its role in cell division had remained elusive (123). ABC transporters typically consists

of a transmembrane domain (TMD) and nucleotide binding domain (NBD) which harnesses the

energy of ATP hydrolysis to power substrate transport across a membrane (124). However, by

26
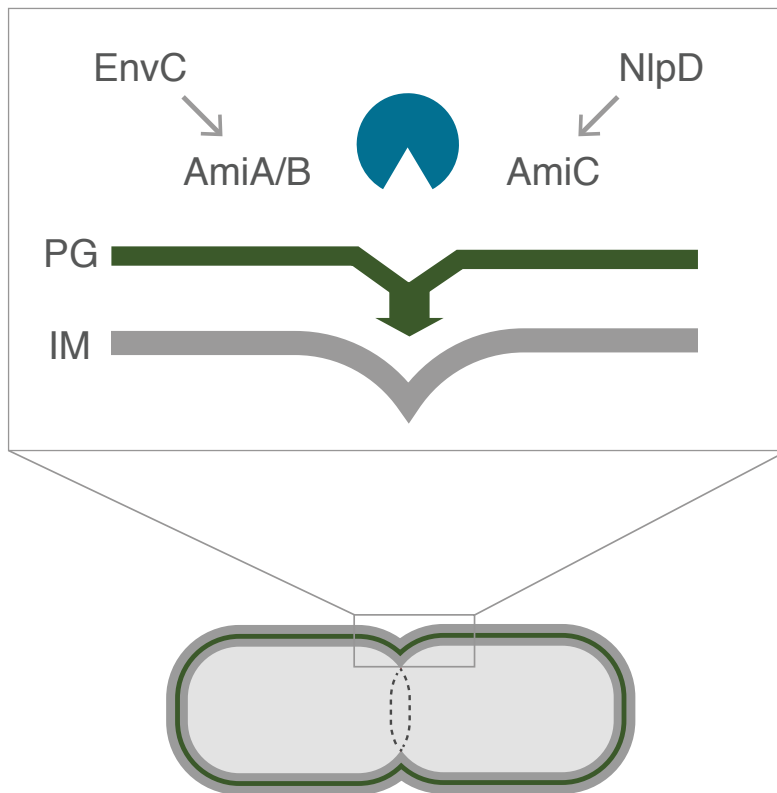
Figure 1.6. Two-redundant septal PG splitting pathways in *E. coli*. Below is a schematic of a dividing cell. The box contains a close-up diagram of the division site highlighting the amidases and their activating, cognate LytM factor. For the purposes of this diagram the outer membrane (OM) has been omitted.

using a number of complementary approaches, I discovered that EnvC is recruited to the septal ring by a direct protein-protein interaction with FtsX (TMD). Moreover, the ability of FtsE (NBD) to bind and hydrolyze ATP did not affect recruitment of EnvC to the divisome, but was critical for promoting cell division. These results suggest that FtsEX is an ABC transporter-like complex that utilizes the conformational change induced by ATP-binding and hydrolysis to directly modulate the ability of EnvC to activate the amidases *in vivo* (125). Furthermore, evidence that FtsZ and FtsE directly interact (126), provides a potential link between contraction of the Z-ring with hydrolysis of septal PG during cell division (125). In total, these findings support a novel model for how dividing bacterial cells convert the potentially dangerous activity of septal PG splitting into a more discreet and directed process (125).

Chapter 3 discusses the identification of unregulated AmiB variants that bypass the need for EnvC activation. The isolation and characterization of such mutants, which upon expression induce cells lysis, provides evidence that the LytM factors are allosterically activating the amidases. Based on the crystal structure of AmiB from *Bartonella henselae*, the lytic mutations I identified all map to an alpha-helical domain that occludes the amidase active site. The results discussed here suggest that EnvC interacts with AmiB, inducing a conformational change that displaces this regulatory helix and thus allows substrate accessibility to the active site. Moreover, similar lesions in *E. coli's* AmiA, or AmiB from *Vibrio cholerae* result in unregulated amidase activity, therefore suggesting the attractive possibility that this mode of regulation is conserved among other bacteria. Taken together, these findings exemplify the use of reversible conformational regulation to control PG hydrolase activity.

In Chapter 4, I summarize the major findings and implications from this work and address the impact these results have on our current understanding of how the cell wall hydrolases are regulated in bacteria. Additionally, I propose a model for how we envision septal PG hydrolysis is controlled and coordinated during cell division. Lastly, I discuss future directions and identify salient questions that remain unanswered in the field.

Section 1.7: References

1. Höltje JV (1998) Growth of the stress-bearing and shape-maintaining murein sacculus of Escherichia coli. *Microbiol Mol Biol Rev* 62:181–203.

2. Ruiz N (2008) Bioinformatics identification of MurJ (MviN) as the peptidoglycan lipid II flippase in Escherichia coli. *Proc Natl Acad Sci USA* 105:15553–15557.

3. Fay A, Dworkin J (2009) Bacillus subtilis homologs of MviN (MurJ), the putative Escherichia coli lipid II flippase, are not essential for growth. *J Bacteriol* 191:6020–6028.

4. Fraipont C et al. (2011) The integral membrane FtsW protein and peptidoglycan synthase PBP3 form a subcomplex in Escherichia coli. *Microbiol* 157:251–259.

5. Sauvage E, Kerff F, Terrak M, Ayala JA, Charlier P (2008) The penicillin-binding proteins: structure and role in peptidoglycan biosynthesis. *FEMS Microbiol Rev* 32:234–258.

6. Derouaux A et al. (2008) The monofunctional glycosyltransferase of Escherichia coli localizes to the cell division site and interacts with penicillin-binding protein 3, FtsW, and FtsN. *J Bacteriol* 190:1831–1834.

7. Spratt BG (1975) Distinct penicillin binding proteins involved in the division, elongation, and shape of Escherichia coli K12. *Proc Natl Acad Sci USA* 72:2999–3003.

8. Lleo MM, Canepari P, Satta G (1990) Bacterial cell shape regulation: testing of additional predictions unique to the two-competing-sites model for peptidoglycan assembly and isolation of conditional rod-shaped mutants from some wild-type cocci. *J Bacteriol* 172:3758–3771.

9. van Heijenoort J (2011) Peptidoglycan Hydrolases of Escherichia coli. *Microbiol Mol Biol Rev* 75:636–663.

10. Cheng Q, Li H, Merdek K, Park JT (2000) Molecular characterization of the beta-N-acetylglucosaminidase of Escherichia coli and its role in cell wall recycling. *J Bacteriol* 182:4836–4840.

11. Park JT, Uehara T (2008) How bacteria consume their own exoskeletons (turnover and recycling of cell wall peptidoglycan). *Microbiol Mol Biol Rev* 72:211–27.

12. Votsch W (2000) Characterization of a beta -N-acetylglucosaminidase of Escherichia coli and Elucidation of Its Role in Muropeptide Recycling and beta -Lactamase Induction. *Journal of Biological Chemistry* 275:39032–39038.

13. Vollmer W, Joris B, Charlier P, Foster S (2008) Bacterial peptidoglycan (murein) hydrolases. *FEMS Microbiol Rev* 32:259–286.

14. Heidrich C, Ursinus A, Berger J, Schwarz H, Höltje J-V (2002) Effects of multiple deletions of murein hydrolases on viability, septum cleavage, and sensitivity to large toxic molecules in Escherichia coli. *J Bacteriol* 184:6093–6099.

15. Lommatzsch J, Templin MF, Kraft AR, Vollmer W, Höltje JV (1997) Outer membrane localization of murein hydrolases: MltA, a third lipoprotein lytic transglycosylase in Escherichia coli. *J Bacteriol* 179:5465–5470.

16. Kraft AR, Prabhu J, Ursinus A, Höltje JV (1999) Interference with murein turnover has no effect on growth but reduces beta-lactamase induction in Escherichia coli. *J Bacteriol* 181:7192–7198.

17. Scheurwater EM, Clarke AJ (2008) The C-terminal domain of Escherichia coli YfhD functions as a lytic transglycosylase. *J Biol Chem* 283:8363–8373.

18. Smith TJ, Blackman SA, Foster SJ (2000) Autolysins of Bacillus subtilis: multiple enzymes with multiple functions. *Microbiol* 146:249–262.

19. Goffin C, Ghuysen JM (1998) Multimodular penicillin-binding proteins: an enigmatic family of orthologs and paralogs. *Microbiol Mol Biol Rev* 62:1079–1093.

20. Henderson TA, Young KD, Denome SA, Elf PK (1997) AmpC and AmpH, proteins related to the class C beta-lactamases, bind penicillin and contribute to the normal morphology of Escherichia coli. *J Bacteriol* 179:6112–6121.

21. Iida K, Hirota Y, Schwarz U (1983) Mutants of Escherichia coli defective in penicillin-insensitive murein DD-endopeptidase. *Mol Gen Genet* 189:215–221.

22. Uehara T, Park JT (2003) Identification of MpaA, an amidase in Escherichia coli that hydrolyzes the gamma-D-glutamyl-meso-diaminopimelate bond in murein peptides. *J Bacteriol* 185:679–682.

23. Lessard IA et al. (1998) Homologs of the vancomycin resistance D-Ala-D-Ala dipeptidase VanX in Streptomyces toyocaensis, Escherichia coli and Synechocystis: attributes of catalytic efficiency, stereoselectivity and regulation with implications for function. *Chem Biol* 5:489–504.

24. Lessard IA, Walsh CT (1999) VanX, a bacterial D-alanyl-D-alanine dipeptidase: resistance, immunity, or survival function? *Proc Natl Acad Sci USA* 96:11028–11032.

25. Heidrich C et al. (2001) Involvement of N-acetylmuramyl-L-alanine amidases in cell separation and antibiotic-induced autolysis of Escherichia coli. *Mol Microbiol* 41:167–178.

26. Uehara T, Park JT (2007) An anhydro-N-acetylmuramyl-L-alanine amidase with broad specificity tethered to the outer membrane of Escherichia coli. *J Bacteriol* 189:5634–5641.

27. Jacobs C et al. (1995) AmpD, essential for both beta-lactamase regulation and cell wall recycling, is a novel cytosolic N-acetylmuramyl-L-alanine amidase. *Mol Microbiol* 15:553–559.

28. Pennartz A, Généreux C, Parquet C, Mengin-Lecreulx D, Joris B (2009) Substrate-induced inactivation of the Escherichia coli AmiD N-acetylmuramoyl-L-alanine amidase highlights a new strategy to inhibit this class of enzyme. *Antimicrob Agents Chemother* 53:2991–2997.

29. Denome SA, Elf PK, Henderson TA, Nelson DE, Young KD (1999) Escherichia coli mutants lacking all possible combinations of eight penicillin binding proteins: viability, characteristics, and implications for peptidoglycan synthesis. *J Bacteriol* 181:3981–3993.

30. Nelson DE, Young KD (2000) Penicillin binding protein 5 affects cell diameter, contour, and morphology of Escherichia coli. *J Bacteriol* 182:1714–1721.

31. Höltje JV, Heidrich C (2001) Enzymology of elongation and constriction of the murein sacculus of Escherichia coli. *Biochimie* 83:103–108.

32. Goodell EW, Schwarz U (1983) Cleavage and resynthesis of peptide cross bridges in Escherichia coli murein. *J Bacteriol* 156:136–140.

33. Goodell EW, Schwarz U (1985) Release of cell wall peptides into culture medium by exponentially growing Escherichia coli. *J Bacteriol* 162:391–397.

34. Goodell EW (1985) Recycling of murein by Escherichia coli. *J Bacteriol* 163:305–310.

35. Pooley HM (1976) Turnover and spreading of old wall during surface growth of Bacillus subtilis. *J Bacteriol* 125:1127–1138.

36. De Boer WR, Kruyssen FJ, Wouters JT (1981) Cell wall turnover in batch and chemostat cultures of Bacillus subtilis. *J Bacteriol* 145:50–60.

37. Carballido-López R, Errington J (2003) A dynamic bacterial cytoskeleton. *Trends Cell Biol* 13:577–583.

38. Daniel RA, Errington J (2003) Control of cell morphogenesis in bacteria: two distinct ways to make a rod-shaped cell. *Cell* 113:767–776.

39. Wachi M et al. (1987) Mutant isolation and molecular cloning of mre genes, which determine cell shape, sensitivity to mecillinam, and amount of penicillin-binding proteins in Escherichia coli. *J Bacteriol* 169:4935–4940.

40. Wachi M, Doi M, Okada Y, Matsuhashi M (1989) New mre genes mreC and mreD, responsible for formation of the rod shape of Escherichia coli cells. *J Bacteriol* 171:6511–6516.

41. van den Ent F, Amos LA, Löwe J (2001) Prokaryotic origin of the actin cytoskeleton. *Nature* 413:39–44.

42. Jones LJ, Carballido-López R, Errington J (2001) Control of cell shape in bacteria: helical, actin-like filaments in Bacillus subtilis. *Cell* 104:913–922.

43. Figge RM, Divakaruni AV, Gober JW (2004) MreB, the cell shape-determining bacterial actin homologue, co-ordinates cell wall morphogenesis in Caulobacter crescentus. *Mol Microbiol* 51:1321–1332.

44. Shih Y-L, Le T, Rothfield L (2003) Division site selection in Escherichia coli involves dynamic redistribution of Min proteins within coiled structures that extend between the two cell poles. *Proc Natl Acad Sci USA* 100:7865–7870.

45. Garner EC et al. (2011) Coupled, circumferential motions of the cell wall synthesis machinery and MreB filaments in B. subtilis. *Science* 333:222–225.

46. Carballido-López R et al. (2006) Actin homolog MreBH governs cell morphogenesis by localization of the cell wall hydrolase LytE. *Dev Cell* 11:399–409.

47. Bisicchia P et al. (2007) The essential YycFG two-component system controls cell wall metabolism in Bacillus subtilis. *Mol Microbiol* 65:180–200.

48. Bisicchia P et al. (2010) Peptidoglycan metabolism is controlled by the WalRK (YycFG) and PhoPR two-component systems in phosphate-limited Bacillus subtiliscells. *Mol Microbiol* 75:972–989.

49. Yamada S et al. (1996) An autolysin ring associated with cell separation of Staphylococcus aureus. *J Bacteriol* 178:1565–1571.

50. Sugai M et al. (1995) Identification of endo-beta-N-acetylglucosaminidase and N-acetylmuramyl-L-alanine amidase as cluster-dispersing enzymes in Staphylococcus aureus. *J Bacteriol* 177:1491–1496.

51. Heilmann C, Hussain M, Peters G, Gotz F (1997) Evidence for autolysin-mediated primary attachment of Staphylococcus epidermidis to a polystyrene surface. *Mol Microbiol* 24:1013–1024.

52. Priyadarshini R, de Pedro MA, Young KD (2007) Role of peptidoglycan amidases in the development and morphology of the division septum in Escherichia coli. *J Bacteriol* 189:5334–5347.

53. Sycuro LK et al. (2010) Peptidoglycan crosslinking relaxation promotes Helicobacter pylori's helical shape and stomach colonization. *Cell* 141:822–833.

54. Huang KC, Mukhopadhyay R, Wen B, Gitai Z, Wingreen NS (2008) Cell shape and cell-wall organization in Gram-negative bacteria. *Proc Natl Acad Sci USA* 105:19282–19287.

55. Uehara T, Bernhardt TG (2011) More than just lysins: peptidoglycan hydrolases tailor the cell wall. *Curr Opin Microbiol* 14:698–703.

56. Russell AB et al. (2011) Type VI secretion delivers bacteriolytic effectors to target cells. *Nature* 475:343–347.

57. Lazarevic V, Margot P, Soldo B, Karamata D (1992) Sequencing and analysis of the Bacillus subtilis lytRABC divergon: a regulatory unit encompassing the structural genes of the N-acetylmuramoyl-L-alanine amidase and its modifier. *J Gen Microbiol* 138:1949–1961.

58. Kuroda A, Sekiguchi J (1993) High-level transcription of the major Bacillus subtilis autolysin operon depends on expression of the sigma D gene and is affected by a sin (flaD) mutation. *J Bacteriol* 175:795–801.

59. Helmann JD, Márquez LM, Chamberlin MJ (1988) Cloning, sequencing, and disruption of the Bacillus subtilis sigma 28 gene. *J Bacteriol* 170:1568–1574.

60. Kuroda A, Sekiguchi J (1991) Molecular cloning and sequencing of a major Bacillus subtilis autolysin gene. *J Bacteriol* 173:7304–7312.

61. Losick R, Stragier P (1992) Crisscross regulation of cell-type-specific gene expression during development in B. subtilis. *Nature* 355:601–604.

62. Errington J (1993) Bacillus subtilis sporulation: regulation of gene expression and control of morphogenesis. *Microbiol Rev* 57:1–33.

63. Dubrac S, Bisicchia P, Devine KM, Msadek T (2008) A matter of life and death: cell wall homeostasis and the WalKR (YycGF) essential signal transduction pathway. *Mol Microbiol* 70:1307–1322.

64. Ng W-L et al. (2003) Constitutive expression of PcsB suppresses the requirement for the essential VicR (YycF) response regulator in Streptococcus pneumoniae R6. *Mol Microbiol* 50:1647–1663.

65. Ng W-L, Kazmierczak KM, Winkler ME (2004) Defective cell wall synthesis in Streptococcus pneumoniae R6 depleted for the essential PcsB putative murein hydrolase or the VicR (YycF) response regulator. *Mol Microbiol* 53:1161–1175.

66. Fabret C, Hoch JA (1998) A two-component signal transduction system essential for growth of Bacillus subtilis: implications for anti-infective therapy. *J Bacteriol* 180:6375–6383.

67. Dubrac S, Boneca IG, Poupel O, Msadek T (2007) New insights into the WalK/WalR (YycG/YycF) essential signal transduction pathway reveal a major role in controlling cell wall metabolism and biofilm formation in Staphylococcus aureus. *J Bacteriol* 189:8257–8269.

68. Dubrac S, Msadek T (2004) Identification of genes controlled by the essential YycG/YycF two-component system of Staphylococcus aureus. *J Bacteriol* 186:1175–1181.

69. Martin PK, Li T, Sun D, Biek DP, Schmid MB (1999) Role in cell permeability of an essential two-component system in Staphylococcus aureus. *J Bacteriol* 181:3666–3673.

70. Senadheera MD et al. (2005) A VicRK signal transduction system in Streptococcus mutans affects gtfBCD, gbpB, and ftf expression, biofilm formation, and genetic competence development. *J Bacteriol* 187:4064–4076.

71. Fukuchi K et al. (2000) The essential two-component regulatory system encoded by yycF and yycG modulates expression of the ftsAZ operon in Bacillus subtilis. *Microbiol* 146:1573–1583.

72. Hancock LE, Perego M (2004) Systematic inactivation and phenotypic characterization of two-component signal transduction systems of Enterococcus faecalis V583. *J Bacteriol* 186:7951–7958.

73. Kallipolitis BH, Ingmer H (2001) Listeria monocytogenes response regulators important for stress tolerance and pathogenesis. *FEMS Microbiol Lett* 204:111–115.

74. Lange R et al. (1999) Domain organization and molecular characterization of 13 two-component systems identified by genome sequencing of Streptococcus pneumoniae. *Gene* 237:223–234.

75. Yamamoto H et al. (2008) Post-translational control of vegetative cell separation enzymes through a direct interaction with specific inhibitor IseA in Bacillus subtilis. *Mol Microbiol* 70:168–182.

76. Fukushima T et al. (2010) A role for the essential YycG sensor histidine kinase in sensing cell division. *Mol Microbiol* 79:503–522.

77. Fukushima T, Szurmant H, Kim E, Perego M, Hoch J (2008) A sensor histidine kinase coordinates cell wall architecture with cell division in Bacillus subtilis. *Mol Microbiol* 69:621–632.

78. Pereira S, Henriques A, Pinho M, de Lencastre H, Tomasz A (2009) Evidence for a dual role of PBP1 in the cell division and cell separation of Staphylococcus aureus. *Mol Microbiol* 72:895–904.

79. Koch AL (1990) Additional arguments for the key role of "smart" autolysins in the enlargement of the wall of gram-negative bacteria. *Res Microbiol* 141:529–541.

80. Rechenberg von M, Ursinus A, Höltje JV (1996) Affinity chromatography as a means to study multienzyme complexes involved in murein synthesis. *Microb Drug Resist* 2:155–157.

81. Romeis T, Höltje JV (1994) Specific interaction of penicillin-binding proteins 3 and 7/8 with soluble lytic transglycosylase in Escherichia coli. *J Biol Chem* 269:21603–21607.

82. Hett EC, Chao MC, Rubin EJ (2010) Interaction and modulation of two antagonistic cell wall enzymes of mycobacteria. *PLoS Pathog* 6:e1001020.

83. Odintsov SG, Sabala I, Marcyjaniak M, Bochtler M (2004) Latent LytM at 1.3A resolution. *J Mol Biol* 335:775–785.

84. Firczuk M, Mucha A, Bochtler M (2005) Crystal structures of active LytM. *J Mol Biol* 354:578–590.

85. Schlag M et al. (2010) Role of staphylococcal wall teichoic acid in targeting the major autolysin Atl. *Mol Microbiol* 75:864–873.

86. Ruggiero A et al. (2010) Structure and functional regulation of RipA, a mycobacterial enzyme essential for daughter cell separation. *Structure* 18:1184–1190.

87. Bublitz M et al. (2009) Structural basis for autoinhibition and activation of Auto, a virulence-associated peptidoglycan hydrolase of Listeria monocytogenes. *Mol Microbiol* 71:1509–1522.

88. Kessler E, Safrin M, Gustin JK, Ohman DE (1998) Elastase and the LasA protease of Pseudomonas aeruginosa are secreted with their propeptides. *J Biol Chem* 273:30225–30231.

89. de Souza RF, Anantharaman V, de Souza SJ, Aravind L, Gueiros-Filho FJ (2008) AMIN domains have a predicted role in localization of diverse periplasmic protein complexes. *Bioinformatics* 24:2423–2426.

90. Bernhardt TG, de Boer PAJ (2003) The Escherichia coli amidase AmiC is a periplasmic septal ring component exported via the twin-arginine transport pathway. *Mol Microbiol* 48:1171–1182.

91. Koch AL, Kirchner G, Doyle RJ, Burdett ID (1985) How does a Bacillus split its septum right down the middle? *Ann Inst Pasteur Microbiol* 136A:91–98.

92. Cheung HY, Freese E (1985) Monovalent cations enable cell wall turnover of the turnover-deficient lyt-15 mutant of Bacillus subtilis. *J Bacteriol* 161:1222–1225.

93. Jolliffe LK, Doyle RJ, Streips UN (1981) The energized membrane and cellular autolysis in Bacillus subtilis. *Cell* 25:753–763.

94. Kemper MA, Urrutia MM, Beveridge TJ, Koch AL, Doyle RJ (1993) Proton motive force may regulate cell wall-associated enzymes of Bacillus subtilis. *J Bacteriol* 175:5690–5696.

95. Calamita HG, Ehringer WD, Koch AL, Doyle RJ (2001) Evidence that the cell wall of Bacillus subtilis is protonated during respiration. *Proc Natl Acad Sci USA* 98:15260–15263.

96. Moynihan PJ, Clarke AJ (2011) O-Acetylated peptidoglycan: Controlling the activity of bacterial autolysins and lytic enzymes of innate immune systems. *Int J Biochem Cell Biol* 43:1655–1659.

97. Blaauwen den T, de Pedro MA, Nguyen-Distèche M, Ayala JA (2008) Morphogenesis of rod-shaped sacculi. *FEMS Microbiol Rev* 32:321–344.

98. de Boer PA (2010) Advances in understanding E. coli cell fission. *Current Opin Microbiol* 13:730–737.

99. Bi EF, Lutkenhaus J (1991) FtsZ ring structure associated with division in Escherichia coli. *Nature* 354:161–164.

100. Adams DW, Errington J (2009) Bacterial cell division: assembly, maintenance and disassembly of the Z ring. *Nat Rev Microbiol* 7:642–653.

101. Durand-Heredia JM, Yu HH, De Carlo S, Lesser CF, Janakiraman A (2011) Identification and Characterization of ZapC, a Stabilizer of the FtsZ Ring in Escherichia coli. *J Bacteriol* 193:1405–1413.

102. Ebersbach G, Galli E, Møller-Jensen J, Löwe J, Gerdes K (2008) Novel coiled-coil cell division factor ZapB stimulates Z ring assembly and cell division. *Mol Microbiol* 68:720–735.

103. Galli E, Gerdes K (2010) Spatial resolution of two bacterial cell division proteins: ZapA recruits ZapB to the inner face of the Z-ring. *Mol Microbiol* 76:1514–1526.

104. Hale CA et al. (2011) Identification of Escherichia coli ZapC (YcbW) as a component of the division apparatus that binds and bundles FtsZ polymers. *J Bacteriol* 193:1393–1404.

105. Pichoff S, Lutkenhaus J (2002) Unique and overlapping roles for ZipA and FtsA in septal ring assembly in Escherichia coli. *EMBO J* 21:685–693.

106. Addinall SG, Cao C, Lutkenhaus J (1997) FtsN, a late recruit to the septum in Escherichia coli. *Mol Microbiol* 25:303–309.

107. Chen JC, Beckwith J (2001) FtsQ, FtsL and FtsI require FtsK, but not FtsN, for co-localization with FtsZ during Escherichia coli cell division. *Mol Microbiol* 42:395–413.

108. Hale CA, de Boer PA (1999) Recruitment of ZipA to the septal ring of Escherichia coli is dependent on FtsZ and independent of FtsA. *J Bacteriol* 181:167–176.

109. Hale CA, de Boer PAJ (2002) ZipA is required for recruitment of FtsK, FtsQ, FtsL, and FtsN to the septal ring in Escherichia coli. *J Bacteriol* 184:2552–2556.

110. Mercer KLN, Weiss DS (2002) The Escherichia coli cell division protein FtsW is required to recruit its cognate transpeptidase, FtsI (PBP3), to the division site. *J Bacteriol* 184:904–912.

111. Weiss DS, Chen JC, Ghigo JM, Boyd D, Beckwith J (1999) Localization of FtsI (PBP3) to the septal ring requires its membrane anchor, the Z ring, FtsA, FtsQ, and FtsL. *J Bacteriol* 181:508–520.

112. Goehring NW, Beckwith J (2005) Diverse paths to midcell: assembly of the bacterial cell division machinery. *Curr Biol* 15:R514–26.

113. Buddelmeijer N, Judson N, Boyd D, Mekalanos JJ, Beckwith J (2002) YgbQ, a cell division protein in Escherichia coli and Vibrio cholerae, localizes in codependent fashion with FtsL to the division site. *Proc Natl Acad Sci USA* 99:6316–6321.

114. Aarsman MEG et al. (2005) Maturation of the Escherichia coli divisome occurs in two steps. *Mol Microbiol* 55:1631–1645.

115. Peters NT, Dinh T, Bernhardt TG (2011) A Fail-Safe Mechanism in the Septal Ring Assembly Pathway Generated by the Sequential Recruitment of Cell Separation Amidases and Their Activators. *J Bacteriol* 193:4973–4983.

116. Finn RD et al. (2008) The Pfam protein families database. *Nucleic Acids Res* 36:D281–288.

117. Chung HS et al. (2009) Rapid β-lactam-induced lysis requires successful assembly of the cell division machinery. *Proc Natl Acad Sci USA* 106:21872–21877.

118. Uehara T, Parzych KR, Dinh T, Bernhardt TG (2010) Daughter cell separation is controlled by cytokinetic ring-activated cell wall hydrolysis. *EMBO J* 29:1412–1422.

119. Uehara T, Dinh T, Bernhardt TG (2009) LytM-domain factors are required for daughter cell separation and rapid ampicillin-induced lysis in Escherichia coli. *J Bacteriol* 191:5094–5107.

120. Browder H, Zygmunt W, Young J, Tavormina P (1965) Lysostaphin: Enzymatic Mode of Action. *Biochem Biophys Res Commun* 19:383–389.

121. Bernhardt TG, de Boer PAJ (2004) Screening for synthetic lethal mutants in Escherichia coli and identification of EnvC (YibP) as a periplasmic septal ring factor with murein hydrolase activity. *Mol Microbiol* 52:1255–1269.

122. Paradis-Bleau C et al. (2010) Lipoprotein cofactors located in the outer membrane activate bacterial cell wall polymerases. *Cell* 143:1110–1120.

123. Schmidt KL et al. (2004) A predicted ABC transporter, FtsEX, is needed for cell division in Escherichia coli. *J Bacteriol* 186:785–793.

124. Rees DC, Johnson E, Lewinson O (2009) ABC transporters: the power to change. *Nat Rev Mol Cell Biol* 10:218–227.

125. Yang DC et al. (2011) An ATP-binding cassette transporter-like complex governs cell-wall hydrolysis at the bacterial cytokinetic ring. *Proc Natl Acad Sci USA* 108:E1052–60.

126. Corbin BD, Wang Y, Beuria TK, Margolin W (2007) Interaction between cell division proteins FtsE and FtsZ. *J Bacteriol* 189:3026–3035.

Chapter 2

An ABC transporter-like complex governs cell well hydrolysis at the bacterial cytokinetic ring

Attributions

The work presented in this chapter was a collaborative effort among all the listed authors. Monica Markovski performed the initial screen that identified both *envC* and *ftsEX* as being synthetically lethal with the loss of PBP1b. Nick Peters verified these results by generating the spot dilution images (Figure 2.3), which additionally illustrated other shared synthetic lethal mutant phenotypes of *ftsEX* and *envC*. He also performed the localization experiments looking at the dependency of EnvC on FtsEX for recruitment to the septal ring (Figure 2.6) and did Western blot analysis on these samples showing that there was no appreciable difference in EnvC-mCherry accumulation in FtsEX$^+$ versus FtsEX$^-$ cells (Figure 2.7). Katherine Parzych did the experiments confirming that Δ*envC* and Δ*ftsEX* phenocopy each other in a Δ*nlpD* strain background (Figure 2.4). She also determined the stability of WT EnvC in FtsEX$^-$ cells (Figure 2.5A). Desirée Yang performed the fractionation experiments determining the subcellular localization of EnvC in WT and FtsEX$^-$ cells (Figure 2.5B). Additionally, she did all the interaction studies including the bacterial two-hybrid assay and purified protein pull-downs (Figure 2.8). Desirée Yang also performed all the localization experiments looking at EnvC recruitment or lack thereof in the ^{Loop1}FtsX-deletion derivatives as well as the ATPase-defective FtsE mutants (Figures 2.9 - 2.12). Finally, the measurements represented in Tables 2.1 and 2.2 where performed by Desirée Yang. Thomas Bernhardt composed the manuscript and all remaining authors helped to revise and edit the paper.

Chapter 2: An ABC transporter-like complex governs cell wall hydrolysis at the bacterial cytokinetic ring

Desirée C. Yang[1], Nick T. Peters[1†], Katherine R. Parzych[1†], Tsuyoshi Uehara[1], Monica Markovski[1], and Thomas G. Bernhardt[1]

[1]Department of Microbiology and Immunobiology, Harvard Medical School, Boston, MA 02115

[†]These authors contributed equally to this work; reprinted with permission from PNAS

Section 2.1: Abstract

ABC transporters are ubiquitous membrane protein complexes that move substrates

across membranes. They do so using ATP-induced conformational changes in their nucleotide

binding domains (NBDs) to alter the conformation of the transport cavity formed by their

transmembrane domains (TMDs). In *Escherichia coli,* an ABC transporter-like complex

composed of FtsE (NBD) and FtsX (TMD) has long been known to be important for cytokinesis,

but its role in the process has remained mysterious. Here we identify FtsEX as a regulator of cell

wall hydrolysis at the division site. Cell wall material synthesized by the division machinery is

initially shared by daughter cells and must be split by hydrolytic enzymes called amidases to

drive daughter cell separation. We recently showed that the amidases require activation at the

cytokinetic ring by proteins with LytM domains, of which EnvC is the most critical. In this

report, we demonstrate that the FtsEX directly recruits EnvC to the septum via an interaction

between EnvC and a periplasmic loop of FtsX. Importantly, we also show that FtsEX variants

predicted to be ATPase defective still recruit EnvC to the septum but fail to promote cell

separation. Our results thus suggest the attractive possibility that amidase activation via EnvC in

the periplasm is regulated by conformational changes in the FtsEX complex mediated by ATP

hydrolysis in the cytoplasm. Since FtsE has been reported to interact with the tubulin-like FtsZ protein, this provides a potential mechanism for coupling amidase activity with the contraction of the FtsZ cytoskeletal ring.


Section 2.2: Introduction

Cytokinesis in *Escherichia coli* and other bacteria is mediated by a ring-shaped multi-protein machine called the "septal ring" or "divisome" (1). Assembly of this machine begins with the polymerization of the tubulin-like FtsZ protein into a ring-like structure just underneath the cell membrane at the prospective site of division (2). Several FtsZ-binding proteins have been identified in *E. coli* (FtsA, ZipA, ZapA, and ZapC). Along with the ZapA-binding protein ZapB, they appear to play partially redundant roles in the formation and stabilization of the Z-ring structure (3-10). Once formed, the Z-ring promotes septal ring assembly by facilitating the recruitment of the remaining essential and non-essential division proteins to the division site according to a mostly linear dependency pathway (1).

Because the functions of many of its components are ill-defined, the mechanism(s) by which the septal ring promotes cell constriction remain largely mysterious (1). One of the most enigmatic division factors has been the ABC-transporter-like complex formed by FtsE and FtsX (FtsEX) (11). ABC transporters are integral membrane protein complexes that use the energy of ATP hydrolysis to transport substrates across membranes (12). They are typically composed of two polytopic transmembrane domains (TMDs) and a pair of cytosolic nucleotide binding domains (NBDs) often called ATP-binding cassettes (ABCs). Structural studies of complete ABC-transporters indicate that these complexes undergo remarkable conformational changes in

response to nucleotide binding and hydrolysis (12). The NBD subunits interconvert between an open and a closed conformation at the membrane surface during an ATP hydrolysis cycle (12). These conformational changes are, in turn, transmitted to the TMD subunits to promote transitions between outward-facing and inward-facing conformations of the central cavity formed by the TMDs (12). Transport is thus promoted by alternating access of the substrate-binding site to opposing sides of the membrane.

The role of the FtsEX complex in cell division has remained unclear for some time (13, 14). FtsE is the NBD component of the complex and FtsX is the TMD component (15) (Figure 2.1A-B). Both factors localize to the septal ring and are conditionally essential for cell division (11). In medium of low osmotic strength, such as LB without added NaCl, cells lacking FtsEX display a lethal division defect (11, 15). They form smooth filaments that assemble Z-rings, but these structures are compromised because they fail to recruit FtsK and other downstream division factors (11). This phenotype along with the observation that FtsE and FtsX interact with several different division proteins (16, 17) has lead to the idea that one important function of FtsEX is to stabilize the septal ring structure (18-20). Consistent with this idea, the division defect of FtsEX⁻ cells can be partially suppressed by the overproduction of other division proteins (FtsZ, FtsN, or FtsP) (18). Increasing the osmolarity of the medium and lowering the growth temperature also restores division function to FtsEX⁻ mutants (11, 15, 18, 19). The mechanisms by which high osmolarity or division protein overproduction bypass the FtsEX requirement for cell division are not known. However, these growth conditions presumably allow essential division proteins downstream of FtsEX in the recruitment hierarchy to assemble at the division site in the absence of the complex. Indeed, FtsN has been shown to localize to
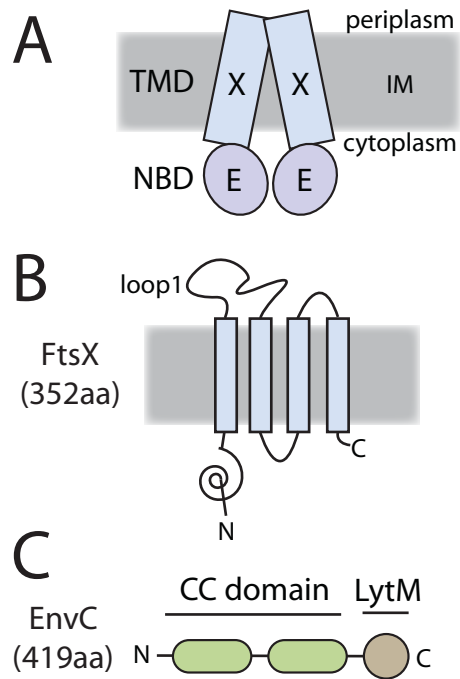
Figure 2.1. Domain structure of FtsEX and EnvC. (**A**) Diagram of the FtsEX ABC system. FtsX (X) is the TMD component, and FtsE (E) is the ATPase component (15). The complex is in the inner membrane (IM) with FtsE located on the cytoplasmic face of the membrane. (**B**) Membrane topology of FtsX as determined by Weiss and coworkers (20). The loop1 domain is composed of residues 93–223. Membrane orientation is the same as in *A*. (**C**) Domain structure of EnvC. EnvC is a periplasmic protein. It possesses an N-terminal signal sequence (residues 1–34), two relatively long segments predicted to form coiled coils (CC domain, residues 35–277), and a C-terminal LytM domain (residues 278–419) needed for amidase activation.

sites of constriction in FtsEX⁻ cells grown in LB with 1% NaCl (11). Over the years, many

functions for FtsEX have been proposed, most of them assuming that it must transport a substrate

(20) (and references therein). In this report, we present evidence that FtsEX may not be a

transporter at all but is instead an important regulator of cell wall turnover at the division site.

Most bacteria surround themselves with a polysaccharide cell wall matrix called

peptidoglycan (PG) (21). This meshwork is essential for cellular integrity and is composed of

glycan strands connected to one another by crosslinks between attached peptide moieties (21)

(Figure 2.2). During cytokinesis in Gram-negative bacteria, septal PG is synthesized by the

divisome (1). This material is thought to be initially shared by the developing daughter cells and

must be split to facilitate outer membrane constriction and daughter cell separation (1) (Figure

2.2). Septal PG splitting is mediated by the periplasmic PG amidases, AmiA, AmiB, and AmiC

(22). Amidases are PG hydrolases that break crosslinks in the PG meshwork by cleaving bonds

that link stem peptides to the glycan strands. Mutants lacking amidase activity complete inner

membrane constriction and fusion. However, they fail to split septal PG and form long chains of

cells connected by shared layers of PG and a partially constricted outer membrane layer (22, 23).

The amidases must be tightly controlled to prevent them from creating lesions in the cell

wall that can result in cell lysis. Part of this regulation appears to rely on the fact that the PG

amidases alone are weakly active enzymes (24). To efficiently hydrolyze PG, they require

activation by EnvC and NlpD (24), divisome-associated proteins with LytM domains (Pfam,

Peptidase_M23) (25, 26). EnvC specifically activates AmiA and AmiB while NlpD specifically

activates AmiC (24). Accordingly, mutants lacking both EnvC and NlpD have a chaining

phenotype that resembles a triple amidase mutant (25). A major unresolved question has been
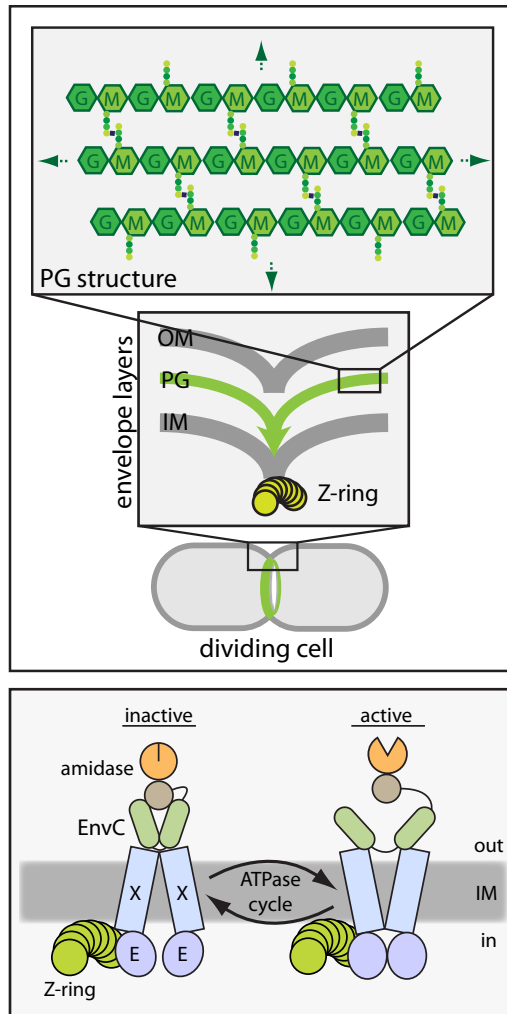
Figure 2.2. Coordinated envelope constriction in Gram-negative bacteria and model for regulated PG hydrolase activity at the division site. (*Upper*) Diagrams showing a dividing cell with an assembled cytokinetic ring apparatus (green) (bottom diagram), a close-up diagram of the division site highlighting the coordinated constriction of the envelope layers (IM, inner membrane; OM, outer membrane; PG, peptidoglycan; Z-ring, FtsZ cytoskeletal ring) (middle diagram), and a diagram of the PG chemical structure (G, *N*-acetylglucosamine; M, *N*-acetylmuramic acid) (top diagram). Colored dots in the top diagram represent attached peptides. The PG structure continues in all directions to envelop the cell (green arrows). (*Lower*) A schematic diagram of a putative FtsEX–EnvC–amidase complex at the Z-ring. We propose that conformational changes in FtsEX induced by FtsE-mediated ATP hydrolysis are transmitted to EnvC to control its ability to activate the amidases so that they can cleave the septal PG (not drawn).

understanding how the LytM factors are themselves controlled so that amidase activity at the septum is properly coordinated with other activities of the septal ring, such as membrane invagination and septal PG synthesis.

Using a genetic screen designed to identify factors involved in cell wall assembly (27), we found that mutations in *ftsEX* and *envC* are synthetically lethal with loss-of-function mutations in a common set of genes. This suggested that FtsEX and EnvC might participate in the same biochemical pathway. Indeed, when grown under permissive conditions, FtsEX⁻ cells phenocopy the cell separation defect displayed by EnvC⁻ cells. We further show that EnvC requires FtsEX for its recruitment to the division site and that EnvC interacts directly with the large periplasmic loop domain of FtsX. Importantly, we also show that FtsEX variants predicted to be ATPase defective still recruit EnvC to the septum but fail to promote cell separation. Our results thus suggest the attractive possibility that FtsX regulates amidase activation by EnvC in the periplasm via conformational changes induced by FtsE-mediated ATP hydrolysis on the opposite side of the membrane. Since FtsE has been reported to interact with FtsZ (16), this provides a potential mechanism for directly coupling septal PG hydrolysis with the contraction of the Z-ring during cell constriction. Interestingly, the accompanying report by Sham and co-workers (28) similarly connects FtsEX with cell separation in the Gram-positive pathogen *Streptococcus pneumoniae*, indicating that the regulation of cell wall turnover is likely to be a broadly conserved function for FtsEX.

Section 2.3: Results

ftsEX and _envC_ mutants share common genetic interactions

To identify factors important for cell wall biogenesis, we recently performed a genetic

screen for mutations synthetically lethal with the inactivation of the PG synthase PBP1b (_slb_

mutants) (27). In addition to mutants in the _lpoA_ gene coding for a lipoprotein cofactor required

for the activity of PBP1a (27, 29), we isolated mutants with transposon insertions in _envC_ and

ftsEX. The _ftsEX_ mutant was isolated in a screen performed at room temperature, a condition

that we find suppresses the lethal effects of FtsEX inactivation. To confirm the synthetic

lethality of the mutant combinations, Δ_envC_ and Δ_ftsEX_ alleles were transduced into strain

MM11 [P$_{ara}$::_ponB_] harboring the low copy plasmid pTB63 [_ftsQAZ_], which expresses the

ftsQAZ operon from native promoters and suppresses the FtsEX⁻ growth defect. In MM11, the

native _ponB_ promoter was replaced with P$_{ara}$ such that _ponB_ expression is arabinose-dependent

(27). Depletion of PBP1b in the absence of FtsEX or EnvC was confirmed to be lethal (Figure

2.3A). The terminal phenotype in both cases was cell lysis. Since EnvC is needed to activate the

amidases AmiA and AmiB at the developing septum, we tested whether the combined

inactivation of AmiA and AmiB was also lethal upon PBP1b depletion. This indeed proved to be

the case (Figure 2.3A). We do not currently know why the inactivation of FtsEX, EnvC, or

AmiA/AmiB renders PBP1b essential for growth. Nevertheless, the observed phenotypes

suggested to us that FtsEX may function in the process of septal PG splitting with EnvC and the

amidases.

The loss of FtsEX function was previously shown to be synthetically lethal with the

deletion of _ftsP_ (_sufI_) (18). We confirmed this and found that the depletion of EnvC was also

synthetically lethal with Δ*ftsP* (Figure 2.3B-C), thus further connecting the functions of EnvC and FtsEX. As expected for proteins functioning in the same pathway, loss of EnvC function was not lethal upon FtsEX depletion (Figure 2.3B).

FtsEX is required for daughter cell separation

While performing the FtsEX depletion experiments in Figure 2.3B, we found that growth on minimal agar at 37°C partially suppressed the FtsEX⁻ growth defect. We assume this is due to the higher osmolarity of the medium relative to standard LB (0.5% NaCl) and the slower overall growth rate of the cells. The suppression in liquid minimal medium was even more pronounced, especially when cells were grown at 30°C. Here, FtsEX⁻ cells displayed a much more mild division defect resembling that typically observed for EnvC⁻ cells (25) (see below). A similar division defect was also observed for Δ*envC* and Δ*ftsEX* mutants harboring an *ftsQAZ* overproducing plasmid (pTB63) when we grew them in LB (1% NaCl) (Figure 2.4A-C). It thus appeared that under conditions that suppressed the septal ring stability defect of FtsEX⁻ cells, a potential role for the FtsEX complex in EnvC-mediated cell separation was revealed. Interestingly, we note that, although not as severe as the FtsEX⁻ division defect, EnvC⁻ cells display a lethal filamentation phenotype when grown in LB without added NaCl at 42°C (30-32). This suggests that at least part of the constriction defect of FtsEX⁻ cells may be the result of EnvC inactivation.

We previously showed that cells lacking EnvC become dependent on NlpD for cell separation (25). Cells lacking EnvC and NlpD appear to be completely defective in cell separation and form very long chains that resemble triple amidase mutants (25) (Figure 2.4D-F).
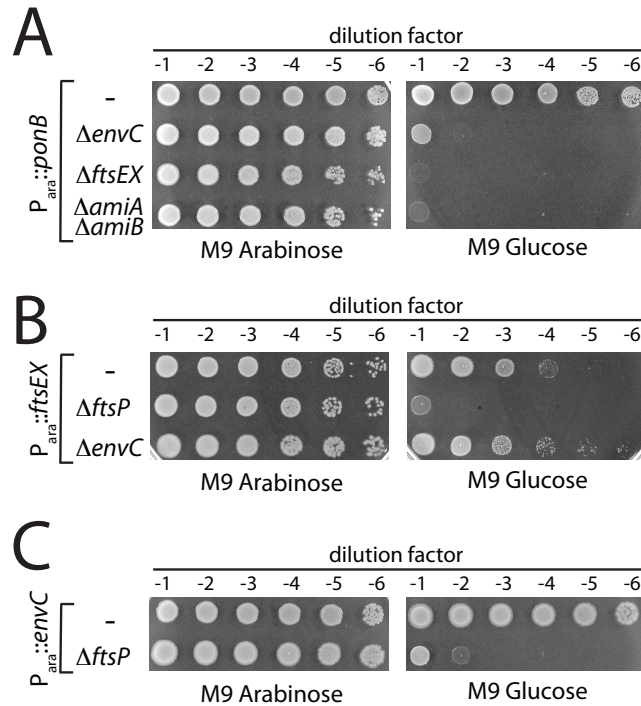
Figure 2.3. Shared synthetic lethal phenotypes of *envC* and *ftsEX* mutants. (**A**) Cells of MM11/ pTB63 (P_{ara}::*ponB*/*ftsQAZ*) and its Δ*envC*, Δ*ftsEX*, or Δ*amiA* Δ*amiB* derivatives were grown overnight in M9 arabinose medium supplemented with 5 μg/mL Tet (Tet⁵) at 37°C. Following normalization for cell density ($OD_{600} = 2$), the resulting cultures were serially diluted (10^{-1} to 10^{-6}), and 5 μL of each dilution was spotted on the indicated medium. Plates were incubated overnight at 37°C and photographed. (**B**) Cells of TU191(attλTU188) [Δ*ftsEX* (P_{ara}::*ftsEX*)] and its Δ*envC* or Δ*ftsP* derivatives were processed as in *A* except growth was in the absence of Tet. (**C**) Cells of TB140(attλTD25) [Δ*envC* (P_{ara}::*envC*)] and its Δ*ftsP* derivative were grown and processed as in *B*.
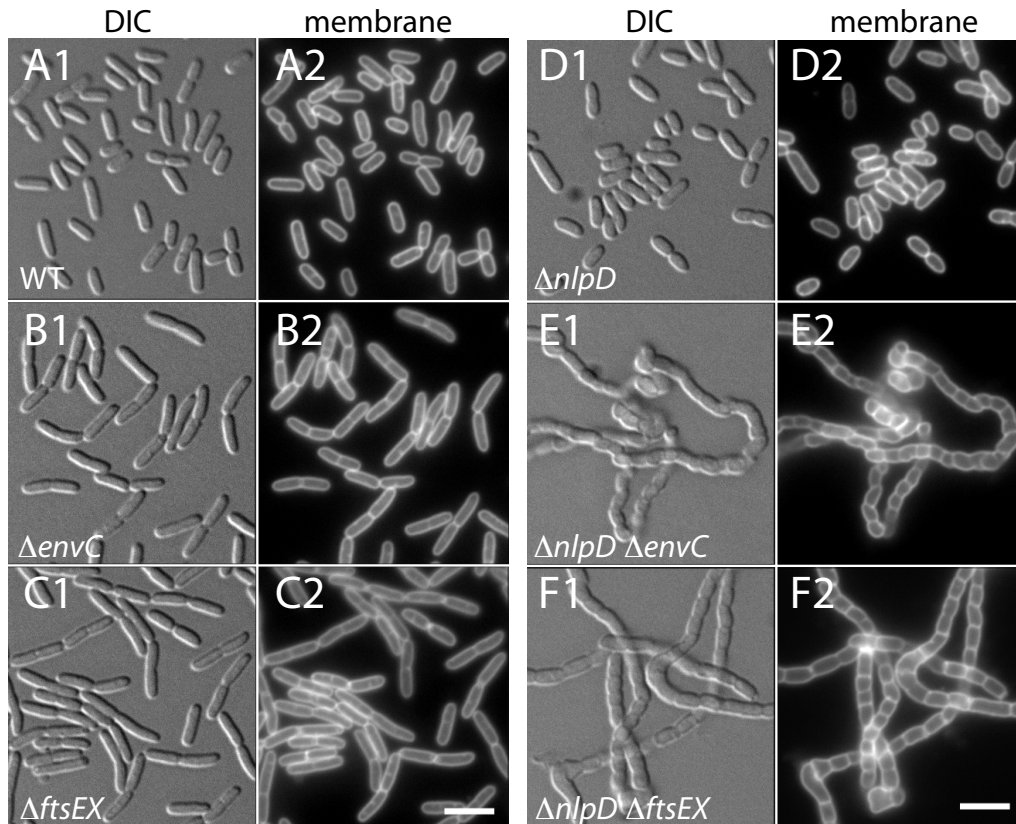
Figure 2.4. FtsEX⁻ and EnvC⁻ cells have similar division defects. Cells of TB28 (WT) (**A**), KP4 (Δ*envC*) (**B**), KP5 (Δ*ftsEX*) (**C**), TB145 (Δ*nlpD*) (**D**), KP6 (Δ*nlpD* Δ*envC*) (**E**), and KP7 (Δ*nlpD* Δ*ftsEX*) (**F**) harboring pTB63 (*ftsQAZ*) were grown overnight in LB-Tet⁵ 1.0% NaCl (**A–C**) or 1.5% NaCl (**D–F**) at 30°C. Cultures were diluted 1:200 into the same medium and grown at 30°C to an OD$_{600}$ of 0.6–0.8. Cells then were incubated with the fixable membrane stain FM1-43FX (5 μg/mL) for 10 min and were fixed. Fixed cells were visualized on 2% agarose pads using differential interference contrast microscopy (DIC) (*A1–F1*) and GFP (*A2–F2*) optics. (Scale bars, 4 microns)

We reasoned that if FtsEX is truly required for EnvC-mediated cell separation, the simultaneous inactivation of FtsEX and NlpD should also result in a severe chaining phenotype. This indeed proved to be the case (Figure 2.4D-F). We therefore conclude that FtsEX is required for EnvC to promote septal PG splitting.

EnvC is stable and released into the periplasm in the absence of FtsEX

A potential reason for the FtsEX-EnvC connection is that EnvC requires FtsEX for its stable accumulation. To investigate this, we compared EnvC levels in total cell extracts prepared from WT versus Δ*ftsEX* cells (Figure 2.5A). Immunoblotting with affinity-purified, anti-EnvC polyclonal antibodies revealed that similar amounts of EnvC accumulate whether or not cells produce FtsEX (Figure 2.5A, compare lanes 1-3 with 7-9). We did, however, observe low concentrations of smaller immuno-reactive species in the Δ*ftsEX* extract that were not seen in the WT or Δ*envC* extracts, indicating that a small portion of EnvC is probably proteolytically processed in the absence of FtsEX (Figure 2.5A). This low level of processing is unlikely to explain the EnvC⁻ phenotype of Δ*ftsEX* cells.

Since FtsEX is related to ABC transporters, one possible way in which it might promote EnvC function is by facilitating its export to the periplasm. To investigate this, we fractionated cells to determine the subcellular localization of EnvC in the presence or absence of FtsEX. WT and Δ*ftsEX* cells were suspended in buffer containing sucrose and converted to spheroplasts by the addition of EDTA and lysozyme. In WT cells, EnvC pelleted with the spheroplasts rather than remaining in the soluble periplasmic fraction like the MalE control (Figure 2.5B, lanes 1-3). In contrast, EnvC was found almost exclusively in the periplasmic fraction from FtsEX⁻ cells.
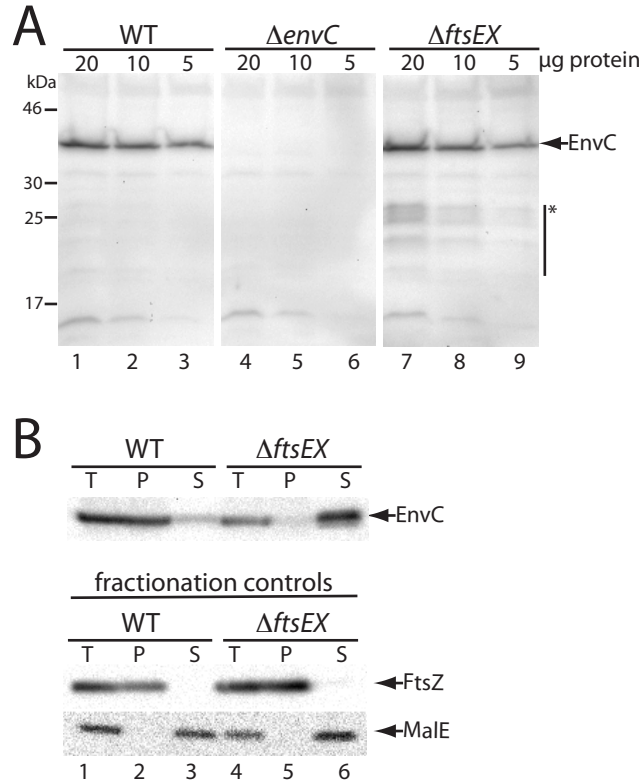
Figure 2.5. Change in EnvC subcellular localization in the absence of FtsEX. (**A**) Cells of TB28 (WT), KP4 (Δ*envC*), or KP5 (Δ*ftsEX*) harboring pTB63 (*ftsQAZ*) were grown overnight in LB (1.0% NaCl)-Tet[5] at 30°C. Cultures were diluted 1:100 into LB-Tet[5] and grown at 30°C to an OD_{600} of 0.66–0.72. Cell extracts then were prepared, and the indicated total protein amounts were subjected to immunoblotting using affinity-purified EnvC antibodies. Arrow indicates position of [FL]EnvC bands, and the bar with the asterisk highlights what appears to be a small amount of EnvC degradation products in extracts from the Δ*ftsEX* mutant. Positions of the molecular weight markers are indicated on the left. (**B**) Cultures of the strains in *A* were grown as above to an OD_{600} of 0.39–0.46. One aliquot of cells was used to prepare a total-cell extract. The remaining cells were converted to spheroplasts and pelleted by centrifugation. The resulting pellet (P) and supernatant (S) fractions along with the total-cell extract (T) were analyzed by SDS-PAGE and immunoblotting for EnvC, FtsZ, and MalE as indicated. FtsZ and MalE served as markers for the cytoplasm/spheroplast membranes and periplasm, respectively.

The FtsZ and MalE fractionation controls indicated that this change in EnvC localization was not due to altered fractionation properties of the FtsEX⁻ cells (Figure 2.5B, lanes 4-6). Thus, FtsEX is not required for the export of EnvC to the periplasm. This is consistent with previous reports suggesting that EnvC is a Sec substrate (32) and that its signal sequence can be functionally replaced by alternative signal peptides for Tat- or Sec- mediated transport (24, 26). Furthermore, the fractionation results suggest that EnvC remains associated with the outer face of the inner membrane of WT cells, possibly through an interaction with FtsX, and that it is released into the periplasm in the absence of this interaction (see below).

FtsEX is required for the recruitment of EnvC to the septal ring

In addition to subcellular fractionations, we also investigated the role of FtsEX in the recruitment of EnvC to the septal ring. To do so, we constructed an FtsEX depletion strain NP69 (*attλ*TU188)(*att*HKTB316) [Δ*ftsEX* Δ*envC zapA-gfp* (P$_{ara}$::*ftsEX*)(P$_{lac}$::*envC-mCherry*)]. In this strain, the native *ftsEX* locus was deleted and a second copy of *ftsEX* under arabinose promoter (P$_{ara}$) control was integrated at the λ *att* site. The strain also encodes *zapA-gfp* at the native *zapA* locus and expresses *envC-mCherry* from an expression cassette integrated at the HK022 *att* site. When grown in M9 maltose medium containing a small amount of arabinose (0.01%), cells of NP69(*attλ*TU188)(*att*HKTB316) divided normally and displayed bands of both EnvC-mCherry and ZapA-GFP at the division sites of most cells (Figure 2.6A). Conversely, when the same cells were grown in M9 maltose medium containing a small amount of glucose (0.01%) to repress P$_{ara}$::*ftsEX*, they displayed the heterogeneous cell constriction and separation phenotype typical of FtsEX⁻ and EnvC⁻ cells (Figure 2.6B). While most cells appeared capable of cell division,

54

P_{ara}::*ftsEX* (+Arabinose)

A1   A2   A3

EnvC-mCherry   ZapA-GFP

P_{ara}::*ftsEX* (-Arabinose)

B1

EnvC-mCherry

B2

ZapA-GFP

B3
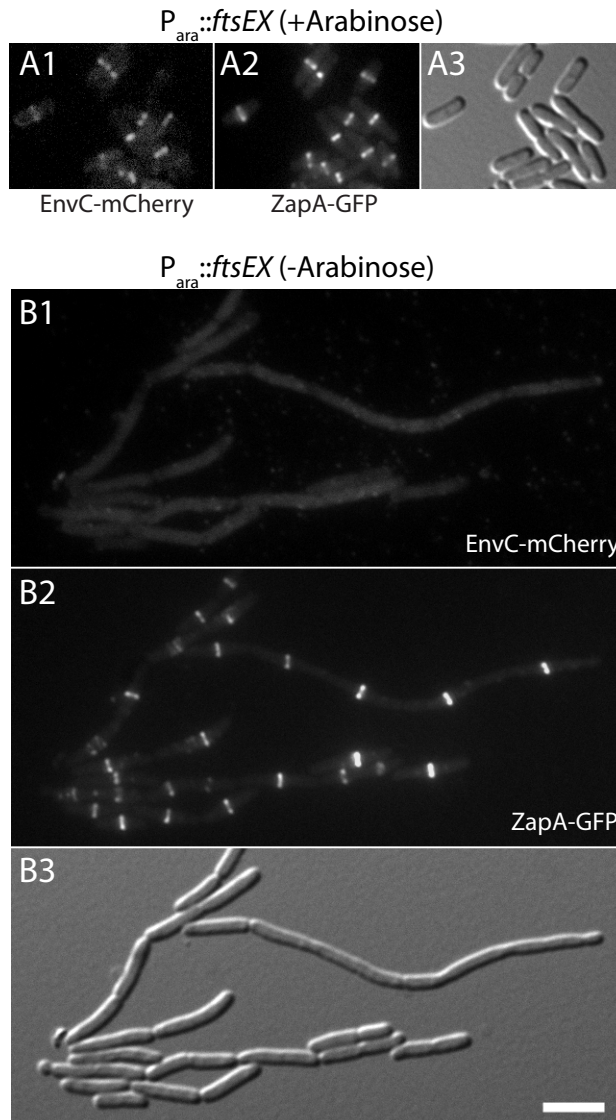
Figure 2.6. FtsEX is required for the recruitment of EnvC to the division site. Cells of NP69 (attλTU188)(attHKTB316) [Δ*ftsEX* Δ*envC zapA-gfp* (P_{ara}::*ftsEX*)(P_{lac}::*envC-mCherry*)] were grown overnight in M9 maltose supplemented with 0.01% arabinose. Cells were washed twice with and resuspended in an equal volume of M9 medium without added sugar. They then were diluted 1:100 into M9 maltose, and growth was continued at 30°C with the addition of either 0.01% arabinose (**A**) or 0.01% glucose (**B**). When the cultures reached an OD_{600} of 0.4–0.6, cells were visualized on 2% agarose pads using mCherry (*Panel 1*), GFP (*Panel 2*), or DIC (*Panel 3*) optics. (Scale bar, 4 microns) Note that a peripheral EnvC-mCherry signal was not observed in *B* as might be expected for a periplasmic protein, likely because too little fusion protein is present to raise the peripheral signal above background.

55

many were elongated and appeared to have difficulty completing cell separation. The Z-ring

marker, ZapA-GFP, formed rings/bands in these elongated cells at fairly regular intervals, but

EnvC-mCherry failed to be recruited to these structures (Figure 2.6B). Immunoblot analysis

indicated that this localization defect was not due to excessive degradation of the EnvC-mCherry

fusion (Figure 2.7). We thus conclude that FtsEX is required for the recruitment of EnvC to the

septal ring.

The large periplasmic loop of FtsX interacts directly with EnvC

Our results thus far suggested that FtsEX may directly interact with EnvC to recruit it to

the division site. The large periplasmic loop of FtsX (residues 93-223, ^{Loop1}FtsX) (Figure 2.1B)

seemed a likely candidate for mediating the interaction with EnvC. We therefore tested the

potential interaction between full-length, mature EnvC (^{FL}EnvC) and ^{Loop1}FtsX using a bacterial

two-hybrid (BACTH) assay based on the reconstitution of adenylate cyclase activity from the

fragments T18 and T25 (33). ^{FL}EnvC-T25 showed a strong interaction signal when paired with a

^{Loop1}FtsX-T18 fusion (Figure 2.8A). EnvC contains three identifiable domains: a signal peptide

(residues 1-34), a coiled coil (CC) domain (residues 35-271), and a LytM domain (residues

318-413) (26, 31, 32) (Figure 2.1C). An interaction signal with ^{Loop1}FtsX-T18 was not detected

when an EnvC truncation lacking the CC domain (^{Lyt}EnvC) was fused to T25 in place of ^{FL}EnvC

(Figure 2.8A). This result suggests that the EnvC-FtsX interaction is mediated by contacts

between ^{Loop1}FtsX and the CC domain of EnvC (^{CC}EnvC). However, for reasons that are not

clear, T25 fusions to ^{CC}EnvC did not show an interaction signal when co-expressed with

^{Loop1}FtsX-T18.
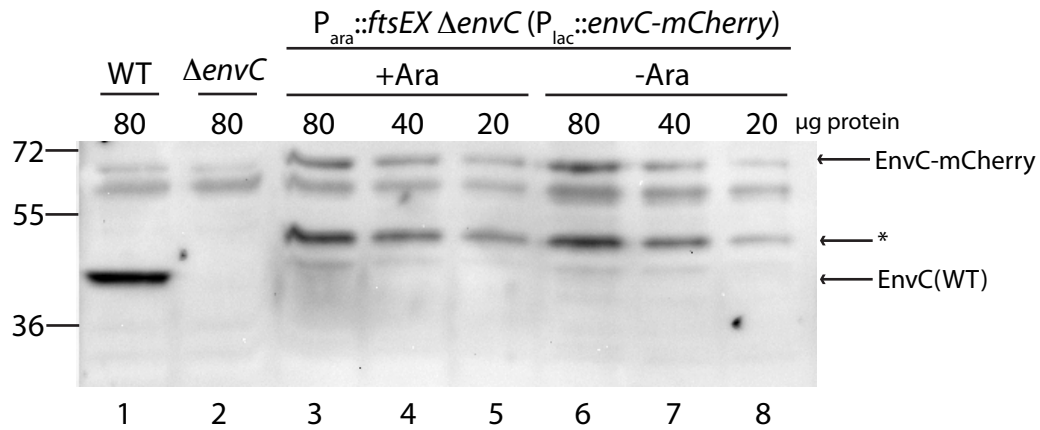
Figure 2.7. EnvC-mCherry accumulation in FtsEX[+] and FtsEX^{-} cells. Cells of TB28 [WT], TB140 [ΔenvC], and NP69(attλTU188)(attHKTB316) [ΔftsEX ΔenvC zapA-gfp (P$_{ara}$::ftsEX) (P$_{lac}$::envC-mCherry)] were grown as described in the legend for Figure 2.6. When the cultures reached an OD$_{600}$ of 0.4-0.6, cells were harvested for whole-cell extract preparation. Proteins in the resulting extracts were separated by SDS-PAGE, transferred to PVDF, and EnvC was detected with affinity purified anti-EnvC antibodies. Relevant genotypes and growth conditions are indicated above the corresponding lanes as well as the amount of total protein (μg) loaded per lane. Asterisk indicates an EnvC-mCherry breakdown product observed in both FtsEX[+] and FtsEX^{-} cells.
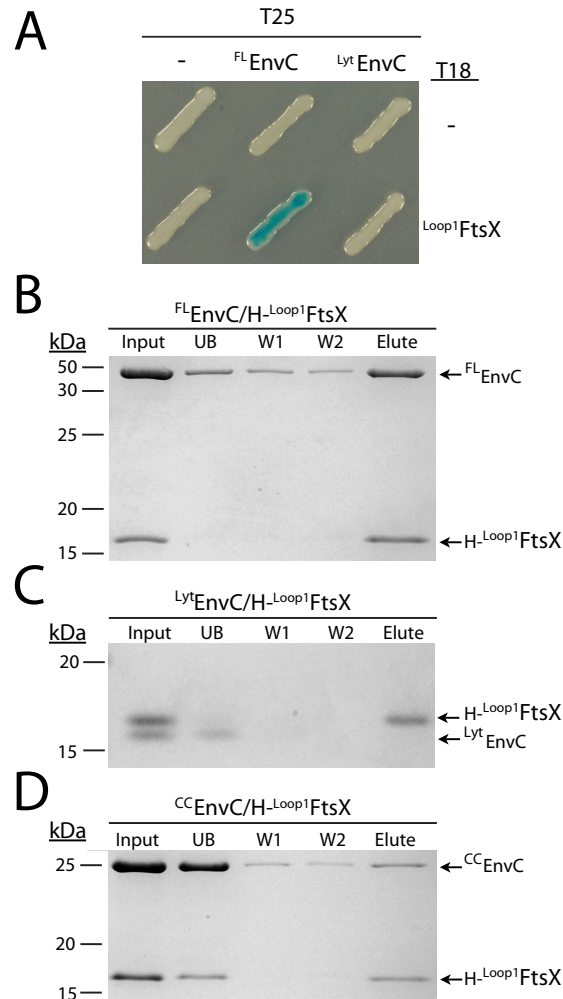
Figure 2.8. EnvC interacts directly with the large periplasmic loop of FtsX. (**A**) Plasmid pairs encoding the indicated [FL]EnvC-T25 or [Lyt]EnvC-T25 and [Loop1]FtsX-T18 fusion proteins were cotransformed into BTH101 (*cya*-99). Individual colonies were patched on M9-glucose supplemented with Amp, Kan, X-Gal, and 1 mM IPTG. Plates were incubated at room temperature and photographed after 72 h. For this particular BACTH assay, interacting partners bring together T18 and T25 to reconstitute adenylate cyclase activity. This activity is detected using *lacZ* induction as a reporter. (**B–D**) Purified H-[Loop1]FtsX was incubated with [FL]EnvC (**B**), [Lyt]EnvC (**C**), or [CC]EnvC (**D**) for 100 min at room temperature in binding buffer [20 mM Tris-HCl (pH 7.4), 150 mM NaCl]. Ni-NTA magnetic agarose beads (Qiagen) then were added to each reaction and were incubated further for 120 min at 4°C with rotation. The magnetic beads were captured with a magnet and were washed twice with binding buffer containing 50 mM imidazole. Proteins retained on the resin were eluted with sample buffer containing EDTA (100 mM). Proteins in the initial reaction (Input), initial supernatant (UB), wash supernatants (W1 and W2), and eluate (Elute) were separated on a 15% Tris-Tricine polyacrylamide gel and stained with Coomassie Brilliant Blue. All proteins were present in the initial binding reaction at a concentration of 4 μM. Positions of molecular weight markers (numbers in kDa) are given to the left of each gel. Control reactions indicated that none of the purified EnvC derivatives could be pulled up with H-GFP.

To further investigate the interaction between FtsX and EnvC, we purified untagged versions of ^{FL}EnvC, ^{Lyt}EnvC, and ^{CC}EnvC as well as a 10xHis (H)-tagged version of ^{Loop1}FtsX (H-^{Loop1}FtsX). We then tested for interactions using "pull-up" assays with magnetic Ni-NTA beads. When ^{FL}EnvC was incubated with H-^{Loop1}FtsX, it was found in the eluate from Ni-NTA beads following two wash steps (Figure 2.8B). Consistent with the BACTH results, this was not the case when ^{Lyt}EnvC was incubated with H-^{Loop1}FtsX (Figure 2.8C). Here, ^{Lyt}EnvC was found primarily in the unbound (UB) fraction. When we incubated ^{CC}EnvC with H-^{Loop1}FtsX, only about half of the H-^{Loop1}FtsX was retained by the beads. It was accompanied in the eluate by a small fraction (about 10%) of the total ^{CC}EnvC, indicating that the two domains weakly interact. The remaining H-^{Loop1}FtsX was found in the unbound fraction with the majority of ^{CC}EnvC. Since H-^{Loop1}FtsX bound efficiently to the beads in the presence of ^{FL}EnvC and ^{Lyt}EnvC, the addition of ^{CC}EnvC appears to adversely affect the accessibility of the H-tag on H-^{Loop1}FtsX. This may be the result of ^{CC}EnvC inducing some sort of conformational change in H-^{Loop1}FtsX, but further investigation is required to test this possibility.

To determine the physiological relevance of the EnvC-^{Loop1}FtsX interaction, we investigated the effect of deleting various portions of the FtsX loop domain on the recruitment of EnvC to the division site. To do so, we generated a construct expressing the *ftsEX* operon under control of P$_{lac}$ with the *ftsX* reading frame fused to the coding sequence for GFP. The expression construct thus produces untagged FtsE as well as FtsX-GFP. For convenience, we will refer to the fusion as FtsEX-GFP. In addition to the WT fusion, we also generated several variants deleted for various portions of the Loop1 domain of FtsX. When produced as the only source of FtsEX in strain DY18(*att*λTD80)(*att*HKDY156) [Δ*ftsEX* Δ*envC* (P$_{lac}$::*envC-mCherry*)

59

(P_{lac}::*ftsEX-gfp*)], the FtsEX-GFP fusion corrected the Δ*ftsEX* division phenotype, localized to

the division site, and was functional for the recruitment of EnvC-mCherry to the septal ring

(Figure 2.9A). All of the Loop1 deletion derivatives of FtsX-GFP we tested (Δ152-161,

Δ146-165, Δ137-176, and Δ109-213) localized to the division site (Figure 2.9B and Figure 2.10),

indicating that the Loop1 domain is not an important localization determinant for FtsX.

However, even the derivative with the smallest deletion (Δ152-161) failed to recruit EnvC to the

septum, and cells expressing these derivatives displayed an EnvC⁻ like division defect (Figure

2.9B and Figure 2.10). We conclude that the Loop1-EnvC interaction we detected in the

BACTH and *in vitro* assays is required for the recruitment of EnvC to the septal ring.

The ATPase activity of FtsE is likely required for amidase activation by EnvC

Weiss and co-workers recently showed that FtsE residues in and around the Walker A

(GxxGxGKS/T, where x is any residue) and Walker B ($\phi\phi\phi$D, where ϕ is a hydrophobic

residue) motifs predicted to be important for ATP hydrolysis are required for FtsEX to function

in cell division (20). Interestingly, however, these residues were not found to be needed for the

stability of FtsE or the recruitment of either FtsE or FtsX to the division site (20). Also, unlike

ftsEX null mutants, division proteins downstream of FtsEX in the localization hierarchy were

recruited to the septal ring in the presence of these predicted ATPase defective variants when

mutant cells were grown under non-permissive conditions (20). Thus, by all indications,

complete septal rings were forming in the filamentous cells producing the FtsE mutants; they

were just unable to promote cell constriction without ATP hydrolysis by FtsEX (20).
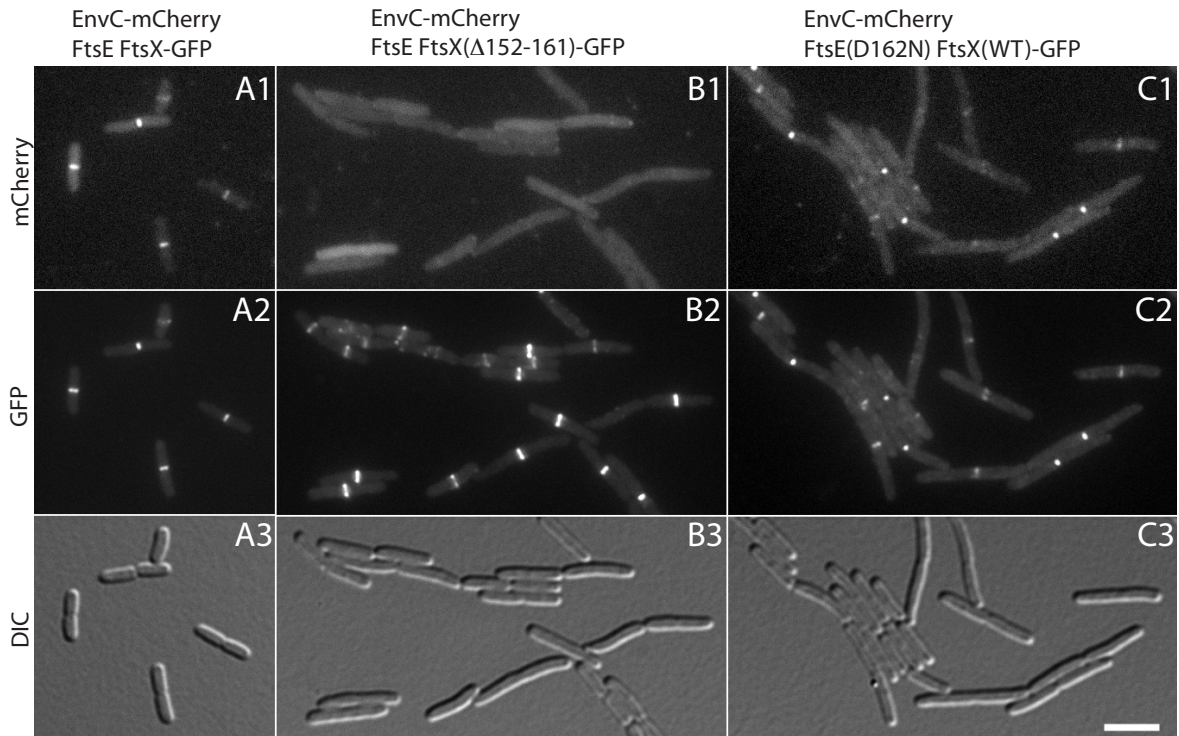
Figure 2.9. EnvC localization in cells producing FtsEX variants. Cells of DY18(*att*λTD80) [Δ*ftsEX* Δ*envC* (P_lac::*envC-mCherry*)] harboring the integrated expression constructs *att*HKDY156 (P_lac::*ftsEX-GFP*) (**A**), *att*HKDY161 (P_lac::*ftsEX^Δ152-161-GFP*) (**B**), or *att*HKDY167 [P_lac::*ftsE(D162N)X-GFP*] (**C**) were grown overnight at 30°C in LB (1% NaCl). They then were diluted 1:100 into M9 maltose supplemented with 500 μM IPTG. When cells reached an OD_600 of 0.42–0.54, they were visualized as described in the legend for Figure 2.6.
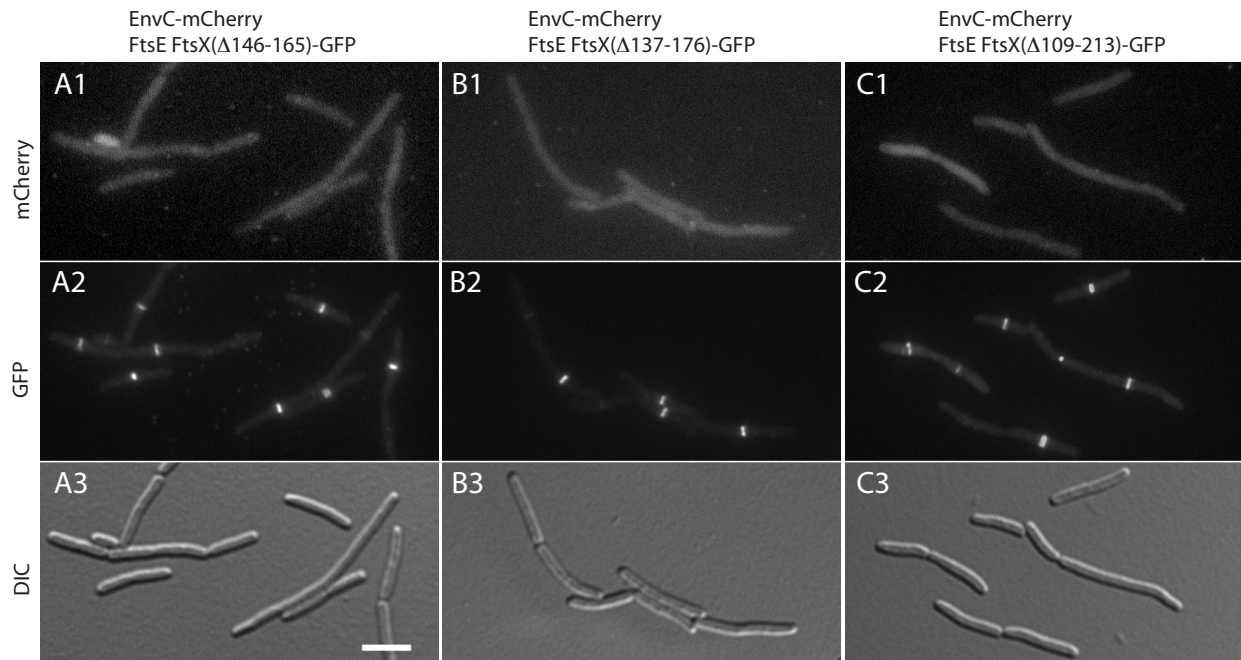
Figure 2.10. EnvC localization in cells producing Loop1FtsX deletions. Cells of DY18 (*attλ*TD80) [Δ*ftsEX* Δ*envC* (Plac::*envC-mCherry*)] harboring the integrated expression constructs (*att*HKDY162) [Plac::*ftsEX (Δ146-165)-GFP*] (**A**), (*att*HKDY163) [Plac::*ftsEX(Δ137-176)-GFP*] (**B**), or (*att*HKDY165) [Plac::*ftsEX (Δ109-213)-GFP*] (**C**) were grown and visualized as described in the legend for Figure 2.9.

Our results thus far indicate that FtsEX directly recruits EnvC to the septal ring. Given

the findings of Arends et al. (2009), we also wondered if the ATPase activity of FtsE might be

required to stimulate amidase activation by EnvC. We therefore generated *ftsE*(K41M), *ftsE*

(D162N), and *ftsE*(E163Q) derivatives of the P$_{lac}$::*ftsEX-gfp* construct described above. The

encoded FtsE variants (FtsE*) in these constructs are similar to those studied previously by

Arends et al. (2009), except that more conservative amino acid changes were made. The K41M

substitution in the Walker A motif of FtsE is predicted to greatly reduce affinity for ATP (34).

The Walker B residue, D162, is predicted to coordinate Mg^{2+} in the active site (34).

Substitutions at this residue in other NBDs abrogate ATP binding (34). An acidic residue, E163

in FtsE, typically follows the Walker B motif in ABC transporters. The role of this residue in the

ATPase catalytic mechanism is controversial (34). NBDs with Glu to Gln substitutions at this

position still bind ATP, but depending on the particular transporter, they may or may not retain

residual ATPase activity (34).

The ability of the FtsE* variants to promote cell separation was first assessed by

producing them from the P$_{lac}$::*ftsEX-gfp* construct in Δ*ftsEX* Δ*nlpD* cells. As expected, a

construct producing WT FtsE completely reversed the severe chaining phenotype of the FtsEX$^-$

NlpD$^-$ mutants (Figure 2.11, Table 2.1). Constructs producing the FtsE* variants, on the other

hand, all failed to restore normal cell separation (Figure 2.11, Table 2.1). However, the mutants

did not behave identically. While FtsE(D162N) appeared to be completely defective for cell

separation, the FtsE(K41M) and FtsE(E163Q) variants appeared to retain partial function (Table

2.1). Based on results from the related LolCDE system, FtsE(K41M) is likely to retain weak

affinity for ATP (35). This may allow enough ATPase activity to reduce the length of the chains
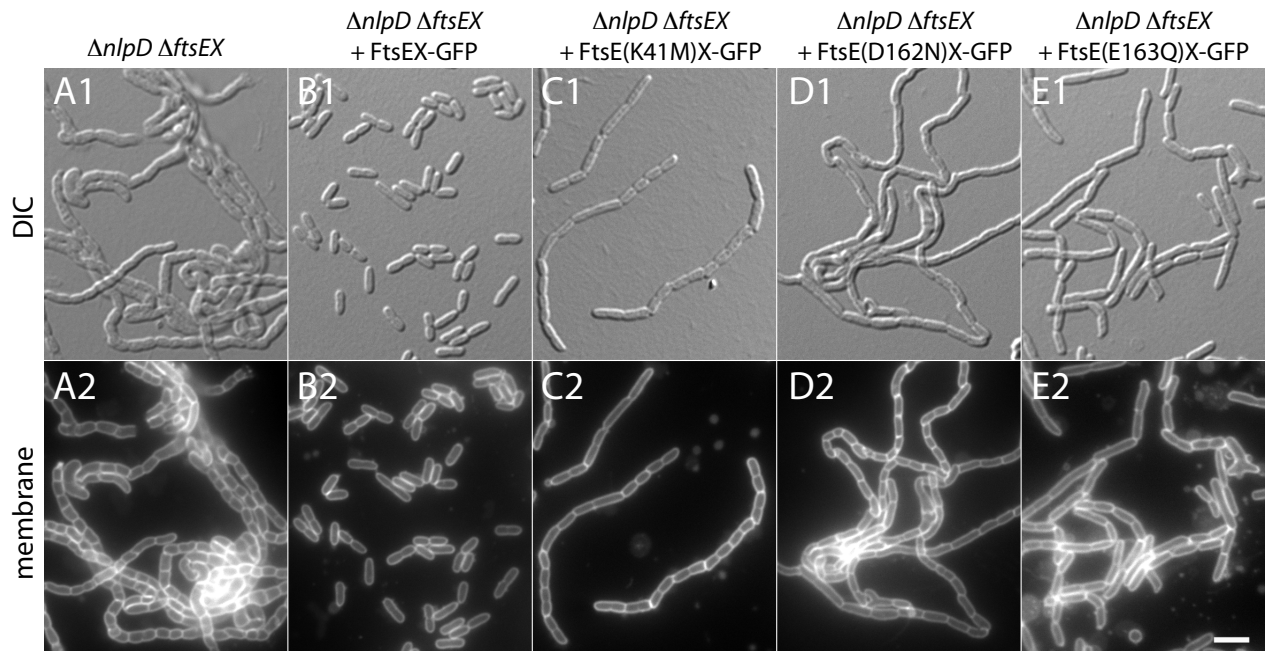
Figure 2.11. FtsE ATP-binding site lesions result in a cell-separation defect. Cells of KP7/ pTB63 (*ΔftsEX ΔnlpD*/*ftsQAZ*) without an integrated expression cassette (**A**) or harboring *att*HKDY156 (P$_{lac}$::*ftsEX-GFP*) (**B**), *att*HKDY166 [P$_{lac}$::*ftsE(K41M)X-GFP*] (**C**), *att*HKDY167 [P$_{lac}$::*ftsE(D162N)X-GFP*] (**D**), or *att*HKDY168 [P$_{lac}$::*ftsE(E163Q)X-GFP*] (**E**) were grown and visualized as described in the legend to Figure 2.4, except that the medium contained 500 µM IPTG.

Table 2.1. Cell separation phenotypes of FtsE* NlpD⁻ cells.

strain	genotype	#cells[a]	# cell units[b]	total L (μm)[c]	avg. L (μm)[c]	total septa	L/septum	septa/cell
KP7	Δ*ftsEX* Δ*nlpD*	4	225	388	97	218	1.8	55
KP7 (attHKDY156)	Δ*ftsEX* Δ*nlpD* (P$_{lac}$::*ftsEX-GFP*)	144	200	475	3.3	56	8.5	0.4
KP7 (attHKDY166)	Δ*ftsEX* Δ*nlpD* (P$_{lac}$::*ftsE(K41M)X-GFP*)	31	202	491	15.8	171	2.9	6
KP7 (attHKDY167)	Δ*ftsEX* Δ*nlpD* (P$_{lac}$::*ftsE(D162N)X-GFP*)	9	214	434	48.2	208	2.1	23
KP7 (attHKDY168)	Δ*ftsEX* Δ*nlpD* (P$_{lac}$::*ftsE(E163Q)X-GFP*)	74	200	618	8	127	4.9	2

[a]Cell chains were considered as a single cell regardless of the number of segments they contained.
[b]Indicates the number of cell compartments in chaining cells.
[c]Length measurements represent a minimum because many of the cell chains extended beyond the field of view.

observed in Δ*ftsEX* Δ*nlpD* cells. For FtsE(E163Q), its ability to shorten Δ*ftsEX* Δ*nlpD* chains

may either indicate that ATP-binding alone is sufficient for low-level cell separation activity, or

that the E/Q substitution in FtsEX does not completely abolish ATPase activity. Measurement of

the ATPase activity of FtsE and the FtsE* variants is required to distinguish between these

possibilities, but this has not been possible due to problems with FtsE solubility when it was

overproduced. Nevertheless, the (partial) loss-of-function phenotypes displayed by the FtsE*

variants clearly highlight a role for key ATP-binding site residues in FtsE for it to promote proper

cell separation. Importantly, FtsX-GFP remained capable of recruiting to septal rings in cells

producing the FtsE* variants and the efficiency with which EnvC-mCherry was recruited to the

FtsX-containing rings was largely unaffected by the FtsE lesions (Figure 2.9C, Figure 2.12, and

Table 2.2). Furthermore, based on the results of Arends et al. (2009) with similar mutants, we

assume that the FtsE* variants described here are also normally recruited to the septal ring.

Thus, FtsE*X-EnvC complexes are likely forming at the division site in cells expressing the

*ftsE** alleles but they fail to function or function poorly in the septal PG splitting process. We

therefore infer that the ATPase activity of the FtsEX complex plays an important role in

promoting amidase activation by EnvC at the septum.

Section 2.4: Discussion

    The role of the FtsEX ABC system in cytokinesis has long remained mysterious. In this

study, we have genetically and physically connected FtsEX with the process of septal PG

splitting. Our results indicate that the complex is directly responsible for the recruitment of the

amidase activator EnvC to the cytokinetic ring. Importantly, we also showed that variants of the
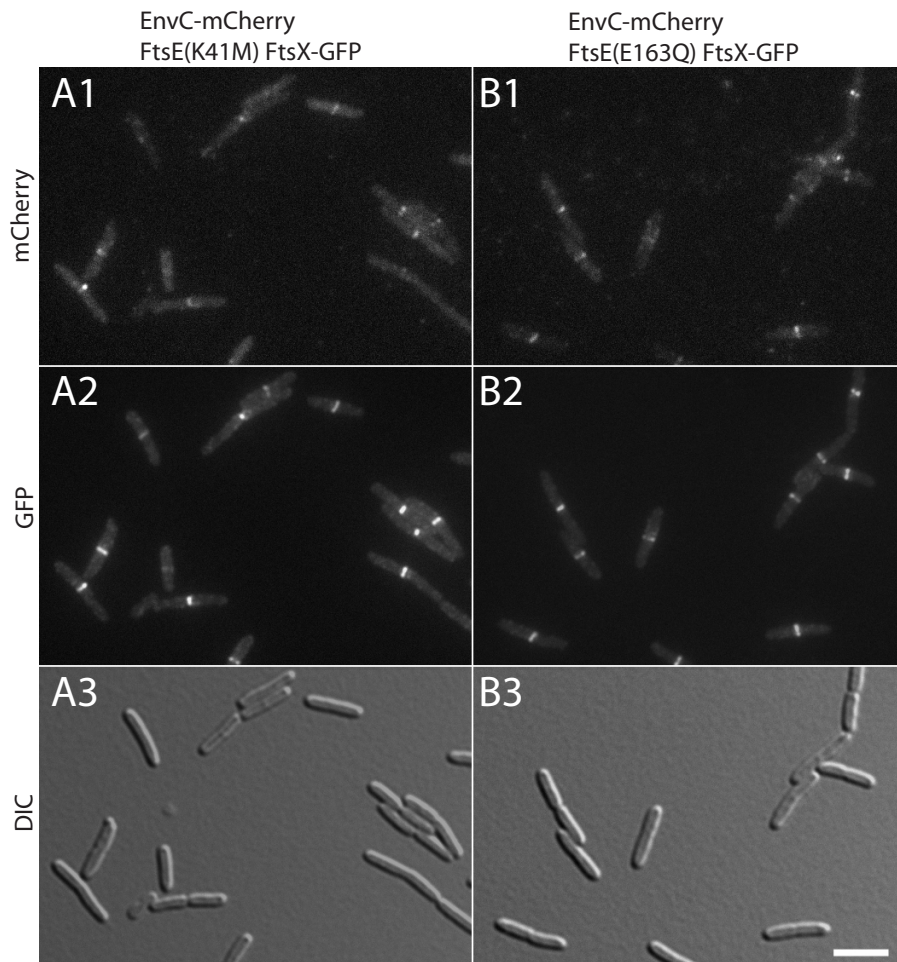
Figure 2.12. EnvC localization in cells producing FtsE* variants. Cells of DY18(*attλ*TD80) [Δ*ftsEX* Δ*envC* (P$_{lac}$::*envC-mCherry*)] harboring the integrated expression constructs (attHKDY166) [P$_{lac}$::ftsE(K41M)X-GFP] (**A**) or (attHKDY168) [P$_{lac}$::ftsE(E163Q)X-GFP] (**B**) were grown and visualized as described in the legend for Figure 2.9.

Table 2.2. Length and localization measurements of FtsE* cells producing FtsX-GFP and EnvC-mCherry.

Strain	genotype	#cells	total L (μm)	avg. L (μm)	# of FtsX-rings	# of EnvC-rings	% co-localization of FtsX and EnvC*	L/FtsX-ring (μm)	L/EnvC-ring (μm)	L/septum (μm)
DY18 (attHKDY156) (attλTD80)	ΔftsEX ΔenvC (P$_{lac}$::ftsEX-GFP) (P$_{lac}$::envC-mCherry)	125	457	3.7	115	93	81	4.0	4.9	9.3
DY18 (attHKDY166) (attλTD80)	ΔftsEX ΔenvC (P$_{lac}$::ftsE(K41M)X-GFP) (P$_{lac}$::envC-mCherry)	125	692	5.5	124	95	77	5.5	9.0	13.6
DY18 (attHKDY167) (attλTD80)	ΔftsEX ΔenvC (P$_{lac}$::ftsE(D162N)X-GFP) (P$_{lac}$::envC-mCherry)	125	1096	8.8	131	109	83	8.4	13.2	12.2
DY18 (attHKDY168) (attλTD80)	ΔftsEX ΔenvC (P$_{lac}$::ftsE(E163Q)X-GFP) (P$_{lac}$::envC-mCherry)	125	655	5.2	124	91	73	7.2	9.0	12.1

*Reflects the number of FtsX-GFP rings clearly associated with a ring of EnvC-mCherry.

FtsEX complex predicted to have inactive ATPase subunits still recruited EnvC to the septum but failed to induce septal PG splitting. Thus, in addition to connecting EnvC to the septal ring, FtsEX appears to use its ATPase activity to promote amidase activation. An attractive possibility is that it does so using ATPase-induced conformational changes similar to those observed in other ABC systems (12) to allosterically regulate EnvC activity in the periplasm (Figure 2.13).

Consistent with this model, sequence analysis groups FtsEX with a sub-class of ABC systems comprised mainly of substrate binding protein (SBP)-dependent importers like the maltose transporter (MalFGK$_2$) (34). The structure of MalFGK$_2$ in complex with maltose binding protein (MalE) indicates that ATP-driven conformational changes in the transporter can alter the conformation of periplasmic MalE (36). In this case, MalE is converted from its closed, maltose-bound conformation to an open conformation that releases maltose into the outward-facing cavity of the transporter for subsequent import (36). We therefore propose that EnvC may be an SBP analog for FtsEX and envision that the conformation of EnvC is similarly modulated by the ABC system so that it interconverts between an "on" and "off" state during an ATPase cycle (Figure 2.13). Such a model is appealing for several reasons. Most significantly, it would provide a means for converting septal PG hydrolysis into a discrete process with a fixed number of PG bonds being broken per ATP hydrolyzed. This would afford the septal ring exquisite control over PG hydrolysis, which seems highly desirable given the inherent risks involved in promoting localized PG degradation. Additionally, since FtsE interacts with FtsZ in the cytoplasm, the ATPase activity of FtsE could be directly coupled to Z-ring dynamics. Thus, the FtsEX complex could serve as a molecular governor to properly coordinate the rate of septal PG hydrolysis with the contraction of the Z-ring. Finally, in addition to connecting the Z-ring with
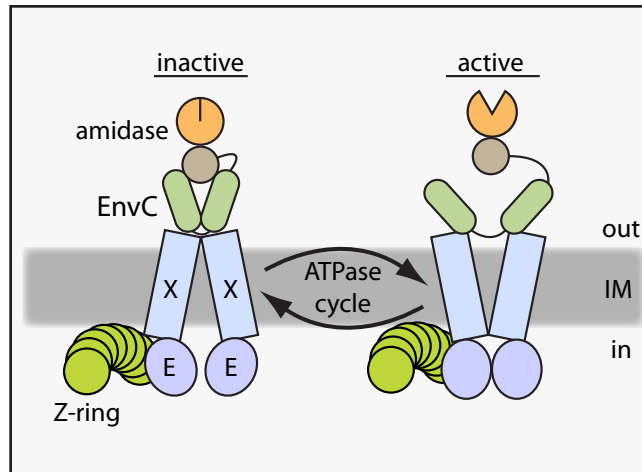
Figure 2.13. Model for FtsEX function in regulating PG hydrolase activity at the division site. Shown is a schematic diagram of a putative FtsEX-EnvC-amidase complex at the Z-ring. We propose that conformational changes in FtsEX induced by FtsE-mediated ATP hydrolysis are transmitted to EnvC to control its ability to activate the amidases so that they can cleave the septal PG (not drawn). The model is not meant to reflect actual interaction stoichiometries, because they have yet to be determined. In addition, it is not yet clear if the amidases remain in complex with EnvC as drawn or if this interaction is also regulated. See text for details.

septal PG hydrolysis, interactions of FtsX with other transmembrane components of the divisome may help couple the activity of the integral membrane PG synthases with the cell separation amidases. For example, the FtsEX complex may only promote EnvC-activated amidase activity when it is engaged with an active PG synthetic complex.

Control of EnvC activity by FtsEX is likely mediated in part by the observed interaction between the CC domain of EnvC and [Loop1]FtsX. Consistent with this possibility, the CC domain of EnvC was previously shown to be important for EnvC regulation (24). An EnvC truncation lacking the CC domain ([Lyt]EnvC) failed to be recruited to the division site and inappropriately activated AmiA and AmiB to induce cell lysis (24). Since cell lysis is not triggered when [FL]EnvC is displaced from the septum by [CC]EnvC overproduction (24) or by the deletion of *ftsEX*, proper regulation of amidase activation appears to entail more than just controlling EnvC localization. Because [FL]EnvC activates the amidases just as well as [Lyt]EnvC *in vitro* (24), we suspect that there is either something about the physiochemical environment of the periplasm that promotes the direct inhibition of [FL]EnvC activity by the CC domain itself or that inhibition is mediated by an additional factor that associates with the CC domain. According to our model for EnvC regulation by FtsEX, it is this auto- or trans-inhibition of EnvC that is cycled on and off in response to the ATPase activity of FtsEX (Figure 2.13).

While we favor a model in which FtsEX serves as a transmembrane allosteric regulator of EnvC, scenarios in which FtsEX transports a molecule needed for EnvC activity are difficult to exclude. Arguing against a transport function is the fact that FtsEX is most similar to the LolCDE ABC system. Rather than catalyzing the transport of a substrate across a membrane, LolCDE facilitates the transfer of lipoproteins from the outer leaflet of the inner membrane to the

periplasmic LolA carrier protein for their ultimate insertion into the outer membrane (37). The

individual TMD components of both FtsEX and LolCDE have only four transmembrane helices,

unlike most ABC-transporters, which typically have at least six (20, 34, 38). Moreover, the

membrane spanning helices of FtsX do not contain any charged amino acids as might be

expected for a factor that transports an electrolyte (20). Based on these observations, Weiss and

colleagues have also proposed that FtsEX may not be a transporter (20). Rather, they

hypothesized that, as we propose here, FtsE uses ATP hydrolysis to drive a periplasmic activity

via conformational changes in FtsX (20). Reconstitution of EnvC regulation by FtsEX is

required to definitively demonstrate an allosteric control mechanism. So far, our attempts at

reconstitution have been unsuccessful. Addition of purified [Loop1]FtsX or full-length FtsX to

mixtures of EnvC and AmiB did not affect amidase activation using our standard reaction

conditions (24). This suggests that the full FtsEX complex may be needed to observe regulation

in vitro. Unfortunately, efforts to purify the complete FtsEX complex have been hampered by

the insolubility of FtsE when it is overproduced. This hurdle must be overcome before

additional attempts at reconstitution can be pursued.

A role for FtsEX in the process of septal PG splitting appears to be conserved. In an

accompanying report (28), Sham et al. directly connect the essential cell separation factor PcsB

(39) with FtsEX in *S. pneumoniae*. While their sequences are largely unrelated, the domain

structures of PcsB and EnvC are strikingly similar. Like EnvC, PcsB has an N-terminal region

predicted to form coiled-coils and a C-terminal PG hydrolase-like CHAP domain (39). However,

it is currently not known whether PcsB directly degrades PG or if, analogous to EnvC, it is an

activator of other PG hydrolases. Nevertheless, the results of Sham et al. (2011) (28) indicate

that PcsB activity is likely governed by FtsEX to properly control the process of septal PG splitting in *S. pneumoniae*. Interestingly, FtsEX does not appear to be involved in cell division in *Bacillus subtilis* (40). We suspect this has to do with the different septal geometries of these organisms. Gram-negative bacteria like *E. coli* and ovococci like *S. pneumoniae* appear to couple septal PG splitting with the invagination of their cytoplasmic membrane to give their pre-divisional cells a constricted appearance (1, 41). This mode of division likely requires regulators of PG hydrolysis like FtsEX to be associated with the septal ring. *B. subtilis* and many other Gram-positive bacteria, on the other hand, first construct a flat septum, the splitting of which appears to be uncoupled from membrane constriction and fission (42). Septal PG splitting in these cells is therefore likely to have regulatory requirements that differ from those of constricting cells. It is not clear what the function of FtsEX is in cells with a flat septal morphology, but it may involve the regulation of PG hydrolysis needed for other aspects of cell wall growth and remodeling.

In conclusion, we have identified a role for the FtsEX ABC system in the regulation of septal PG hydrolysis by the amidases AmiA and AmiB and the LytM factor EnvC. A second pathway for septal PG splitting involving AmiC and the LytM factor NlpD is also operative in *E. coli* (24). How this system is regulated is currently not known. However, since NlpD is an outer membrane lipoprotein (43) rather than a periplasmic protein like EnvC, its activity is likely to be modulated by a distinct mechanism. To our knowledge, this report describes the first example of an ABC system being implicated in the transmembrane regulation of enzymatic activity. Given the diversity and ubiquity of ABC systems in nature (34), it is likely that the ATP-driven

conformational changes in these membrane complexes have been adapted to regulate a variety of biological processes.

Section 2.5: Material and methods

Media, bacterial strains, and plasmids

Cells were grown in LB [1% tryptone, 0.5% yeast extract, (0.5%-1.5% NaCl as indicated)] or minimal M9 medium (44) supplemented with 0.2% casamino acids and 0.2% sugar (glucose, maltose, or arabinose as indicated). Unless otherwise indicated, antibiotics were used at 5, 10, 15, 20, or 50 µg/ml for tetracycline (Tet), chloramphenicol (Cam), ampicillin (Amp), kanamycin (Kan), or spectinomycin (Spec), respectively.

The bacterial strains used in this study are listed in Table 2.3. All strains used in the reported experiments are derivatives of MG1655 (45). Plasmids used in this study are listed in Table 2.4. Vectors with R6K origins are all derivatives of the CRIM plasmids developed by Wanner and co-workers (46). They were either maintained in the cloning strain DH5α(λ*pir*) where they replicate as plasmids, or they were integrated into phage attachment sites (HK022 or λ) using the helper vectors pTB102 (47) or pInt-ts (46), respectively, as described previously (46). Single copy integrants were identified using diagnostic PCR (46). Integrated vectors were transferred between strains by P1-mediated transduction. In all cases, PCR was performed using KOD polymerase (Novagen) according to the instructions. Unless otherwise indicated, MG1655 chromosomal DNA was used as a template. Restriction sites for use in plasmid constructions are italicized and underlined in the primer sequences given below. Plasmid DNA and PCR

fragments were purified using the Qiaprep spin miniprep kit (Qiagen) or the Qiaquick PCR

purification kit (Qiagen), respectively.

Synthetic lethal screen

The screen for mutants with a Slb phenotype was performed as previously described (27).

Briefly, TU122/pTU110 [*ΔlacIZYA ΔponB*/P$_{lac}$::*ponB lacZ*] was mutagenized with the EzTn-

Kan2 transposome (Epicentre) as previously described (26). Mutants were selected for Kan

resistance at room temperature, yielding a library of 75,000 independent transposon insertions.

This mutant library was plated on LB (0.5% NaCl) agar supplemented with 50 µM IPTG and X-

gal (40 µg/ml) at 30°C and room temperature to identify mutants with a Slb phenotype. In

addition to the transposon insertions in *ponA* and *lpoA* described previously (27), we also

isolated mutants with insertions in *envC* (between codon 74 and 75) and *ftsX* (within codon 59).

Fluorescence microscopy and protein methods

Fluorescence microscopy was performed as described previously (25). See figure

legends for specific growth conditions employed for each experiment. Cell fixation and

membrane staining was performed as described previously (25). The BACTH assay and Ni-

NTA "pull-up" assays are described in the legend to Figure 2.8.

Protein Purification, pull-up assays, and two-hybrid analysis

[FL]EnvC and [Lyt]EnvC were purified as described previously (24). [CC]EnvC was

overexpressed and purified with a 6xHis-SUMO (H-SUMO) tag fused to its N-terminus. H-

SUMO-^{CC}EnvC was purified from BL21(λDE3)/pDY151 and a 10xHis-tagged version of ^{Loop1}FtsX [H-^{Loop1}FtsX] was purified from BL21(λDE3)/pDY138. Overnight cultures were grown at 37°C in LB supplemented with ampicillin (50 µg/ml) and glucose (0.2%). The cultures were diluted 1:100 into 0.1 L of LB supplemented with ampicillin (50 µg/ml) and glucose (0.04%), and cells were grown at 30°C to an OD_{600} of 0.81 and 0.86 respectively. IPTG was added to 1 mM and the cultures were grown for an additional 3 hrs at 30°C. Cells were harvested by centrifugation and the cell pellets were resuspended in 3 ml of buffer A (50 mM Tris-HCl pH 8.0, 300 mM NaCl, 10% glycerol) with 20 mM imidazole and stored at -80°C. Cells were thawed, disrupted by sonication, and cell debris was pelleted by centrifugation at 20,000 x g for 20 min at 4°C. The supernatants were passed through 0.2 µM syringe filters and loaded onto ProPur IMAC mini spin columns (Nunc) equilibrated in buffer A with 20 mM imidazole. Columns were washed 3x using buffer A with 50 mM imidazole and eluted using buffer A with 300 mM imidazole. For H-SUMO-^{CC}EnvC, the H-SUMO tag was cleaved with 6xHis-tagged SUMO protease (H-SP) as previously described (24). The cleavage reaction was passed through Ni-NTA resin (ProPur IMAC midi spin column) to remove free H-SUMO and H-SP, yielding a pure preparation of untagged ^{CC}EnvC. Amicon Centrifugal Filter Units (MWCO 10 kDa) were used to concentrate both protein preparations and exchange the buffer to buffer A without imidazole. Protein preparations were stored at -80°C in buffer A. The BACTH assay and Ni-NTA "pull-up" assays are described in the legend to Figure 2.8.

EnvC antisera and affinity purification of anti-EnvC antibodies

Polyclonal rabbit antisera was raised agains purified ^{FL}EnvC by Covance according to their standard protocol. The resulting anti-EnvC antibodies were affinity purified using ^{FL}EnvC coupled to AminoLink resin (Pierce) as described previously for SlmA antibody purification (48).

Cell fractionation and immunoblotting

Whole-cell extracts for Figure 2.5 were prepared as described previously (49). The protein concentration in each extract was determined using the non-interfering protein assay (Genotech) according to the manufacturers instructions. Protein concentrations were normalized between extracts and 20, 10, or 5 μg of total protein from each extract was separated on a 12% SDS-PAGE gel. Proteins were transferred to a PVDF membrane (Whatman) and the membrane was blocked with Rapid-Block (Genotech) for 5 minutes. The membrane was incubated with anti-EnvC antibodies (1:5000 in Rapid-Block) for 1 hour at room temperature. The membrane was washed three times with 25 ml TBST (10 mM Tris-HCl pH7.5, 100 mM NaCl, 0.1% Tween-20) for 10 minutes. Following the wash, the membrane was incubated with goat anti-rabbit antibodies conjugated with HRP (Rockland) (1:20,000 in Rapid-Block) for 1 hour at room temperature. Finally, the membrane was washed an additional four times as above and developed using the Pierce Super-Signal West-Pico reagents. Chemiluminescence was detected using a BioRad Chemidoc system. Cell fractionations and immunoblotting for Figure 2.5B were performed as described previously (50), except that 500 mM NaCl was added to the spheroplasts after they were formed and EnvC was detected as described above. NaCl addition was required

77

to promote the complete release of EnvC to the periplasmic fraction in spheroplasts from FtsEX⁻

cells.

Recombineering

The Δ*ftsEX*::Kan^R allele was constructed by replacing the region between the 2nd codon

of *ftsE* and the 7th codon from the stop codon of *ftsX* with a Kan^R cassette as described

previously (54, 55). The Kan^R cassette was amplified from pKD13 (56) using the primers 5'-

ACTTTATAGAGGCACTTTTTGCCCGAGAGGATTAACAATGATTCCGGGGATCCGTCGA

CC-3' and 5'-

AGAGTATAACACGCTTTTATTATTCAGGCGTAAAGTGGCGTGTAGGCTGGAGCTGCTT

CG-3'. The resulting product was electroporated into strain TB10 as described previously (26),

and the recombinants were selected at 30˚C on an LB plate containing 1% NaCl and 20 μg/ml

kanamycin to generate the chromosomal deletion.

To generate a marker for the Z-ring, a *zapA-gfp* fusion was created at its native

chromosomal locus by λ recombineering (55). *gfp-mut2* (57) coding sequence and a linked *cat*

cassette flanked by *zapA* 3' end sequence and sequence downstream of *zapA* was amplified using

pTB24 (58) as a template and the primers 5'-

ACAAGGTCGCATCACCGAAAAAACTAACCAAAACTTTGAAGATCCCCCCGCTGAATT

CATG-3' and 5'-

TTGTCTTCACGGTTACTCTACCACAGTAAACCGAAAAGTGGTGTAGGCTGGAGCTGC

TTCG-3'. The resulting fragment was used for recombineering in strain TB10 as described

previously (26). The *zapA-gfp* fusion linked to the *cat* cassette was transferred between strains by P1-transduction.

Plasmid construction

pTU188

To construct pTU188 [*attλ cat* P~ara~::*ftsE-ftsX*], a fragment containing *ftsE* and *ftsX* was amplified with the primers 5'-GTCA*TCTAGA*TTTGCCCGAGAGGATTAACAATG-3' and 5'-GTCA*AAGCTT*TTATTATTCAGGCGTAAAGTGGCG-3', digested with XbaI and HindIII, and inserted into the corresponding XbaI-HindIII sites of pTB285 (27).

pTB332-333

For pTB332 [*aph Plac*::*envC(277-419)-T25*], *envC(278-419)* was amplified with the primers 5'-GTAC*AAGCTT*GACCGAAAGCGAAAAATCGCTGATG-3' and 5'-GTCA*GGATCC*TCTCTTCCCAACCACGGCTGTGG-3'. The resulting fragment was digested and ligated with HindIII and BamHI digested pKNT25 (17). pTB333 [*aph* P~lac~:*:envC(34-419)-T25*] was constructed in the same manner except that *envC(34-419)* was amplified with the primers 5'-GTAC*AAGCTT*GGATGAGCGTGACCAACTCAAATCTATTC-3' and 5'-GTCA*GGATCC*TCTCTTCCCAACCACGGCTGTGG-3'.

To construct pTD80 [*attλ cat lacI^q* P~lac~::*envC-mCherry*], the P~lac~::*envC-mCherry* containing

EcoRI-HindIII fragment of pTB316 [*att*HK022 *bla lacI^q* P~lac~::*envC-mCherry*] (25) was used to

replace the corresponding P~ara~::*envC* fragment of pTD25 [*attλ cat* P~ara~::*envC*] (25).

pMT1

pMT1 [*cat* P~ara~::*ftsEX*] was constructed in multiple steps. First, pTU170 [*att*HK022 *bla*

P~syn135~::*gfp-zapA*] was made by ligating the *EcoR*I-*Sal*I digested fragment from pEZ4 (58) into

the *EcoR*I-*Sal*I digested backbone of pTB263 [*att*HK022 *bla* P~lac~::^ss^*dsbA-sfgfp*] (25). Then

pTU176 [*att*HK022 *bla* P~syn135~::^ss^*dsbA-sfgfp*] was made by ligating the ^ss^*dsbA-sfgfp*-containing

*Xba*I-*Hind*III fragment from pTB263 (25) with *Xba*I-*Hind*III digested pTU170 to generate

pTU176. The ^ss^*dsbA-sfgfp*-containing *Xba*I-*Hind*III fragment from pTU176 was ligated with

*Xba*I-*Hind*III digested pBAD18-cat (59) to generate pTU214 [*cat* P~ara~::^ss^*dsbA-sfgfp*]. Using

pTU188 [*attλ cat* P~ara~::*ftsEX*] as a template, *RBSwk2-ftsEX* was amplified with primers 5'-

GTCA*TCTAGA*AAAAAGGAAAAATGATTCGCTTTGAACATGTCAGCAAGG-3' and 5'-

GTCA*AAGCTT*TTATTATTCAGGCGTAAAGTGGCG-3'. The resulting fragment was digested

with *Hind*III and *Xba*I and ligated with pTU214 digested with the same enzymes to generate

pMT1.

pDY133

pDY133 [*bla* P~lac~::^loop1^*ftsX-T18*] was constructed in two steps. First, the *amiA* gene was

amplified using the primers 5'-

GTCA*TCTAGA*AGGATCCGCCAAAGACGAACTTTTAAAAACCAGC-3' and 5'-

GTCA*GAGCTC*GGCTCGAGTCGCTTTTTCGAATGTGCTTTCTGGTTG-3'. The resulting

fragment was digested with *Xba*I and *Sac*I and ligated with pCH363 [*bla* P$_{lac}$::*lacZ-T18*] (58)

digested with the same enzymes to generate pTU236 [*bla* P$_{lac}$::*amiA-T18*]. Second, ^{loop1}*ftsX* was

amplified from pMT1 [*cat* P$_{ara}$::*RBSwk2-ftsEX*] using the primers 5'-

GTCATT*GGATCC*GTGTACAAAAACGTTAACCAGGCGGCG-3' and 5'-

AGTTAAGCTTATTA*CTCGAG*GCGCCCGACCAGCCCGGTCAACGCC-3'. The resulting

fragment was digested with *BamH*I and *Xho*I and ligated with pTU236 [*bla* P$_{lac}$::*amiA-T18*]

digested with the same enzymes to generate pDY133.

pDY138

pDY138 [*bla* P$_{T7}$::*His10-ftsXloop1*] was constructed in several steps. pDY42 [*bla* P$_{T7}$::*His10-*

mcs] was made by using the synthetic oligonucleotides 5'-

CTAGAAATAATTTTGTTTAACTTTAAGAAGGAGATATACCATGCGTGGTTCTCACCACC

ATCACCACCATCACCACCATCATGCTAGCG-3'and 5'-

GATCCGCTAGCATGATGGTGGTGATGGTGGTGATGGTGGTGAGAACCACGCATGGTAT

ATCTCCTTCTTAAAGTTAAACAAAATTATTT-3'. These oligonucleotides were annealed,

resulting in the formation of dsDNA with overhangs complementary to *BamH*I and *Xho*I

restriction sites. pTD68 [*bla* P$_{lac}$::^{ss}*dsbA-linker-^{sf}gfp*] (60) was digested with *BamH*I and *Xho*I,

and the resulting plasmid backbone was ligated with the complementary synthetic dsDNA.

Finally, the ^{loop1}*ftsX* was amplified from pMT1 [*cat* P$_{ara}$::*ftsEX*] using the primers 5'-

GTCATT*GGATCC*GTGTACAAAAACGTTAACCAGGCGGCG-3' and 5'-

AGTTAAGCTTATTA*CTCGAG*GCGCCCGACCAGCCCGGTCAACGCC-3'. The resulting

fragment was digested with *BamH*I and *Xho*I and ligated with pDY42 digested with the same

enzymes to generate pDY138.

pDY151

pDY151 [*bla* P~T7~::*H-SUMO-*^cc^*envC*] was constructed in several steps. First, pTU138 [*att*HK022

bla P~lac~::^ss^*dsbA-envC*(35-419)-^sf^*gfp*] was made by amplifying ^fl^*envC* using the primers 5'-

GTCA*GGATCC*GGTGATGAGCGTGACCAACTCAAATCTATTC-3' and 5'-

GTCA*CTCGAG*TCTTCCCAACCACGGCTGTGG-3'. The resulting fragment was digested

with *BamH*I and *Xho*I and ligated with pTB282 [*att*HK022 *bla* P~lac~::^ss^*dsbA-*^sf^*gfp*] (48) digested

with the same enzymes. Using pTB138 as a template, ^cc^*envC* was amplified with the primers 5'-

GTCA*GGATCC*GGTGATGAGCGTGACCAACTCAAATCTATTC-3' and 5'-

GTCA*CTCGAG*CGGTTTGTAGGTGGTGCCTTTGC-3'. The resulting fragment was digested

with *BamH*I and *Xho*I and ligated with pTB282 (48) digested with the same enzymes to generate

pTU150 [*att*HK022 *bla* P~lac~::^ss^*dsbA-*^cc^*envC-*^sf^*gfp*]. Finally, the ^cc^*envC*-containing *BamH*I-*Xho*I

fragment from pTU150 was ligated with *BamH*I-*Xho*I digested pTD68 [*bla* P~T7~::*H-SUMO-mcs*]

(24) to generate pDY151.

pDY156

pDY156 [*att*HK022 *bla* P~lac~::*ftsEX-sfgfp*] was constructed as follows. *ftsEX* was amplified from

MG1655 with the primers 5'-GTCA*TCTAGA*TTTGCCCGAGAGGATTAACAATG-3' and 5'-

GTCA*CTCGAG*TTCAGGCGTAAAGTGGCGTAAATG-3'. The resulting fragment was

digested with *Xba*I and *Xho*I and ligated with pTB311 [*att*HK022 *bla* P_{lac}::^{ss}*dsbA-amiB(23-445)-*^{sf}*gfp*] (24) digested with the same enzymes.

<u>*pDY158-160*</u>

pDY158 [*attλ cat* P_{ara}::*ftsE(K41M)X*] was made by site-directed mutagenesis of pTU188 [*attλ cat* P_{ara}::*ftsEX*] using the QuickChange method (Stratagene) and the primer 5'-GATCAGCTTCAGGAGGGTACTCATCCCTGCGCCGGAATGACCGGT-3'.

pDY159 [*attλ cat* P_{ara}::*ftsE(D162N)X*] was constructed by site-directed mutagenesis of pTU188 [*attλ cat* P_{ara}::*ftsEX*] using the QuickChange method (Stratagene) and the primer 5'-GTCCAGGTTACCAGTCGGTTCGTTCGCCAGCAGTACCGCGGGCTT-3'.

pDY160 [*attλ cat* P_{ara}::*ftsE(E163Q)X*] was constructed by site-directed mutagenesis of pTU188 [*attλ cat* P_{ara}::*ftsEX*] using the QuickChange method (Stratagene) and the primer 5'-GTCGTCCAGGTTACCAGTCGGTTGGTCCGCCAGCAGTACCGCGGG-3'.

<u>*pDY161-pDY165*</u>

pDY161 [*att*HK022 *bla* P_{lac}::*ftsEX(152-161)-sfgfp*] was constructed as follows. To make the 10aa *ftsX* internal deletion *ftsEX(152-161)*, two overlap extension PCR fragments were amplified with the primers 5'-GTCA*TCTAGA*TTTGCCCGAGAGGATTAACAATG-3' and 5'-GTTTTCTTCCAGCATATCCAGCTCACCCAGTGCGTCTTCACG-3' as well as 5'-CGTGAAGACGCACTGGGTGAGCTGGATATGCTGGAAGAAAAC-3' and

5'GTCA*CTCGAG*TTCAGGCGTAAAGTGGCGTAAATG-3' using pDY156 [*att*HK022 *bla*

P~lac~::*ftsEX-sfgfp*] as the DNA template. The resulting PCR fragments were purified and used

together as the final DNA template to amplify the *ftsEX(152-161)* fragment using the primers 5'-

GTCA*TCTAGA*TTTGCCCGAGAGGATTAACAATG-3' and

5'GTCA*CTCGAG*TTCAGGCGTAAAGTGGCGTAAATG-3'. The resulting fragment was

digested with *Xba*I and *Xho*I and ligated with pTB311 [*att*HK022 *bla* P~lac~::^ss^*dsbA-amiB(23-445)-*

sfgfp] (24) digested with the same enzymes.

<u>pDY162</u>

pDY162 [*att*HK022 *bla* P~lac~::*ftsEX(146-165)-sfgfp*] was constructed as follows. To make the

20aa *ftsX* internal deletion *ftsEX(146-165)*, two overlap extension PCR fragments were amplified

with the primers 5'-GTCA*TCTAGA*TTTGCCCGAGAGGATTAACAATG-3' and 5'-

TGCCGGAAGCGGGTTTTCTTCACGAGAAAGATAGTTCACTTT-3' as well as 5'-

AAAGTGAACTATCTTTCTCGTGAAGAAAACCCGCTTCCGGCA-3' and

5'GTCA*CTCGAG*TTCAGGCGTAAAGTGGCGTAAATG-3' using pDY156 [*att*HK022 *bla*

P~lac~::*ftsEX-sfgfp*] as the DNA template. The resulting PCR fragments were purified and used

together as the final DNA template to amplify the *ftsEX(146-165)* fragment using the primers 5'-

GTCA*TCTAGA*TTTGCCCGAGAGGATTAACAATG-3' and

5'GTCA*CTCGAG*TTCAGGCGTAAAGTGGCGTAAATG-3'. The resulting fragment was

digested with *Xba*I and *Xho*I and ligated with pTB311 [*att*HK022 *bla* P~lac~::^ss^*dsbA-amiB(23-445)-*

sfgfp] (24) digested with the same enzymes.

pDY163 [*att*HK022 *bla* P~lac~::*ftsEX(137-176)-sfgfp*] was constructed as follows. To make the 40aa *ftsX* internal deletion *ftsEX(137-176),* two overlap extension PCR fragments were amplified with the primers 5'-GTCA*TCTAGA*TTTGCCCGAGAGGATTAACAATG-3' and 5'-CTGGAAATCGAGTTTCGGGATGCCTTGCTCGGCCTGCAACTG-3' as well as 5'-CAGTTGCAGGCCGAGCAAGGCATCCCGAAACTCGATTTCCAG-3' and 5'GTCA*CTCGAG*TTCAGGCGTAAAGTGGCGTAAATG-3' using pDY156 [*att*HK022 *bla* P~lac~::*ftsEX-sfgfp*] as the DNA template. The resulting PCR fragments were purified and used together as the final DNA template to amplify the *ftsEX(137-176)* fragment using the primers 5'-GTCA*TCTAGA*TTTGCCCGAGAGGATTAACAATG-3' and 5'GTCA*CTCGAG*TTCAGGCGTAAAGTGGCGTAAATG-3'. The resulting fragment was digested with *Xba*I and *Xho*I and ligated with pTB311 [*att*HK022 *bla* P~lac~::^ss^*dsbA-amiB(23-445)-sfgfp*] (24) digested with the same enzymes.

pDY164 [*att*HK022 *bla* P~lac~::*ftsEX(109-188)-sfgfp*] was constructed as follows. To make the 80aa *ftsX* internal deletion *ftsEX(109-188),* two overlap extension PCR fragments were amplified with the primers 5'-GTCA*TCTAGA*TTTGCCCGAGAGGATTAACAATG-3' and 5'-GATACGATCACGCAGCGTATTTGACGGATAATACTGCGTCGC-3' as well as 5'-GCGACGCAGTATTATCCGTCAAATACGCTGCGTGATCGTATC-3' and 5'GTCA*CTCGAG*TTCAGGCGTAAAGTGGCGTAAATG-3' using pDY156 [*att*HK022 *bla* P~lac~::*ftsEX-sfgfp*] as the DNA template. The resulting PCR fragments were purified and used

together as the final DNA template to amplify the *ftsEX(109-188)* fragment using the primers 5'-GTCA*TCTAGA*TTTGCCCGAGAGGATTAACAATG-3' and 5'GTCA*CTCGAG*TTCAGGCGTAAAGTGGCGTAAATG-3'. The resulting fragment was digested with *Xba*I and *Xho*I and ligated with pTB311 [*att*HK022 *bla* P$_{lac}$::^{ss}*dsbA-amiB(23-445)-sfgfp*] (24) digested with the same enzymes.

pDY165

pDY165 [*att*HK022 *bla* P$_{lac}$::*ftsEX(109-213)-sfgfp*] was constructed as follows. To make the 105aa *ftsX* internal deletion *ftsEX(109-213)*, two overlap extension PCR fragments were amplified with the primers 5'-GTCA*TCTAGA*TTTGCCCGAGAGGATTAACAATG-3' and 5'-CAGCCCGGTCAACGCCGCCAGTGACGGATAATACTGCGTCGC-3' as well as 5'-GCGACGCAGTATTATCCGTCACTGGCGGCGTTGACCGGGCTG-3' and 5'GTCA*CTCGAG*TTCAGGCGTAAAGTGGCGTAAATG-3' using pDY156 [*att*HK022 *bla* P$_{lac}$::*ftsEX-sfgfp*] as the DNA template. The resulting PCR fragments were purified and used together as the final DNA template to amplify the *ftsEX(109-213)* fragment using the primers 5'-GTCA*TCTAGA*TTTGCCCGAGAGGATTAACAATG-3' and 5'GTCA*CTCGAG*TTCAGGCGTAAAGTGGCGTAAATG-3'. The resulting fragment was digested with *Xba*I and *Xho*I and ligated with pTB311 [*att*HK022 *bla* P$_{lac}$::^{ss}*dsbA-amiB(23-445)-sfgfp*] (24) digested with the same enzymes.

pDY166-pDY168

pDY166 [*att*HK022 *bla* P_{lac}::*ftsE(K41M)X-sfgfp*] was constructed by amplifying *ftsE(K41M)X*

with the primers 5'-GTCA*TCTAGA*TTTGCCCGAGAGGATTAACAATG-3' and 5'-

GTCA*CTCGAG*TTCAGGCGTAAAGTGGCGTAAATG-3' using pDY158 [*attλ cat* P_{ara}::*ftsE*

(K41M)X] as the DNA template. The resulting fragment was digested with *Xba*I and *Xho*I and

ligated with pTB311 [*att*HK022 *bla* P_{lac}::^{ss}*dsbA-amiB(23-445)-sfgfp*] (24) digested with the same

enzymes.

pDY167

pDY167 [*att*HK022 *bla* P_{lac}::*ftsE(D162N)X-sfgfp*] was constructed by amplifying *ftsE(D162N)X*

with the primers 5'-GTCA*TCTAGA*TTTGCCCGAGAGGATTAACAATG-3' and 5'-

GTCA*CTCGAG*TTCAGGCGTAAAGTGGCGTAAATG-3' using pDY159 [*attλ cat* P_{ara}::*ftsE*

(D162N)X] as the DNA template. The resulting fragment was digested with *Xba*I and *Xho*I and

ligated with pTB311 [*att*HK022 *bla* P_{lac}::^{ss}*dsbA-amiB(23-445)-sfgfp*] (24) digested with the same

enzymes.

pDY168

pDY168 [*att*HK022 *bla* P_{lac}::*ftsE(E163Q)X-sfgfp*] was constructed by amplifying *ftsE(E163Q)X*

with the primers 5'-GTCA*TCTAGA*TTTGCCCGAGAGGATTAACAATG-3' and 5'-

GTCA*CTCGAG*TTCAGGCGTAAAGTGGCGTAAATG-3' using pDY160 [*attλ cat* P_{ara}::*ftsE*

(E163Q)X] as the DNA template. The resulting fragment was digested with *Xba*I and *Xho*I and

ligated with pTB311 [*att*HK022 *bla* P$_{lac}$::^{ss}*dsbA-amiB(23-445)-sfgfp*] (24) digested with the same

enzymes.

Table 2.3. Bacterial strains used in this study.

Strain[a]	Genotype[b]	Source/Reference[c]
DH5α	F− hsdR17 deoR recA1 endA1 phoA supE44 thi-1 gyrA96 relA1 Δ(lacZYA-argF)U169 ϕ80dlacZΔM15	Gibco BRL
BL21(λDE3)	ompT rB− mB− (P$_{lac}$UV5::T7gene1)	Novagen
BTH101	F−, glnV44(AS), recA1, endA1, gyrA96, thi1, hsdR17, spoT1, rfbD1 cya	(33)
BW25113	Δ(araD-araB)567 ΔlacZ4787(::rrnB-3) rph-1 Δ(rhaD-rhaB)568 hsdR514	(54)
JW5646	BW25113 ΔenvC::Kan^R	(54)
JW2985	BW25113 ΔftsP(sufI)::Kan^R	(54)
MG1655	rph1 ilvG rfb-50	(45)
MM9	TB28 (Kan^R araC P$_{ara}$)::ponB	(27)
MM11	TB28 (frt araC P$_{ara}$)::ponB	(27)
TB10	rph1 ilvG rfb-50 λΔcro-bio nad::Tn10	(51)
TB28	MG1655 ΔlacIZYA::frt	(26)
TB140	TB28 ΔenvC::frt	(25)
TB145	TB28 ΔnlpD747::frt	(25)
TB172	TB28 ΔamiA::frt ΔamiB::frt (Kan^R araC P$_{ara}$)::ponB	P1(MM9) x TU207
TU122	TB28 ΔponB::frt	(27)
TU189	TB10 ΔftsEX::Kan^R	λRec
TU190**	TB28 ΔftsEX::Kan^R	P1(TU189) x TB28(attλTU188)
TU191	TB28 ΔftsEX::frt	TU190/pCP20
TU195**	TB28 ΔftsEX::frt ΔenvC::Kan^R	P1(JW5646) x TU191(attλTU188)
TU196**	TB28 ΔftsEX::frt ΔftsP(sufI)::Kan^R	P1(JW2985) x TU191(attλTU188)
TU205***	TB28 ΔenvC::frt ΔftsP(sufI)::Kan^R	P1(JW2985) x TB140(attλTD25)
TU207	TB28 ΔamiA::frt ΔamiB::frt	(24)
HC260	TB10 zapA-gfp Cam^R	λRec
HC261	TB28 zapA-gfp Cam^R	P1(HC260) x TB28
HC262	TB28 ΔenvC::frt zapA-gfp Cam^R	P1(HC261) × TB140
NP32	TB28 ΔenvC::frt zapA-gfp frt	HC262/pCP20
NP65*	TB28 (frt araC P$_{ara}$)::ponB ΔenvC::Kan^R	P1(JW5646) x MM11/pTB63

Table 2.3 continued.

NP66*	TB28 (*frt araC* P~ara~)::*ponB* Δ*ftsEX*::Kan^R	P1(TU190) x MM11/pTB63
NP69	TB28 Δ*envC*::*frt zapA-gfp frt* Δ*ftsEX*::Kan^R	P1(TU190) x NP32
KP4*	TB28 Δ*envC*::Kan^R	P1(JW5646) x TB28/pTB63
KP5*	TB28 Δ*ftsEX*::Kan^R	P1(TU190) x TB28/pTB63
KP6*	TB28 Δ*nlpD*747::*frt* Δ*envC*::Kan^R	P1(JW5646) x TB145/pTB63
KP7*	TB28 Δ*nlpD*747::*frt* Δ*ftsEX*::Kan^R	P1(TU190) x TB145/pTB63
DY18	TB28 Δ*envC*::*frt* Δ*ftsEX*::Kan^R	P1(TU190) x TB140

[a] Stains marked with a single asterisk were made by transducing Kan^R cassettes into a recipient harboring plasmid pTB63. Stains marked with a double or triple asterisk were made by transducing Kan^R cassettes into recipients harboring *att*λTU188 or *att*λTD25, respectively.

[b] The Kan^R cassette is flanked by *frt* sites for removal by FLP recombinase. An *frt* scar remains following removal of the cassette using FLP expressed from pCP20.

[c] Strain constructions by P1 transduction are described using the shorthand: P1(donor) x recipient. Transductants were selected on LB Kan or Cam plates where appropriate. Strains resulting from the removal of a Drug^R cassette using pCP20 are indicated as: Parental strain/pCP20. λRec indicates strains were constructed by recombineering (see Experimental Procedures for details).

Table 2.4. Plasmids used in this study[a].

Plasmid	Genotype	Origin	Source or reference
pCP20	*bla cat c*I875 *repA*(Ts) P$_R$::*flp*	pSC101	(56)
pInt-ts	*bla c*I875 *repA*(Ts) P$_R$::*int$^\lambda$*	pSC101	(46)
pKNT25	*aph Plac::T25*	p15A	(33)
pCH363	*bla lacI^q* P$_{lac}$::*T18*	pBR/colE1	(58)
pDY133	*bla lacI^q* P$_{T7}$::*^{10}H-^{loop1}ftsX*	pBR/colE1	This study
pDY138	*bla lacI^q* P$_{lac}$:: *^{loop1}ftsX-T18*	pBR/colE1	This study
pDY151	*bla lacI^q* P$_{T7}$::*H-SUMO-envC(35-276)*	pBR/colE1	This study
pDY156	*att*HK *bla* P$_{lac}$::*ftsEX-GFP*	R6K	This study
pDY161	*att*HK *bla* P$_{lac}$::*ftsEX$^{(\Delta152-161)}$-GFP*	R6K	This study
pDY162	*att*HK *bla* P$_{lac}$::*ftsEX$^{(\Delta146-165)}$-GFP*	R6K	This study
pDY163	*att*HK *bla* P$_{lac}$::*ftsEX$^{(\Delta137-176)}$-GFP*	R6K	This study
pDY164	*att*HK *bla* P$_{lac}$::*ftsEX$^{(\Delta109-188)}$-GFP*	R6K	This study
pDY165	*att*HK *bla* P$_{lac}$::*ftsEX$^{(\Delta109-213)}$-GFP*	R6K	This study
pDY166	*att*HK *bla* P$_{lac}$::*ftsE(K41M)X-GFP*	R6K	This study
pDY167	*att*HK *bla* P$_{lac}$::*ftsE(D162N)X-GFP*	R6K	This study
pDY168	*att*HK *bla* P$_{lac}$::*ftsE(E163Q)X-GFP*	R6K	This study
pTB63	*tetAR ftsQAZ*	pSC101	(26)
pTB102	*cat c*I875 *repA*(Ts) P$_R$::*int^{HK022}*	pSC101	(47)
pTB316	*att*HK022 *bla lacI^q* P$_{lac}$::*envC-mCherry*	R6K	(25)
pTB332	*aph P$_{lac}$::envC(277-419)-T25*	p15A	This study
pTB333	*aph P$_{lac}$::envC(34-419)-T25*	p15A	This study
pTD25	*attλ cat* P$_{ara}$::*envC*	R6K	(25)
pTD80	*attλ cat* P$_{lac}$::*envC-mCherry*	R6K	This study
pTU110	*cat lacI^q* P$_{lac}$::*ponB lacZ*	F	(27)
pTU188	*attλ cat* P$_{ara}$::*ftsEX*	R6K	This study

[a] P$_R$, P$_{lac}$, and P$_{ara}$ indicate the phage λR, lactose, and arabinose promoters, respectively. P$_{syn135}$ is a synthetic *lac* promoter with a consensus -35 element and no operators. Numbers in parenthesis indicate the codons included in the relevant clones. The GFP allele used in plasmid constructs was superfolder GFP (52) and mCherry was from Shaner and co-workers (53). The linker LEGPAGL was present between the fusion proteins and the protein of interest.

Acknowledgments

Section 2.6: References

1. de Boer PA (2010) Advances in understanding E. coli cell fission. *Current Opin Microbiol* 13:730–737.

2. Bi EF, Lutkenhaus J (1991) FtsZ ring structure associated with division in Escherichia coli. *Nature* 354:161–164.

3. Dajkovic A, Pichoff S, Lutkenhaus J, Wirtz D (2010) Cross-linking FtsZ polymers into coherent Z rings. *Mol Microbiol* 78:651–668.

4. Pichoff S, Lutkenhaus J (2002) Unique and overlapping roles for ZipA and FtsA in septal ring assembly in Escherichia coli. *EMBO J* 21:685–693.

5. Hale CA, de Boer PA (1997) Direct binding of FtsZ to ZipA, an essential component of the septal ring structure that mediates cell division in E. coli. *Cell* 88:175–185.

6. Hale CA et al. (2011) Identification of Escherichia coli ZapC (YcbW) as a component of the division apparatus that binds and bundles FtsZ polymers. *J Bacteriol* 193:1393–1404.

7. Gueiros-Filho FJ, Losick R (2002) A widely conserved bacterial cell division protein that promotes assembly of the tubulin-like protein FtsZ. *Genes Dev* 16:2544–2556.

8. Durand-Heredia JM, Yu HH, De Carlo S, Lesser CF, Janakiraman A (2011) Identification and Characterization of ZapC, a Stabilizer of the FtsZ Ring in Escherichia coli. *J Bacteriol* 193:1405–1413.

9. Galli E, Gerdes K (2010) Spatial resolution of two bacterial cell division proteins: ZapA recruits ZapB to the inner face of the Z-ring. *Mol Microbiol* 76:1514–1526.

10. Ebersbach G, Galli E, Møller-Jensen J, Löwe J, Gerdes K (2008) Novel coiled-coil cell division factor ZapB stimulates Z ring assembly and cell division. *Mol Microbiol* 68:720–735.

11. Schmidt KL et al. (2004) A predicted ABC transporter, FtsEX, is needed for cell division in Escherichia coli. *J Bacteriol* 186:785–793.

12. Rees DC, Johnson E, Lewinson O (2009) ABC transporters: the power to change. *Nat Rev Mol Cell Biol* 10:218–227.

13. Ricard M, Hirota Y (1973) Process of cellular division in Escherichia coli: physiological study on thermosensitive mutants defective in cell division. *J Bacteriol* 116:314–322.

14. Gill DR, Hatfull GF, Salmond GP (1986) A new cell division operon in Escherichia coli. *Mol Gen Genet* 205:134–145.

15. de Leeuw E et al. (1999) Molecular characterization of Escherichia coli FtsE and FtsX. *Mol Microbiol* 31:983–993.

16. Corbin BD, Wang Y, Beuria TK, Margolin W (2007) Interaction between cell division proteins FtsE and FtsZ. *J Bacteriol* 189:3026–3035.

17. Karimova G, Dautin N, Ladant D (2005) Interaction network among Escherichia coli membrane proteins involved in cell division as revealed by bacterial two-hybrid analysis. *J Bacteriol* 187:2233–2243.

18. Reddy M (2007) Role of FtsEX in cell division of Escherichia coli: viability of ftsEX mutants is dependent on functional SufI or high osmotic strength. *J Bacteriol* 189:98–108.

19. Samaluru H, SaiSree L, Reddy M (2007) Role of SufI (FtSP) in cell division of Escherichia coli: evidence for its involvement in stabilizing the assembly of the divisome. *J Bacteriol* 189:8044–8052.

20. Arends SJR, Kustusch RJ, Weiss DS (2009) ATP-binding site lesions in FtsE impair cell division. *J Bacteriol* 191:3772–3784.

21. Vollmer W, Blanot D, de Pedro MA (2008) Peptidoglycan structure and architecture. *FEMS Microbiol Rev* 32:149–167.

22. Heidrich C et al. (2001) Involvement of N-acetylmuramyl-L-alanine amidases in cell separation and antibiotic-induced autolysis of Escherichia coli. *Mol Microbiol* 41:167–178.

23. Priyadarshini R, de Pedro MA, Young KD (2007) Role of peptidoglycan amidases in the development and morphology of the division septum in Escherichia coli. *J Bacteriol* 189:5334–5347.

24. Uehara T, Parzych KR, Dinh T, Bernhardt TG (2010) Daughter cell separation is controlled by cytokinetic ring-activated cell wall hydrolysis. *EMBO J* 29:1412–1422.

25. Uehara T, Dinh T, Bernhardt TG (2009) LytM-domain factors are required for daughter cell separation and rapid ampicillin-induced lysis in Escherichia coli. *J Bacteriol* 191:5094–5107.

26. Bernhardt TG, de Boer PAJ (2004) Screening for synthetic lethal mutants in Escherichia coli and identification of EnvC (YibP) as a periplasmic septal ring factor with murein hydrolase activity. *Mol Microbiol* 52:1255–1269.

27. Paradis-Bleau C et al. (2010) Lipoprotein cofactors located in the outer membrane activate bacterial cell wall polymerases. *Cell* 143:1110–1120.

28. Sham L-T, Barendt SM, Kopecky KE, Winkler ME (2011) Essential PcsB putative peptidoglycan hydrolase interacts with the essential FtsXSpn cell division protein in Streptococcus pneumoniae D39. *Proc Natl Acad Sci* 108:E1061–9.

29. Typas A et al. (2010) Regulation of peptidoglycan synthesis by outer-membrane proteins. *Cell* 143:1097–1109.

30. Rodolakis A, Thomas P, Starka J (1973) Morphological mutants of Escherichia coli. Isolation and ultrastructure of a chain-forming envC mutant. *J Gen Microbiol* 75:409–416.

31. Ichimura T, Yamazoe M, Maeda M, Wada C, Hiraga S (2002) Proteolytic activity of YibP protein in Escherichia coli. *J Bacteriol* 184:2595–2602.

32. Hara H et al. (2002) Identification and characterization of the Escherichia coli envC gene encoding a periplasmic coiled-coil protein with putative peptidase activity. *FEMS Microbiol Lett* 212:229–236.

33. Karimova G, Pidoux J, Ullmann A, Ladant D (1998) A bacterial two-hybrid system based on a reconstituted signal transduction pathway. *Proc Natl Acad Sci USA* 95:5752–5756.

34. Davidson AL, Dassa E, Orelle C, Chen J (2008) Structure, function, and evolution of bacterial ATP-binding cassette systems. *Microbiol Mol Biol Rev* 72:317–64.

35. Ito Y, Kanamaru K, Taniguchi N, Miyamoto S, Tokuda H (2006) A novel ligand bound ABC transporter, LolCDE, provides insights into the molecular mechanisms underlying membrane detachment of bacterial lipoproteins. *Mol Microbiol* 62:1064–1075.

36. Khare D, Oldham ML, Orelle C, Davidson AL, Chen J (2009) Alternating access in maltose transporter mediated by rigid-body rotations. *Mol Cell* 33:528–536.

37. Yakushi T, Masuda K, Narita S, Matsuyama S, Tokuda H (2000) A new ABC transporter mediating the detachment of lipid-modified proteins from membranes. *Nat Cell Biol* 2:212–218.

38. Daley DO et al. (2005) Global topology analysis of the Escherichia coli inner membrane proteome. *Science* 308:1321–1323.

39. Ng W-L, Kazmierczak KM, Winkler ME (2004) Defective cell wall synthesis in Streptococcus pneumoniae R6 depleted for the essential PcsB putative murein hydrolase or the VicR (YycF) response regulator. *Mol Microbiol* 53:1161–1175.

40. Garti-Levi S, Hazan R, Kain J, Fujita M, Ben-Yehuda S (2008) The FtsEX ABC transporter directs cellular differentiation in Bacillus subtilis. *Mol Microbiol* 69:1018–1028.

41. Higgins ML, Shockman GD (1970) Model for cell wall growth of Streptococcus faecalis. *J Bacteriol* 101:643–648.

42. Burdett ID (1979) Electron microscope study of the rod-to-coccus shape change in a temperature-sensitive rod- mutant of Bacillus subtilis. *J Bacteriol* 137:1395–1405.

43. Ichikawa J, Li C, Fu J, Clarke S (1994) A gene at 59 minutes on the Escherichia coli chromosome encodes a lipoprotein with unusual amino acid repeat sequences. *J Bacteriol* 176:1630–1638.

44. Miller JH (1972) *Experiments in Molecular Genetics* (Cold Spring Harbor Laboratory, Cold Spring Harbor, New York).

45. Guyer MS, Reed RR, Steitz JA, Low KB (1981) Identification of a sex-factor-affinity site in E. coli as gamma delta. *Cold Spring Harb. Symp. Quant. Biol.* 45:135–140.

46. Haldimann A, Wanner BL (2001) Conditional-replication, integration, excision, and retrieval plasmid-host systems for gene structure-function studies of bacteria. *J Bacteriol* 183:6384–6393.

47. Bernhardt TG, de Boer PAJ (2005) SlmA, a nucleoid-associated, FtsZ binding protein required for blocking septal ring assembly over Chromosomes in E. coli. *Mol Cell* 18:555–564.

48. Cho H, McManus HR, Dove SL, Bernhardt TG (2011) Nucleoid occlusion factor SlmA is a DNA-activated FtsZ polymerization antagonist. *Proc Natl Acad Sci USA* 108:3773–3778.

49. Hale CA, de Boer PA (1999) Recruitment of ZipA to the septal ring of Escherichia coli is dependent on FtsZ and independent of FtsA. *J Bacteriol* 181:167–176.

50. Bernhardt TG, de Boer PAJ (2003) The Escherichia coli amidase AmiC is a periplasmic septal ring component exported via the twin-arginine transport pathway. *Mol Microbiol* 48:1171–1182.

51. Johnson JE, Lackner LL, Hale CA, de Boer PAJ (2004) ZipA is required for targeting of DMinC/DicB, but not DMinC/MinD, complexes to septal ring assemblies in Escherichia coli. *J Bacteriol* 186:2418–2429.

52. Pédelacq J-D, Cabantous S, Tran T, Terwilliger TC, Waldo GS (2006) Engineering and characterization of a superfolder green fluorescent protein. *Nat Biotechnol* 24:79–88.

53. Shaner NC et al. (2004) Improved monomeric red, orange and yellow fluorescent proteins derived from Discosoma sp. red fluorescent protein. *Nat Biotechnol* 22:1567–1572.

54. Baba T et al. (2006) Construction of Escherichia coli K-12 in-frame, single-gene knockout mutants: the Keio collection. *Mol Syst Biol* 2:2006.0008.

55. Yu D et al. (2000) An efficient recombination system for chromosome engineering in Escherichia coli. *Proc Natl Acad Sci USA* 97:5978–5983.

56. Datsenko KA, Wanner BL (2000) One-step inactivation of chromosomal genes in Escherichia coli K-12 using PCR products. *Proc Natl Acad Sci USA* 97:6640–6645.

57. Cormack BP, Valdivia RH, Falkow S (1996) FACS-optimized mutants of the green fluorescent protein (GFP). *Gene* 173:33–38.

58. Bendezú FO, Hale CA, Bernhardt TG, de Boer PAJ (2009) RodZ (YfgA) is required for proper assembly of the MreB actin cytoskeleton and cell shape in E. coli. *EMBO J* 28:193–204.

59. Guzman LM, Belin D, Carson MJ, Beckwith J (1995) Tight regulation, modulation, and high-level expression by vectors containing the arabinose PBAD promoter. *J Bacteriol* 177:4121–4130.

60. Morlot C, Uehara T, Marquis KA, Bernhardt TG, Rudner DZ (2010) A highly coordinated cell wall degradation machine governs spore morphogenesis in Bacillus subtilis. *Genes Dev* 24:411–422.

Chapter 3

A conformational switch controls the activation of bacterial cell separation enzymes

Attributions

The work presented in this chapter was performed primarily by Desirée Yang. Kemin Tan and Andrzej Joachimiak carried out the crystallographic studies that generated the crystal structure of AmiB from *Bartonella henselae* [PDB: 3NE8] (Figure 3.6, Figure 3.7, Table 3.5). All remaining experiments and subsequent figures/tables were performed and generated by Desirée Yang. The manuscript was written by Desirée Yang and Thomas Bernhardt for impending submission.

Chapter 3: A conformational switch controls the activation of bacterial cell separation enzymes

Desirée C. Yang[1], Kemin Tan[2], Andrzej Joachimiak[2], Thomas G. Bernhardt[1]

[1]Department of Microbiology and Immunobiology, Harvard Medical School, Boston, MA 02115

[2]Biosciences Division, Argonne National Laboratory, Argonne, IL 60439

Section 3.1: Abstract

Bacterial membranes are typically fortified by a cell wall layer made of peptidoglycan (PG). Biogenesis of this structure requires hydrolytic enzymes as well as synthases. Since breaches in the PG structure can cause cell lysis, the potentially lethal activity of PG hydrolases must be kept in check. Despite the importance of these controls, the cellular mechanisms regulating PG hydrolase activity have largely remained mysterious. We have been investigating the regulation of PG hydrolases called amidases required for splitting shared PG material formed at the division site of *Escherichia coli*. We previously showed that these amidases (AmiA, AmiB, and AmiC) have low basal activities and require activation by cytokinetic-ring-associated factors with LytM domains (EnvC and NlpD) to promote cell separation. Here we identify a domain in the amidase structure responsible for activity regulation. Using a genetic enrichment strategy, we isolated plasmids encoding poorly regulated (lytic) *amiB* mutants. The amino acid substitutions in these AmiB variants led to elevated basal PG hydrolase activity *in vitro* and mapped to a ~50 residue domain that was found to be unique to cell separation amidases of Gram-negative bacteria. Structural analysis of an AmiB ortholog from *Bartonella henselae* revealed that this domain forms an alpha-helix that occludes the amidase active site. Our results

thus support a model in which PG amidase activity is controlled by a conformational switch involving the LytM-stimulated release of the regulatory helix from the amidase active site.

Section 3.2: Introduction

Most bacteria surround themselves with a tough cell wall exoskeleton made of peptidoglycan (PG). This essential layer is constructed from polysaccharide strands crosslinked to one another via attached peptides to form a continuous three-dimensional meshwork that encapsulates the cytoplasmic membrane and protects it from osmotic rupture (1, 2). Assembly of the PG layer requires synthetic enzymes called penicillin binding proteins (PBPs), the primary targets of penicillin and related β-lactam antibiotics (3). In addition to these PG synthases, bacterial cells also produce an array of hydrolytic enzymes that cleave PG bonds (4). The activities of PG hydrolases are used to promote important aspects of growth, division, and development (4). To function in this capacity, however, these enzymes must be tightly regulated (3-5). Otherwise, aberrant cleavage of the PG layer may result in cell lysis. While this fact has been appreciated for some time, the cellular mechanisms responsible for regulating PG hydrolases have largely remained mysterious (3-5).

Cell division in *Escherichia coli* has proven to be an excellent model system for studies of PG hydrolase regulation (6, 7). In most bacteria, the process begins with the polymerization of the tubulin-like FtsZ protein into a ring structure (the Z-ring) just underneath the cytoplasmic membrane at the prospective site of division (8, 9). This structure then promotes the recruitment of a number of essential and non-essential division proteins to the division site, ultimately organizing the formation of a trans-envelope molecular machine capable of driving cell

constriction (9). An important function of this so called septal ring or divisome machine is the highly localized synthesis of the new (septal) PG material that will ultimately fortify the poles of the daughter cells (3). Septal PG appears to be initially shared between the daughters and must be split by PG hydrolases to shape the poles and complete the division process (5). Septal PG splitting in *E. coli* depends critically on the activities of three LytC-type *N*-acetylmuramyl-L-alanine amidases (Pfam: Amidase_3): AmiA, AmiB and AmiC (10, 11). Amidases are PG hydrolases that break the peptide crosslinks in the PG meshwork by cleaving bonds that link stem peptides to the glycan strands (4). The three amidases appear to be largely redundant with mutants lacking individual enzymes dividing essentially normally. However, mutants lacking all three amidases fail to split septal PG and form long chains of cells with distinct cytoplasmic compartments connected by shared layers of PG and a partially constricted outer membrane layer (10, 11).

We previously demonstrated that the cell separation amidases have low basal activities *in vitro*, and that in order to promote division, these enzymes must be activated by septal ring factors with LytM domains: EnvC and NlpD (6, 12). *In vitro* PG hydrolase assays and *in vivo* genetic analyses indicate that EnvC specifically activates AmiA and AmiB while NlpD specifically activates AmiC (6). Accordingly, mutants lacking both EnvC and NlpD have a chaining phenotype that resembles a triple amidase mutant (12). In a subsequent study, we further showed that EnvC activity is controlled by an ATP-binding cassette (ABC) transporter-like complex composed of the ATPase FtsE and transmembrane domain (TMD) subunit FtsX (7). FtsEX directly recruits EnvC to the septal ring via an interaction between EnvC and a periplasmic loop of FtsX (7). Interestingly, FtsEX variants predicted to be ATPase defective still

recruit EnvC to the septum but fail to promote cell separation (7). Our results therefore support a model in which amidase activation via EnvC in the periplasm is regulated by conformational changes in the FtsEX complex mediated by ATP hydrolysis in the cytoplasm. This model is attractive because it provides a means for converting septal PG hydrolysis into a discrete process with a fixed number of PG bonds being broken per ATP hydrolyzed. This conversion, in turn, may afford the divisome exquisite control over the septal PG splitting process through the modulation of the ATPase activity of FtsE. Importantly, a role for FtsEX in the control of septal PG splitting appears to be conserved as Sham et al. (13) have directly connected the essential cell separation factor PcsB (14) with FtsEX in *S. pneumoniae*.

Here we investigate the mechanism by which amidase activity is controlled by the LytM factors. Using a genetic enrichment strategy based on the release of plasmids from lysing cells, we isolated plasmids encoding poorly regulated (lytic) variants of AmiB. The amino acid substitutions in these AmiB variants led to elevated basal PG hydrolase activity *in vitro* and mapped to a ~50 residue domain that was found to be unique to cell separation amidases of Gram-negative bacteria. When similar substitutions were engineered in related amidases, proper regulatory activity was also disrupted. Structural analysis of an AmiB ortholog from *Bartonella henselae* revealed that the identified regulatory domain forms an alpha-helix that occludes the amidase active site. Our results thus support a model in which PG amidase activity at the division site is controlled by a cascade of conformational changes starting with FtsE-mediated ATP hydrolysis in the cytoplasm and culminating with the LytM-stimulated release of a regulatory helix from the amidase active site in the periplasm. We propose that similar conformational control mechanisms are likely to be part of a general cellular strategy used to

regulate PG hydrolases involved in cell growth, division, and other processes requiring

remodeling of the PG matrix.

Section 3.3: Results

Isolation of *amiB* mutants that induce cell lysis

Although we recently showed that the cell separation amidases require activation by their

cognate LytM factor to promote cell separation (6), the mechanism of amidase activation has

remained unclear. We hypothesized that the amidases are likely to be conformationally regulated

and therefore can exist in an "OFF" or an "ON" state. Thus, according to this model, the LytM

proteins would activate the amidases by promoting an OFF to ON conformational transition. If

this were true, we reasoned that we should be able to isolate *amiB* mutants that encode AmiB

variants with an increased propensity to visit the ON conformation in the absence of activation.

We further anticipated that, when exported to the periplasm, the poorly regulated activity of such

mutants would create lesions in the PG matrix and induce cell lysis. A plasmid release

enrichment strategy (Figure 3.1A) (15) (W. Roof and R. Young, unpublished data) was therefore

initiated to isolate lytic *amiB* (^{lyt}*amiB*) mutants. To this end, we generated a library of plasmids

encoding *amiB* under control of the arabinose promoter [P_{ara}::*amiB*] in which the *amiB* gene was

mutagenized by error-prone PCR. The library was transformed into TB28 [WT] cells and the

resulting transformants were pooled and grown in LB broth. Upon reaching an OD_{600} of ~0.3,

amiB was induced by the addition of arabinose to 0.2% and growth was continued for an

additional 3 hrs. During the induction period, we presumed that plasmids encoding ^{lyt}*amiB*

mutants would cause cell lysis, promoting their release into the medium. Therefore, following
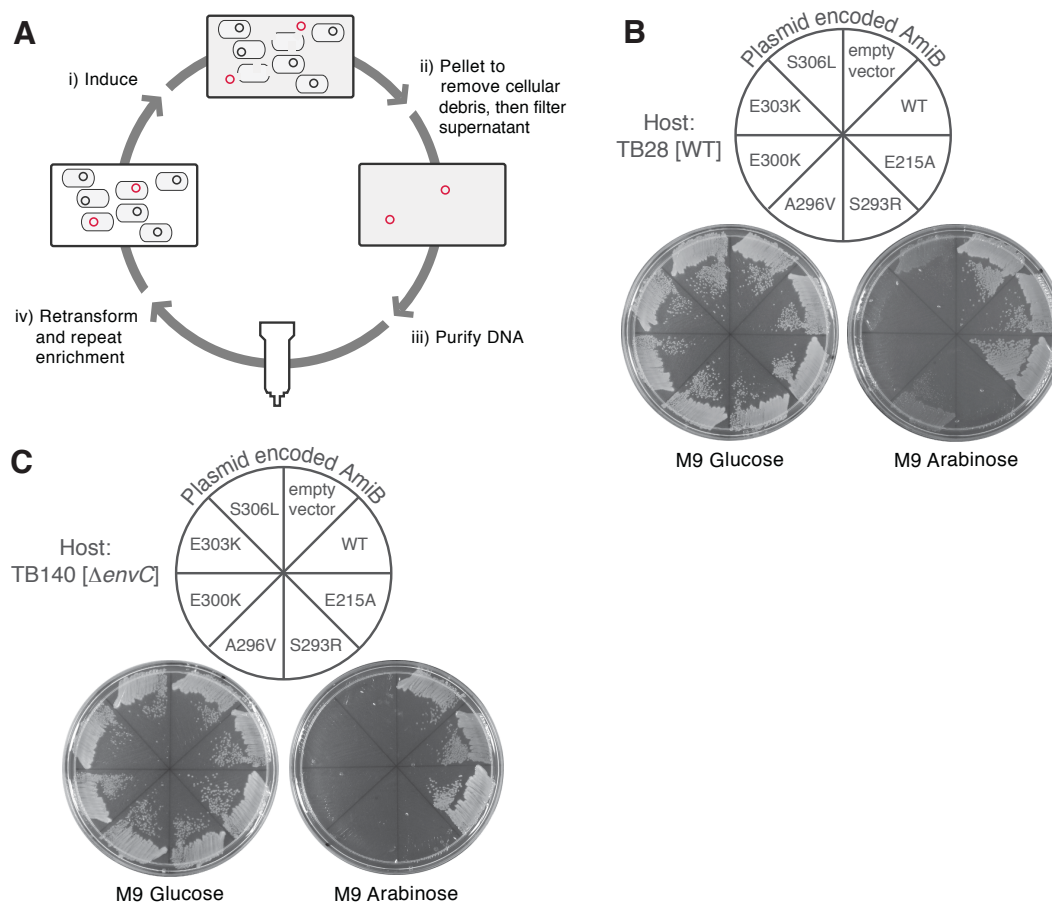
Figure 3.1. Plasmid release enrichment strategy for the isolation of lytic *amiB* (^{lyt}*amiB*) mutants. (**A**) Overview of the plasmid release enrichment protocol. (i) Cells carrying mutagenized *amiB*-containing plasmid (black and red circles) are induced with 0.2% arabinose. (ii) Plasmids encoding rare ^{lyt}*amiB* mutants (red circles) promote cell lysis and are released into the culture supernatant. Cells and cell debris are removed by centrifugation and filtration. (iii) Plasmid DNA is purified from the culture supernatants using Qiagen columns. (iv) Purified DNA can then be retransformed into the parental strain to repeat the enrichment protocol for as many rounds as necessary. (**B**) TB28 [WT] cells carrying an empty vector or expression constructs encoding AmiB (WT), AmiB(E215A) or the indicated ^{Lyt}AmiB variants were struck out on M9-casamino acid (M9-CAA) agar containing either 0.2% glucose or 0.2% arabinose supplemented with 10 μg/ml chloramphenicol (Cm^{10}). Plates were incubated overnight at 37°C and photographed. AmiB(E215A) is a catalytically inactive variant (6). (**C**) TB140 [$\Delta envC$] cells carrying an empty vector or expression constructs encoding AmiB (WT), AmiB(E215A) or the indicated ^{Lyt}AmiB variants were struck out on M9-CAA-Cm^{10} agar containing either 0.2% glucose or 0.2% arabinose. Plates were incubated overnight at 37°C and photographed.

removal of cells and cell debris, we purified plasmid DNA from the growth medium of the induced culture using Qiagen spin columns (see Experimental Procedures). Purified DNA was used to transform TB28 [WT] cells and the transformants were recovered on non-inducing medium. To identify transformants harboring [lyt]*amiB*-containing plasmids, colonies from the primary transformation plate were screened for those that failed to grow or grew poorly on agar containing 0.2% arabinose (inducing conditions).

Using two independently mutagenized plasmid libraries and only one round of plasmid release for each enrichment, 33 out of 116 plasmid-release transformants showed differential growth on arabinose versus glucose media. Plasmid DNA was isolated from each of these candidates and the resident *amiB* genes were sequenced. As expected, a majority of the plasmids (29/33) were found to encode *amiB* mutants (Table 3.1). The three plasmids containing wild-type *amiB* were found to yield much more DNA than the parental vector following plasmid purification (data not shown). We assume these plasmids were released during the enrichment because their apparent copy number increase led to a level of AmiB overproduction that was sufficiently high enough for lysis induction. These isolates were not studied further.

To verify that the plasmid encoded *amiB* mutants isolated in the plasmid release enrichment were indeed [lyt]*amiB* alleles, mutants from unique isolates were subcloned into the parental vector backbone. In each case, TB28 [WT] cells harboring the resulting plasmids were found to be inducer sensitive, indicating that the *amiB* mutants were toxic (Table 3.2 and Figure 3.1B). Site directed mutagenesis was also used to generate constructs producing the AmiB variants: AmiB(H302P), AmiB(S306P), AmiB(D314V), and AmiB(A405V) because plasmids encoding variants with single substitutions at these positions were not isolated in the enrichment.

Table 3.1. Summary of all sequenced [Lyt]AmiB candidates from plasmid release.

PRE Candidate #	Base Pair Change(s)	Amino Acid Change(s)
4[a]	**G**AG$_{303}$→**A**AG	E303K
13[a]	AT**T**$_{125}$→AT**A**, A**G**T$_{293}$→A**A**T	silent, S293I
15[a]	**T**CG$_{306}$→**C**CG, **C**AA$_{422}$→**T**AA	S306P, stop codon
20[a]	AG**T**$_{293}$→AG**A**	S293R
21[a]	GT**G**$_{59}$→GT**T**, T**T**G$_{229}$→T**C**G, G**C**C$_{296}$→G**T**C, G**A**T$_{314}$→G**T**T	silent, L229S, A296V, D314V
26[a]	**G**AG$_{303}$→**A**AG	E303K
29[a]	G**G**T$_{33}$→G**A**T, **G**AG$_{300}$→**A**AG, TC**A**$_{378}$→TC**G**	G33D, E300K, silent
32[b]	G**C**C$_{296}$→G**T**C	A296V
35[b]	**G**AG$_{300}$→**A**AG	E300K
36[b, c]	no mutation	n/a
40[b]	A**G**T$_{293}$→A**A**T	S293I
41[b, c]	no mutation	n/a
45[b]	**C**GC$_{372}$→**T**GC	R372C
48[b]	**C**GC$_{372}$→**T**GC	R372C
49[b]	TC**G**$_{306}$→TT**G**	S306L
50[b]	**C**GC$_{372}$→**T**GC	R372C
52[b]	sequencing results ambiguous, candidate discarded	n/a
56[b]	G**C**C$_{296}$→G**T**C	A296V
64[a]	A**G**C$_{173}$→A**A**C, AG**T**$_{293}$→AG**A**	S173N, S293R
69[a]	**T**CT$_{87}$→**C**CT, TC**G**$_{306}$→TT**G**	S87P, S306L
72[a]	T**G**G$_{8}$→T**T**G, GT**G**$_{99}$→GT**T**, **A**AT$_{263}$→**G**AT, AT**G**$_{295}$→AT**A**, AT**T**$_{408}$→AT**C**, GG**T**$_{427}$→GG**A**	W8L, silent, N263D, M295I, silent, silent
77[a]	TC**G**$_{306}$→TT**G**	S306L
80[a]	C**A**C$_{302}$→C**C**C, CT**G**$_{371}$→CT**A**, G**C**A$_{405}$→G**T**A	H302P, silent, A405V
81[a]	TC**G**$_{306}$→TT**G**, CT**G**$_{395}$→CT**A**	S306L, silent
91[a]	AC**G**$_{40}$→AC**C**, **G**GT$_{170}$→**T**GT, AG**T**$_{293}$→AG**A**	silent, G170C, S293R
95[b, c]	no mutation	n/a
98[b]	G**C**C$_{296}$→G**T**C	A296V

Table 3.1 continued.

PRE Candidate #	Base Pair Change(s)	Amino Acid Change(s)
99[b]	CG**G**$_{214}$→CG**T**, T**C**G$_{306}$→T**T**G	silent, S306L
103[b]	C**A**G$_{333}$→C**T**G	Q333L
104[b]	**C**GC$_{372}$→**T**GC	R372C
107[b]	T**C**G$_{306}$→T**T**G	S306L
108[b]	AT**G**$_{295}$→AT**A**	M295I
112[b]	A**G**T$_{293}$→A**A**T	S293I

[a] isolate from library #1
[b] isolate from library #2
[c] copy number mutant
n/a = not applicable

Table 3.2. AmiB variants isolated in the plasmid release enrichment.

Variants from Enrichment	Lytic Activity[e]	
	WT	**Δ*envC***
W8L, N263D, M295I[a]	+++	+++
G33D, E300K[a]	+++	+++
S87P, S306L	+++	+++
G170C, S293R[a]	+++	+++
S173N, S293R	+++	+++
L229S, A296V, D314V[a]	+++	+++
S293I[b, d]	+++	+++
S293R[d]	+++	+++
M295I[b, d]	+++	+++
A296V[b, d]	+++	+++
E300K[b, d]	+++	+++
H302P, A405V[a, d]	+++	+++
E303K[d]	+++	+++
S306L[b, d]	+++	+++
S306P[c, d]	+++	+++
Q333L[d]	+	+++
R372C[d]	+	+++
Site-Directed Variants		
H302P	+++	+++
S306P	+++	+++
D314V	-	-
A405V	-	-

[a] also contain silent mutation(s)
[b] variant isolated from two independent libraries
[c] variant contains a premature stop at codon 422

AmiB(H302P) and AmiB(S306P) were found to be toxic whereas the others were not (Table

3.2). Finally, a subset of the mutant *amiB* isolates were confirmed to have lytic activity in liquid

broth (Figure 3.2) and to produce equivalent levels of protein relative to wild-type *amiB* (Figure

3.3). As expected for mutants thought to possess elevated basal activity, the AmiB variants were

also found to be toxic in a strain lacking their cognate activator EnvC (Figure 3.1C). We thus

conclude that the [lyt]*amiB* alleles isolated in the plasmid release enrichment procedure encode

poorly regulated AmiB variants that induce cell lysis when overproduced *in vivo*.

Substitutions in the [Lyt]AmiB variants cluster within a predicted regulatory domain

LytC-type amidases are widely distributed within the bacterial domain and are also

encoded in the genomes of many bacteriophages (16). These enzymes can be grouped into at

least three different functional classes: i) phage-encoded enzymes (endolysins) that are likely

used to elicit host cell lysis at the end of an infection cycle (e.g. PLY-PSA) (17), ii) enzymes

encoded by sporulating bacteria that are likely used to promote mother cell lysis for the release

of mature spores (e.g. LytC) (18), and iii) enzymes encoded by Gram-negative proteobacteria

that are likely employed to promote cell separation (e.g. AmiB) (10). Interestingly, a sequence

alignment of selected amidases from these three functional classes revealed that the predicted

cell separation enzymes contain an ~50 amino acid insertion in their amidase domain that is

absent in the lytic amidases (Figure 3.4 and Figure 3.5). Strikingly, 25/29 [lyt]*amiB* candidates

sequenced encoded proteins with at least one amino acid substitution within this region (residues

292-340 of *E. coli* AmiB) (Table 3.1, Figure 3.4). Our results therefore implicate the ~50 amino

acid insertion in the cell separation amidases as a regulatory domain.
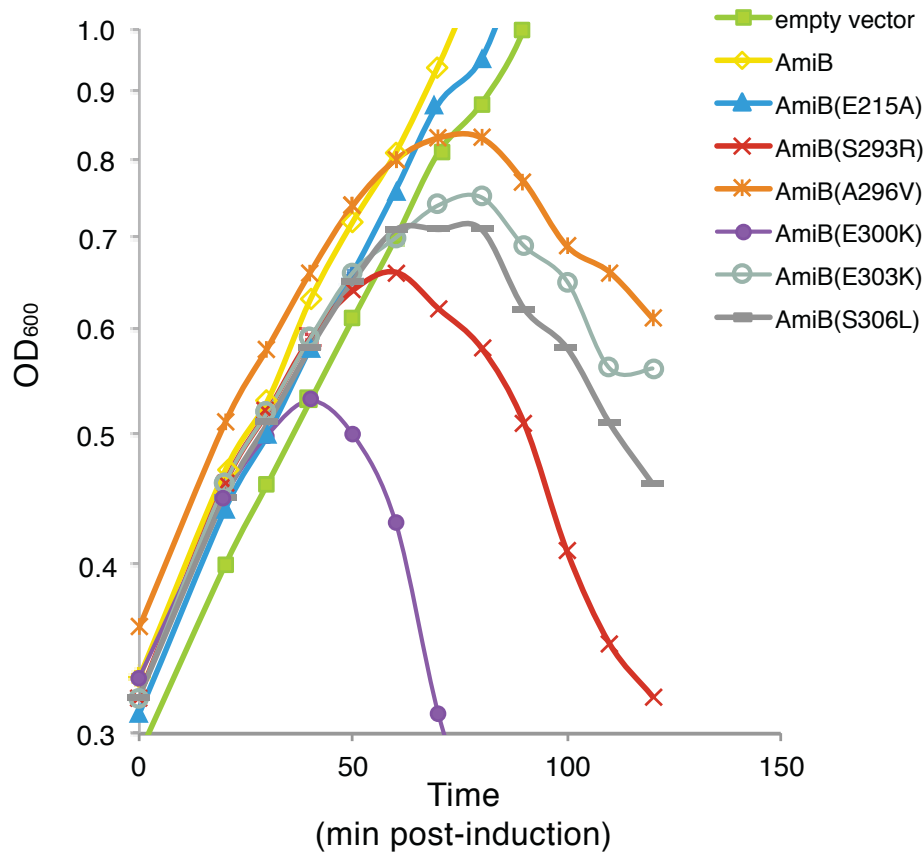
Figure 3.2. Overproduction of the [Lyt]AmiB variants induces lysis. TB170 [Δ*amiB*] carrying an empty vector or expression constructs encoding AmiB (WT), AmiB(E215A) or the indicated [Lyt]AmiB variants were were grown at 37°C in M9-CAA-Cm[10] supplemented with 0.2% maltose to an OD_{600} of about 0.3. At $t = 0$, arabinose was added to a final concentration of 0.2% and growth was monitored by following culture OD_{600}. Samples for immunoblot analysis were taken just prior to lysis at $t = 50$ (see Figure 3.3). Growth of cells harboring the empty vector, AmiB (WT) or AmiB(E215A) control constructs continued without observable lysis.
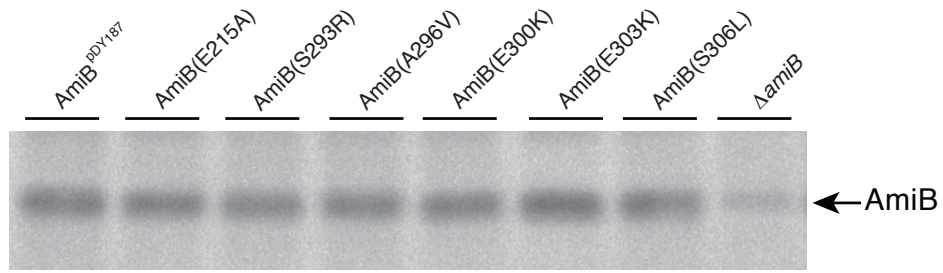
Figure 3.3. ^{Lyt}AmiB variants accumulate at levels similar to AmiB(WT). Cells of TB170 [Δ*amiB*] were grown as described in the legend for Figure 3.2. At *t* = 50 min, cells were harvested for whole-cell extract preparation. Proteins in the resulting extracts were separated by SDS-PAGE, transferred to PVDF, and AmiB was detected with anti-AmiB antisera. 1.5 *µ*g of total protein was loaded into each lane.
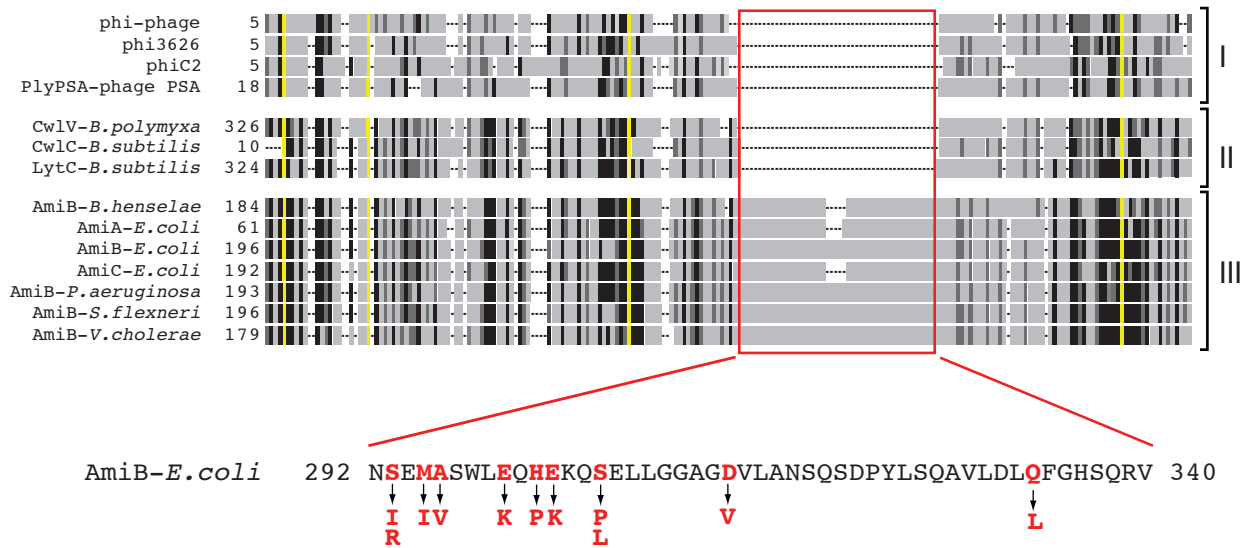
Figure 3.4. Amino acid substitutions in the ^{Lyt}AmiB variants map to a potential regulatory domain. Shown is a schematic representation of a multiple sequence alignment generated using amidase sequences from bacteria and phages. Identities and similarities are indicated by the black and dark grey regions, respectively. Residues essential for catalysis are highlighted in yellow. Gaps in the alignment are indicated as dashed lines. The amidases are grouped into the following categories: (I) phage endolysins, (II) bacterial amidases involved in mother cell lysis following sporulation, and (III) cell separation amidases. The red box highlights what appears to be a ~50 amino acid insertion region found only in the cell separation amidases. The sequence of the insertions from *E. coli* AmiB is shown below the alignment. Residues in red were altered in ^{Lyt}AmiB variants. The identity of the substitutions are indicated by the arrows. See Figure 3.5 for the complete sequence alignment.

```
phi-phage          5  VNCGHTKTGAGSGAIGKI--NESIETRNVGYKVIDKLKTLGNN---V-VDCTIDK
phi3626            5  ERGGHNFQAT--GAVGLI--NETVE-DRKVLAAAYKYTKAAGY---D-VLDVTPG    I
phiC2             5  ITVGHSILKS--GACTSAD-GVVNE-YQYNKSLAPVLADTFRKE-GHKVDVIIC-
PlyPSA-phage PSA  18  MSRGHSDKCV--GAEDIL--SEIKE-AEKVLNAA---SDELKREGHN-VKTFIDR
CwlV-B.polymyxa  326  IDAGHGAKDS--GAVGIS--RKNYE-KTFNLAMALKVESILKQN-PK-LEVVLTR
CwlC-B.subtilis   10  ----HGGSDP--GATGN---G-LQE-KTLTLQIALALRTILTNEYEG-VSLLLSR    II
LytC-B.subtilis  324  IDPGHGDQDS--GAIGN---G-LLE-KEVNLDIAKRVNTKLNAS--G-ALPVLSR
AmiB-B.henselae  184  LDPGHGGIDG--GARGVT--G-ILE-KDVTLAFARALRDELQKG-SH-TIVALTR
AmiA-E.coli       61  LDPGHGGIDT--GAIGRN--G-SKE-KHVVLAIAKNVRSILRN--HG-IDARLTR
AmiB-E.coli      196  IDAGHGGQDP--GAIGPG--G-TRE-KNVTIAIARKLRTLLNDD-PM-FKGVLTR    III
AmiC-E.coli      192  LDPGHGGEDS--GAVGKY--K-TRE-KDVVLQIARRLRSLIEKE-GN-MKVYMTR
AmiB-P.aeruginosa 193 IDAGHGGEDP--GALGPG--G-LHE-KNITLSIARELQRQINQV-RG-YRAELTR
AmiB-S.flexneri  196  IDAGHGGQDP--GAIGPG--G-TRE-KNVTIAIARKLRTLLNDD-PM-FKGVLTR
AmiB-V.cholerae  179  IDAGHGGEDP--GSIGPT--R-KYE-KDITLSVSKKLADQLNAV-PG-MKAVLTR


phi-phage         54  ASTQ-SEC----LSKIATQANRQDLDWFISIHFNAGK-----GRGCEVYTYKGKQ
phi3626           51  NCDS-NTD----LILGVNKAERFGAELFLSYHFDKCYDEYNGALGVACWICATGG    I
phiC2             54  PEKQ-FKTKNEEKSYKIPRVNSGGYDLLIELHLNASN-G--QGKGSEVLYYSNKG
PlyPSA-phage PSA  64  TSTTQSAN----LNKIVNWHNANPADVHISVHLNAGK-----GTGVEVWYYAGDE
CwlV-B.polymyxa  374  SDDT-FLE----LKQRVKVAENLKANVFVSIHANSSGSS--ASNGTETYYQRS--
CwlC-B.subtilis   53  TSDQ-YVS----LNDRTNAANNWGADFFLSIHVNSGG-----GTGFESYIYPDVG    II
LytC-B.subtilis  369  SNDT-FYS----LQERVNKAASAQADLFLSIHANANDSS--SPNGSETYYDTTYQ
AmiB-B.henselae  231  DSDI-FLR----LSERVKKAQEFDADLFISIHADTIDVH--SLRGATVYTISDE-
AmiA-E.coli      107  SGDT-FIP----LYDRVEIAHKHGADLFMSIHADGFTNP--KAAGASVFALSNRG
AmiB-E.coli      243  DGDY-FIS----VMGRSDVARKQNANFLVSIHADAAPNR--SATGASWVLSNRR    III
AmiC-E.coli      239  NEDI-FIP----LQVRVAKAQKQRADLFVSIHADAFTSR--QPSGSSVFALSTKG
AmiB-P.aeruginosa 240 TGDY-FIP----LRKRTEIARKKGADLFVSIHADAAPSR--SAFGASVFALSDRG
AmiB-S.flexneri  243  DGDY-FIS----VMGRSDVAHKQNANFLVSIHADAAPNR--SATGASVWVLSNRR
AmiB-V.cholerae  226  RGDY-FVN----LNKRTEIARRSKAHLLVSVHADAFHTP--QPRGGSVFVLNTRR


phi-phage         99  ------------------------------------------------------YQDAI
phi3626          101  KA----------------------------------------------------EEYAK    I
phiC2            105  ------------------------------------------------------LEYA
PlyPSA-phage PSA 110  KG----------------------------------------------------RKLAV
CwlV-B.polymyxa  420  AS----------------------------------------------------KAFAN
CwlC-B.subtilis   98  APT---------------------------------------------------TTYQS    II
LytC-B.subtilis  417  AAN---------------------------------------------------SKRLAE
AmiB-B.henselae  278  ASDAIAKSLAESENKVDLLDGLP-----KEESLELTDILLDLTRRETHAFSINFA
AmiA-E.coli      155  ASSAMAKYLSERENRADEVAGKK----ATDKDHLLQQVLFDLVQTDTIKNSLTLG
AmiB-E.coli      291  ANSEMASWLEQHEKQSELLGGAGDVLANSQSDPYLSQAVLDLQFGHSQRVGYDVA
AmiC-E.coli      287  ATSTAAKYLAQTQNASDLIGGVS-----KSGDRYVDHTMFDMVQSLTIADSLKFG    III
AmiB-P.aeruginosa 288 ATSETARWLADSENRSDLIGGDGSV-SLGDKDQMLAGVLLDLSMTATLSSSLDVG
AmiB-S.flexneri  291  ANSEMASWLEQHEKLSELLGGAGDVLANSQSDPYLSQAVLDLQFGHSQRVGYDVA
AmiB-V.cholerae  274  ANTEIARWVENHEQQSELLGGAGEVLSKTNNDRNVSQTLLDLQFSHSQKEGYKVA


phi-phage        104  DVCKKISD-L-GFTNRGVKDGSGLY-VVKKTKAKSMLIEVCFVDSEDANKYL--S
phi3626          108  SIVDTIAAGT-GLKNRGVKVNPKLYE-LRKTSMPAVIVEVCFCEATEDVRIYK-E    I
phiC2            109  TRICDKLGTV---FKNRGAKLDKRLYILNSSKPTAVLIESFFCDNKEDYDKAKKL
PlyPSA-phage PSA 117  EISAKMAKAL-GLPNRGAKATKDLRF-LNSTKGTAVLLEVCFVDRKEDANAIHKS
CwlV-B.polymyxa  427  VMHKYFAPAT-GLTDRGIR-YGNFH-VIRETTMPAVLLEVGYLSNAKEEATLFDE
CwlC-B.subtilis  106  TIHSEVIQAV-DFADRGKK-TANFH-VLRESAMPALLTENGFIDTVSDANKLKTS    II
LytC-B.subtilis  426  QIQPKLAANL-GTRDRGVK-TAAFY-VIKYSKMPSVLVETAFITNASDASKLKQA
AmiB-B.henselae  328  NNVVSNLSKSHINLINNPHR-YADFQVLKAPDVPSVLIEIGYLSNKEDEKLLNNP
AmiA-E.coli      206  SHILKKIKPVH-KLHSRNTE-QAAFVVLKSPSVPSVLVETSFITNPEEERLLGTA
AmiB-E.coli      346  TSMISQLQRIG-EIHKRRPE-HASLGVLRSPDIPSVLVETGFISNNSEERLLASD    III
AmiC-E.coli      337  KAVLNKLGKIN-KLHKNQVE-QAGFAVLKAPDIPSILVETAFISNVEEERKLKTA
AmiB-P.aeruginosa 342 HKVLTNVGRIT-SLHKRRVE-QAGFMVLKSPDIPSILVETGFISNVNESRKLASA
AmiB-S.flexneri  346  TSMISQLQRIG-EIHKRRPE-HASLGVLRSPDIPSVLVETGFISNNSEERLLASD
AmiB-V.cholerae  329  TNILREMGKVA-HLHKTEPV-NASLAVLKSPDIPSVLVETGFISNPSEEKLLIQR
```

Figure 3.5. Multiple sequence alignment of different subclasses of amidases. The Pfam: Amidase_3 domain from the listed organisms were aligned using T-coffee (http::/tcoffee.crg.cat/apps/tcoffee/index.html). Black and grey boxes highlight identities and similarities, respectively. Residues that when substituted confer the ^{Lyt}AmiB phenotype are boxed in red. Positions corresponding to the residues important for catalysis (20, 17) (PDB 1JWQ) are highlighted in yellow.
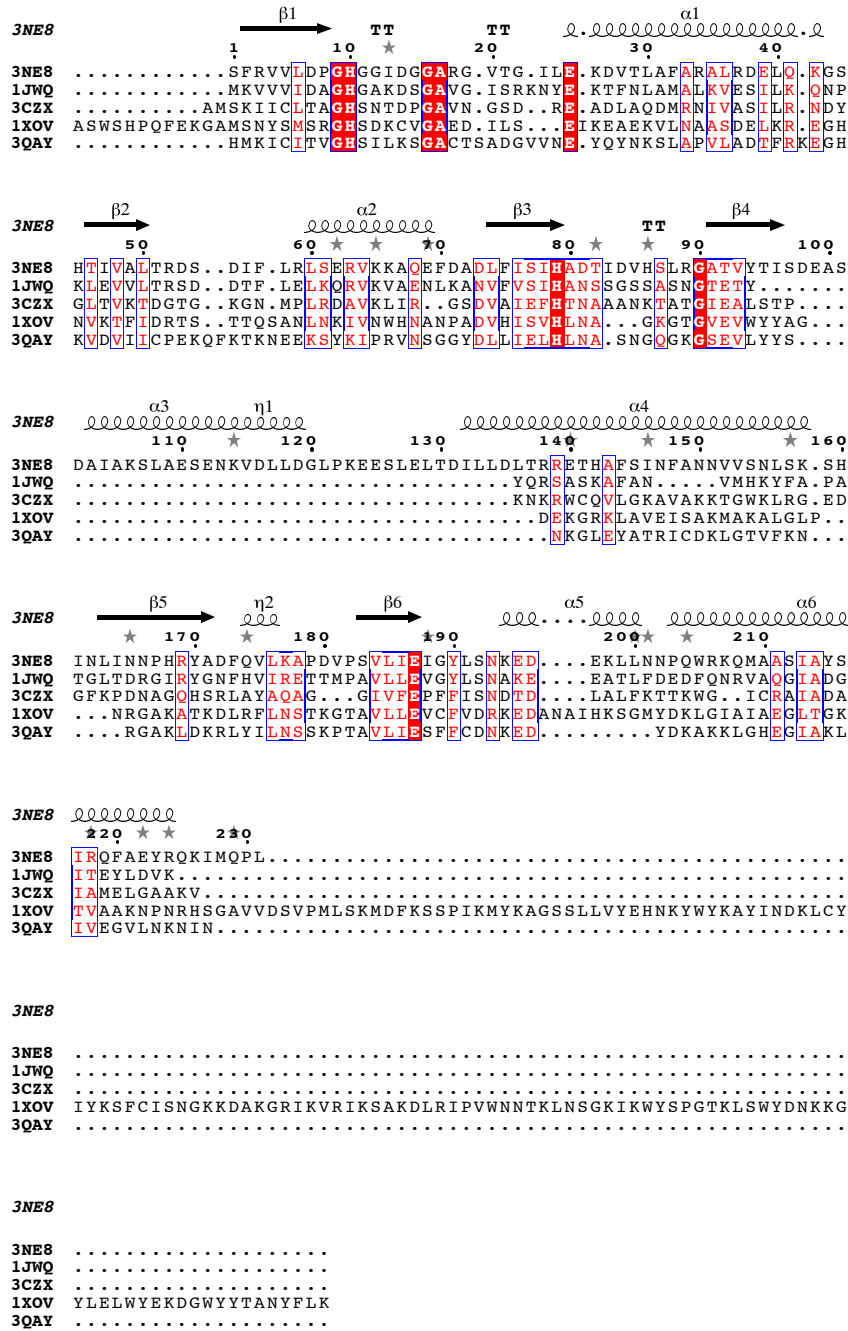
Structural analysis of an AmiB ortholog

The structures of several phage or mother cell lysis amidases have been solved: CD27L, PLY-PSA, and CwlV (17, 19) (PDB: 3QAY, 1XOV, 1JWQ). They are metallo-enzymes and all contain a Zn^{2+}-binding site in the middle of the cleft which is thought to be the catalytic center where the PG peptide substrate is presumably bound and cleaved (17, 19, 20) (Figure 3.6). The metal ion is coordinated by two histidines and one glutamic acid. These residues are highly conserved in LytC-type amidases and all of them have been demonstrated to be critical for catalysis (20). The Zn^{2+} ion in these structures is openly accessible and coordinated by a water molecule in addition to the residues in the active site cleft (17, 19) (Figure 3.6A). Thus, the activity of these enzymes is unlikely to be autoregulated.

Here we report the first structure of a predicted cell separation amidase, AmiB from *Bartonella henselae* ([BH]AmiB). The core structure of [BH]AmiB is similar to that of the lytic amidases (Figure 3.6A-B). A structural alignment between [BH]AmiB and CwlV yields a root mean square derivation value of 1.4Å over 167 amino acids even though their sequences identity is less than 35%. As in other amidases, the LytC-domain of [BH]AmiB is an α/β fold with a highly twisted central β-sheet that has an order of 2-1-3-6-4-5, in which the strands 4 and 5 are antiparallel to the others (Figure 3.6 and Figure 3.7). The β-sheet is flanked by four helices on one side, α1, consecutive α6 and α7, and an extensive α4. On the other side it is packed by two short parallel helices, α2 and α5. The packing of these two short helices helps create an extensive shallow cleft across the β-strands.

In the active site, the Zn^{2+} has an octahedral-like coordination with five short bonds (2.00-2.25Å) and one long bond (>2.55Å). In addition to the conserved two histidines and one
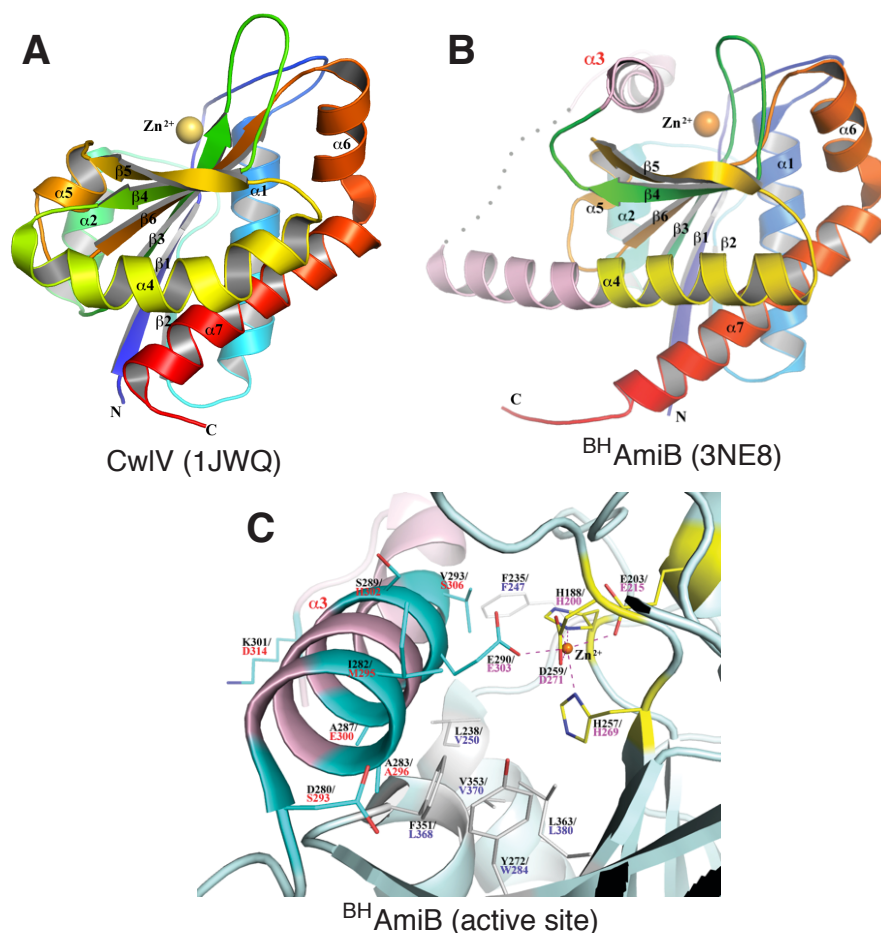
Figure 3.6. The structures of CwlV and ^{BH}AmiB. (**A**) A cartoon diagram of CwlV drawn in rainbow-colors with the N-terminus in blue and the C-terminus in red. The catalytic Zn^{2+} ion is drawn as a yellow sphere. All secondary structures are labeled. In numbering α-helices, α3 is skipped for the comparison to ^{BH}AmiB, which has an extra helix. Therefore, all corresponding secondary structures in CwlV and ^{BH}AmiB have the same numberings. The N- and C-termini are labeled as N and C, respectively. (**B**) A carton diagram of ^{BH}AmiB active domain drawn in similar rainbow-colors except of the insertion region, which is colored in light pink. The structurally disordered loop region between α3 and α4 helices is represented by a dotted line. The unique α3 helix is labeled in red. (**C**) The active site of ^{BH}AmiB is inactivated and blocked by α3 helix. All residues are drawn in stick format and the Zn^{2+} as an orange sphere. The Zn^{2+} is coordinated by H188, E203, H257, D259 (bidentate) and E290 with their carbon atoms drawn in yellow. Their corresponding residues in *E.coli* AmiB are provided underneath those of ^{BH}AmiB in magenta. The ^{BH}AmiB residues corresponding to those *E.coli* AmiB residues with their mutations reported in this report are drawn with their carbon atoms in cyan. The residue T315 of ^{BH}AmiB and its corresponding residue Q333 of *E.coli* AmiB are located in the N-terminal region of α4 helix and they are out of the view in this figure. The hydrophobic residues on the floor of binding cleft are also displayed.

```
                              β1
3NE8          ──────────────────►      TT        TT              ℓ.ℓℓℓℓℓℓℓℓℓℓℓℓℓℓ.ℓ
                        1         10   ★          20           30          40
3NE8    ............SFRVVLDPGHGGIDGGARG.VTG.ILE.KDVTLAFARALRDELQ.KGS
1JWQ    ............MKVVVIDAGHGAKDSGAVG.ISRKNYE.KTFNLAMALKVESILK.QNP
3CZX    ...........AMSKIICLTAGHSNTDPGAVN.GSD..RE.ADLAQDMRNIVASILR.NDY
1XOV    ASWSHPQFEKGAMSNYSMSRGHSDKCVGAED.ILS...EIKEAEKVLNAASDELKR.EGH
3QAY    ............HMKICITVGHSILKSGACTSADGVVNE.YQYNKSLAPVLADTFRKEGH


            β2                        α2              β3              β4
3NE8    ──────►              ℓℓℓℓℓℓℓℓℓ           ──────►      TT      ──────►
             50             60 ★    ★   70           80 ★      ★  90           100
3NE8    HTIVALTRDS..DIF.LRLSERVKKAQEFDADLFISIHADTIDVHSLRGATVYTISDEAS
1JWQ    KLEVVLTRSD..DTF.LELKQRVKVAENLKANVFVSIHANSSGSSASNGTETY.......
3CZX    GLTVKTDGTG..KGN.MPLRDAVKLIR..GSDVAIEFHTNAAANKTATGIEALSTP....
1XOV    NVKTFIDRTS..TTQSANLNKIVNWHNANPADVHISVHLNA...GKGTGVEVWYYAG...
3QAY    KVDVIICPEKQFKTKNEEKSYKIPRVNSGGYDLLIELHLNA.SNGQGKGSEVLYYS....


              α3             η1                              α4
3NE8    ℓℓℓℓℓℓℓℓℓℓℓℓℓ       ℓℓℓ                 ℓℓℓℓℓℓℓℓℓℓℓℓℓℓℓℓℓℓ
            110     ★    120          130        140     ★  150         ★ 160
3NE8    DAIAKSLAESENKVDLLDGLPKEESLELTDILLDLTRRETHAFSINFANNVVSNLSK.SH
1JWQ    ...................................YQRSASKAFAN.....VMHKYFA.PA
3CZX    ...................................KNKRWCQVLGKAVAKKTGWKLRG.ED
1XOV    ..................................DEKGRKLAVEISAKMAKALGLP..
3QAY    .................................NKGLEYATRICDKLGTVFKN...


            β5          η2         β6           α5               α6
3NE8    ──────►        ℓℓℓ      ──────►    ℓℓℓ...ℓℓℓℓ   ℓℓℓℓℓℓℓℓℓℓℓℓ
              ★   170     ★  180         190       200★    ★  210
3NE8    INLINNPHRYADFQVLKAPDVPSVLIEIGYLSNKED....EKLLNNPQWRKQMAASIAYS
1JWQ    TGLTDRGIRYGNFHVIRETTMPAVLLEVGYLSNAKE....EATLFDEDFQNRVAQGIADG
3CZX    GFKPDNAGQHSRLAYAQAG...GIVFEPFFISNDTD....LALFKTTKWG..ICRAIADA
1XOV    ...NRGAKATKDLRFLNSTKGTAVLLEVCFVDRKEDANAIHKSGMYDKLGIAIAEGLTGK
3QAY    ....RGAKLDKRLYILNSSKPTAVLIESFFCDNKED.........YDKAKKLGHEGIAKL


3NE8    ℓℓℓℓℓℓℓℓ
            220 ★   ★     230
3NE8    IRQFAEYRQKIMQPL.........................................
1JWQ    ITEYLDVK...............................................
3CZX    IAMELGAAKV.............................................
1XOV    TVAAKNPNRHSGAVVDSVPMLSKMDFKSSPIKMYKAGSSLLVYEHNKYWYKAYINDKLCY
3QAY    IVEGVLNKNIN............................................


3NE8
3NE8    .......................................................
1JWQ    .......................................................
3CZX    .......................................................
1XOV    IYKSFCISNGKKDAKGRIKVRIKSAKDLRIPVWNNTKLNSGKIKWYSPGTKLSWYDNKKG
3QAY    .......................................................


3NE8
3NE8    ....................
1JWQ    ....................
3CZX    ....................
1XOV    YLELWYEKDGWYYTANYFLK
3QAY    ....................
```

Figure 3.7. Secondary structure of AmiB from *Bartonella henselae* and sequence alignment with several other LytC-type amidases. The topmost line denotes the secondary structure of 3NE8 (AmiB *Bartonella henselae*). α, alpha-helices; β, beta-sheets, TT, turn turn; 3NE8, AmiB *Bartonella henselae*; 1JWQ, CwlV *Bacillus polymyxa*; 3CZX, amidase *Nisseria meningitidis*; 1XOV, PlyPSA bacteriophage PSA of *Listeria monocytogenes*; 3QAY, CD27L *Clostridia difficile*.

glutamate also found in unregulated amidases, an aspartate (D259 of BH-amidase) forms

bidentate bonds (one short and one long bonds) to Zn^{2+}, replacing two coordinating water

molecules, for example, in CwlV. The aspartate is conserved in all regulated amidases while it is

substituted by an asparagine in most unregulated amidases. The sixth coordinate of the Zn^{2+} in

the [BH]AmiB is contributed by a glutamic acid (E290 of [BH]AmiB) from the regulation α3 helix,

which is packed parallel onto the presumably PG-binding cleft. In this way, the helix completely

buries the catalytic Zn^{2+}-binding site as well as blocks the access to the cleft by substrate (Figure

3.6B).

The PG-binding cleft is rich in hydrophobic residues (Figure 3.6C). The α3 helix is quite

amphipathic with a polar side and a non-polar side. The Zn^{2+}-binding E290 of [BH]AmiB is the

only polar residue on the non-polar side of the helix. It is the non-polar side of the helix that sits

on the PG-binding cleft, creating a predominant hydrophobic interaction between the regulation

helix and the PG-binding cleft. The binding of the glutamate (E290 of [BH]AmiB) to Zn^{2+} is the

only conserved specific interaction, seemingly helping position the helix on the cleft. From the

sequences alignment of the "regulated" amidases, we predicted that the ~50 amino acid

insertions of these enzymes have similar conformations, characterized by an extra regulation

helix, which may serve as a "plug" to keep the active site of AmiB inactive and inaccessible to

substrate.

Strikingly, and in perfect agreement with the genetic analysis, the region of [BH]AmiB

corresponding to the ~50 amino acid insertion identified in cell separation amidases is in part

composed of a helical domain (α3, D280-L296) that completely buries the active site Zn^{2+} ion

and occludes the active site cleft (Figure 3.6 and Figure 3.7). The insertion domain then

continues from α3 to include an unstructured loop region and the first half of the extended α4 helix. This is in contrast to amidases without the insertion domain in which the β4 strand is directly linked to a much shorter α4 helix as observed, for example, in CwlV (Figure 3.6 and Figure 3.7). The α3 helix is amphipathic with the non-polar face inserting into the predominantly hydrophobic active site cleft. There are only four hydrogen bonds across the interface between the α3 helix and the active site. They as well as the salt bridges involving D280 of [BH]AmiB at the beginning of the α3 helix are not conserved in the insertion domains of other cell separation amidases. Thus, the overall association between the α3 helix and PG-binding groove is largely composed of non-specific hydrophobic interactions except for Zn^{2+}-binding by the conserved glutamate residue of the helical insertion (E290 of [BH]AmiB), which replaces the coordinating water molecule observed in structures of the phage and sporulation amidases.

Importantly, mapping the amino acid substitutions found in the [Lyt]AmiB variants onto the [BH]AmiB crystal structure show that these residues are primarily located on helix α3. Moreover, the majority of these residues are also found on the face of α3 that is interacting with the active site cleft. When modeled in the structure, the substituting residues, especially the positively charged lysines and arginine, likely cause α3 to fit poorly into the active site cleft and are predicted to destabilize the cleft-helix interaction. Additionally, in the case of the E303K substitution, the conserved glutamate that coordinates the active site Zn^{2+} is converted to a basic residue that is likely to have an unfavorable electrostatic interaction with the positively charged metal ion. Thus, in most cases, the [Lyt]AmiB variants are predicted to have a destabilized cleft-helix interaction. The tight correspondence between the genetic and structural data, as well as

the conservation of the regulatory domain among predicted cell separation amidases, strongly suggests that these enzymes are autoinhibited by a regulatory helix analogous to α3 in [BH]AmiB. Furthermore, the results imply that the LytM-domain activators must somehow promote the release of the regulatory helix from the active site cleft to stimulate amidase activity.

[Lyt]AmiB variants have elevated basal activity *in vitro*

The [BH]AmiB structure indicates that the interaction between the regulatory helix and the active site cleft is likely to be weakened in the *E. coli* [Lyt]AmiB variants. These enzymes should therefore have active sites that are more accessible and thus have higher basal PG hydrolase activities. To test this, we purified three of the most toxic [Lyt]AmiB variants [AmiB(S293R), AmiB(E300K), and AmiB(E303K)] as well as a variant containing all three substitutions [AmiB (triple)] and compared their basal activities to the wild-type enzyme using a dye-release assay for PG hydrolysis in which the liberation of dye from labeled PG is a reflection of PG hydrolase activity. PG sacculi covalently labeled with Remazol Brilliant Blue (RBB) were incubated with the amidases (2 µM) at 37°C for 30 min. Undigested PG was pelleted by centrifugation and the absorbance of the supernatants was measured at 595 nm. As observed previously, AmiB(WT) led to minimal dye release in the absence of activation (Figure 3.8A). The [Lyt]AmiB variants with single substitutions in the regulatory helix were all found to have increased basal activity compared to AmiB(WT) (Figure 3.8A). The effects of the single substitutions were additive with AmiB(triple) displaying roughly three times the basal activity of the [Lyt]AmiB variants identified in the enrichment (Figure 3.8A). Basal PG hydrolytic activity is therefore inversely correlated
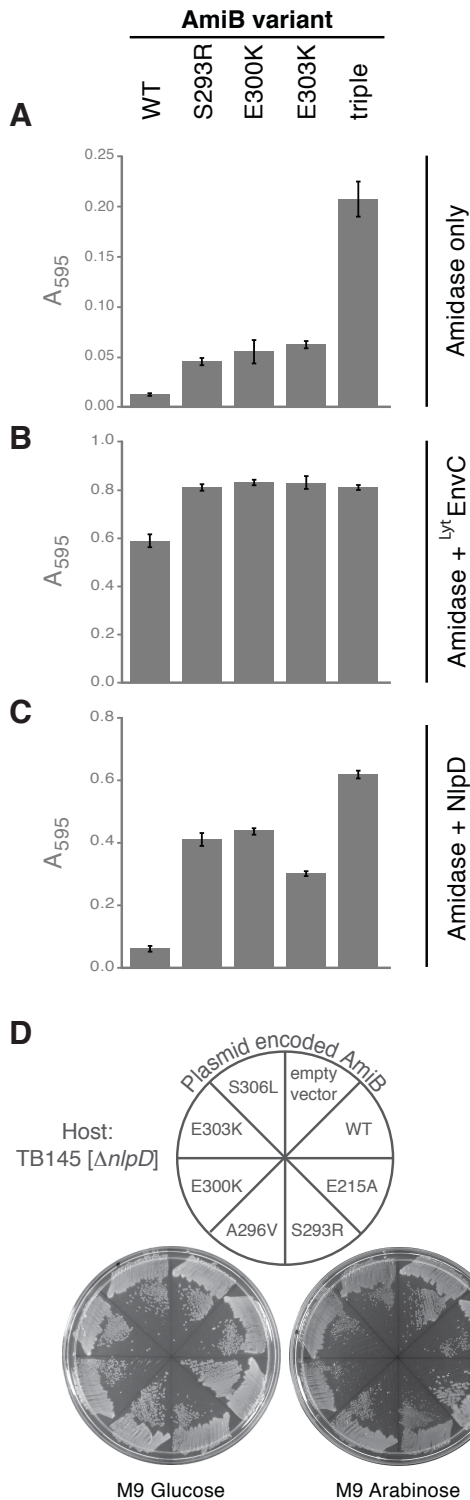
Figure 3.8. [Lyt]AmiB variants have elevated basal PG hydrolase activity. (**A**) Dye-release assays measuring basal PG hydrolase activity of the [Lyt]AmiB variants relative to AmiB(WT). The variant referred to as "triple" is AmiB (S293R, E300K, E303K). The indicated proteins ($2\ \mu$M) were incubated with RBB-labeled PG at 37°C for 30 min. Undigested PG was pelleted by centrifugation and the absorbance of the supernatants was measured at 595 nm. Reactions were performed in triplicate and the error bars indicate the standard deviation. (**B-C**) Same as in (**A**) except [Lyt]EnvC ($2\ \mu$M) or NlpD ($2\ \mu$M) were combined with the amidases. Supernatants from control reactions containing [Lyt]EnvC only ($2\ \mu$M), NlpD only ($2\ \mu$M), lysozyme ($4\ \mu$M) or buffer alone had the following A_{595} readings (average +/- std. dev.): 0.02 +/- 0.002, 0.04 +/- 0.008, 0.56 +/- 0.022 and 0.007 +/- 0.002. (**D**) TB145 [$\Delta nlpD$] cells carrying an empty vector or expression constructs encoding AmiB (WT), AmiB(E215A) or the indicated [Lyt]AmiB variants were struck out on M9-CAA-Cm[10] agar containing either 0.2% glucose or 0.2% arabinose. Plates were incubated overnight at 37°C and photographed.

with the apparent stability of the regulatory helix-active site cleft interaction.

All of the [Lyt]AmiB variants tested retained the ability to be activated by the LytM domain of EnvC [[Lyt]EnvC] and possessed slightly higher activity levels following activation than the wild-type enzyme (Figure 3.8B). Strikingly, unlike AmiB(WT), which can only be activated by EnvC, the [Lyt]AmiB variants were also activated by the non-cognate LytM factor, NlpD (Figure 3.8C). This observation suggests that the apparent stability of the regulatory helix-active site cleft interaction is an important determinant of the specificity of the amidases for their cognate LytM activators. The observed mis-activation appeared to be physiologically relevant as the [Lyt]AmiB variants with single substitutions required NlpD activity to elicit cell lysis (Figure 3.8D and Figure 3.9A-C). AmiB(triple), on the other hand, was capable of inducing lysis of both WT and NlpD⁻ cells (Figure 3.9A-C). Thus, a threshold level of mis-regulated amidase activity appears necessary for the induction of cell lysis. In WT cells this is accomplished by the aberrant activation of the [Lyt]AmiB variants by a non-cognate LytM activator. However, given enough basal activity, as in the case of AmiB(triple), lysis can be induced independently of the activators.

The autoinhibition mechanism for amidase regulation is conserved

We tested the potential conservation of the amidase autoregulatory mechanism by mutating *E. coli amiA* and *Vibrio cholerae amiB* ([VC]*amiB*) so that they encoded enzymes with the equivalent substitution as the [Lyt]AmiB variant AmiB(E303K) (Figure 3.11A). Production of the wild-type versions of each enzyme was not lethal. However, AmiA(E167K) and [VC]AmiB (E286K) were lethal in both WT and NlpD⁻ cells (Figure 3.11B-C). Purified AmiA(E167K) had

elevated PG hydrolase activity *in vitro* relative to AmiA(WT) (Figure 3.11D). As for the

^{Lyt}AmiB variants, AmiA(E167K) retained the ability to be activated by EnvC (Figure 3.11E). It

was also mis-activated by the non-cognate NlpD activator (Figure 3.11F), underscoring the likely

role of the regulatory helix-active site interaction in determining amidase-activator specificity.

Interestingly, the basal activity of AmiA(E167K) approached that of AmiB(triple). This

relatively high basal activity is probably responsible for the NlpD-independence of AmiA

(E167K) toxicity *in vivo*. Unfortunately, solubility problems prevented us from purifying

^{VC}AmiB and ^{VC}AmiB(E286K) to test their basal activities. Nevertheless, their behavior *in vivo*,

combined with the genetic, structural, biochemical, and bioinformatic results for the other

amidases, strongly supports the idea that there is a conserved conformational control mechanism

governing cell separation amidase activity at the cytokinetic ring of *E. coli* and related Gram-

negative bacteria.


Section 3.4: Discussion

Septal murien splitting by PG hydrolases during cell division is a delicate process and

bacteria must employ numerous control mechanisms to regulate these enzymes in order to avoid

unwanted disasters. In *E. coli,* the LytC-type *N*-acetylmuramyl-L-alanine amidases - AmiA,

AmiB and AmiC - are critical for cell division along with their cognate activating LytM factors,

EnvC and NlpD (6, 10-12, 21). Until now a detailed mechanism of amidase activation by the

LytM factors had yet to be elucidated. Therefore, to begin investigating how the LytM factors

stimulate amidase activity *in vivo* we set out to isolate poorly regulated (lytic) variants of AmiB

(^{Lyt}AmiB). We reasoned that identification of such variants would support a model where the
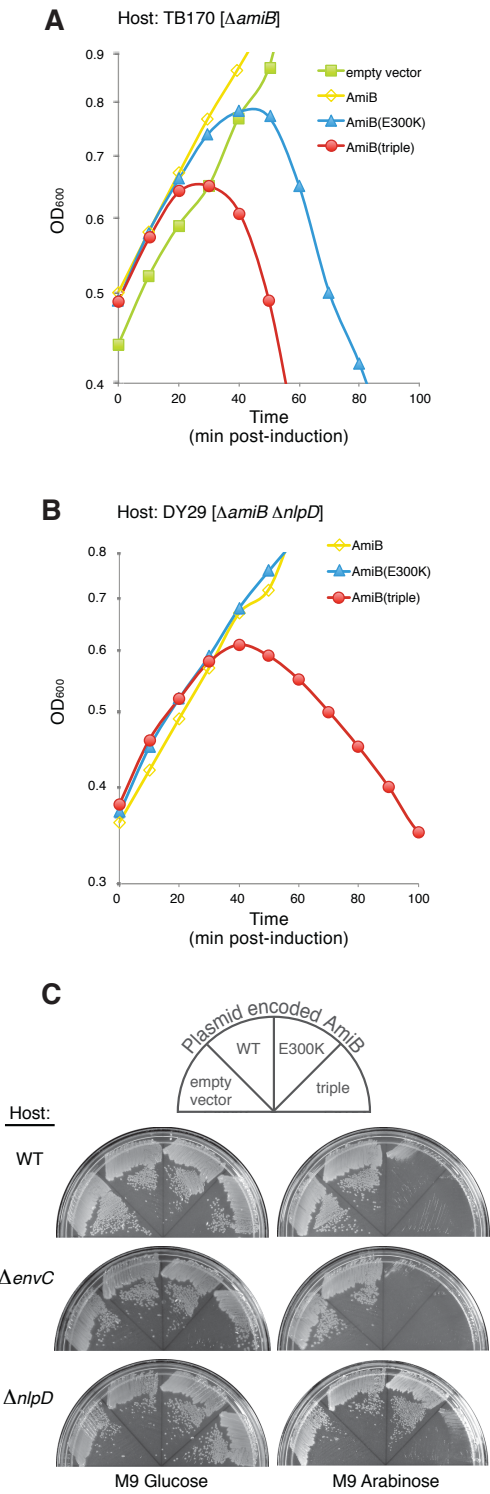
Figure 3.9. AmiB(triple) lacks an NlpD requirement for lysis induction. (**A**) TB170 [$\Delta amiB$] cells carrying an empty vector or expression constructs encoding AmiB (WT), AmiB(E300K), or AmiB(triple) were grown at 37°C in M9-CAA-Cm^{10} medium supplemented with 0.2% maltose to an OD$_{600}$ of 0.4-0.5. At $t = 0$, arabinose was added to a final concentration of 0.2% and growth was monitored by following culture OD$_{600}$. Samples for immunoblot analysis were taken just prior to lysis at $t = 30$ (see Figure 3.10). (**B**) DY29 [$\Delta amiB$ $\Delta nlpD$] cells carrying an empty vector or expression constructs encoding AmiB (WT), AmiB(E300K), or AmiB(triple) were grown at 37°C in M9-CAA-Cm^{10} medium supplemented with 0.2% maltose to an OD$_{600}$ of 0.4-0.5. At $t = 0$, arabinose was added to a final concentration of 0.2% and growth was monitored by following culture OD$_{600}$. Samples for immunoblot analysis were taken just prior to lysis at $t = 40$ (see Figure 3.10). (**C**) TB28 [WT], TB140 [$\Delta envC$], or TB145 [$\Delta nlpD$] carrying an empty vector or expression constructs encoding AmiB (WT), AmiB (E300K), or AmiB(triple) were struck out on M9-CAA-Cm^{10} agar containing either 0.2% glucose or 0.2% arabinose. Plates were incubated overnight at 37°C and photographed. triple = AmiB(S293R, E300K, E303K).

123
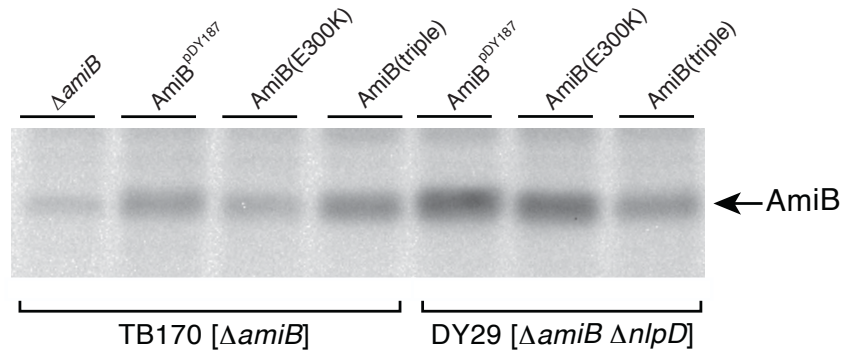
Figure 3.10. AmiB(triple) accumulates to levels similar to other ^{Lyt}AmiB variants and AmiB (WT). Cells of TB170 [Δ*amiB*] or DY29 [Δ*amiB* Δ*nlpD*] were grown as described in the legend for Figure 3.9A-B. At $t = 30$ or 40 min respectively, cells were harvested for whole-cell extract preparation. AmiB variants were detected as described in Figure 3.3. 1.5 μg of total protein was loaded into each lane.
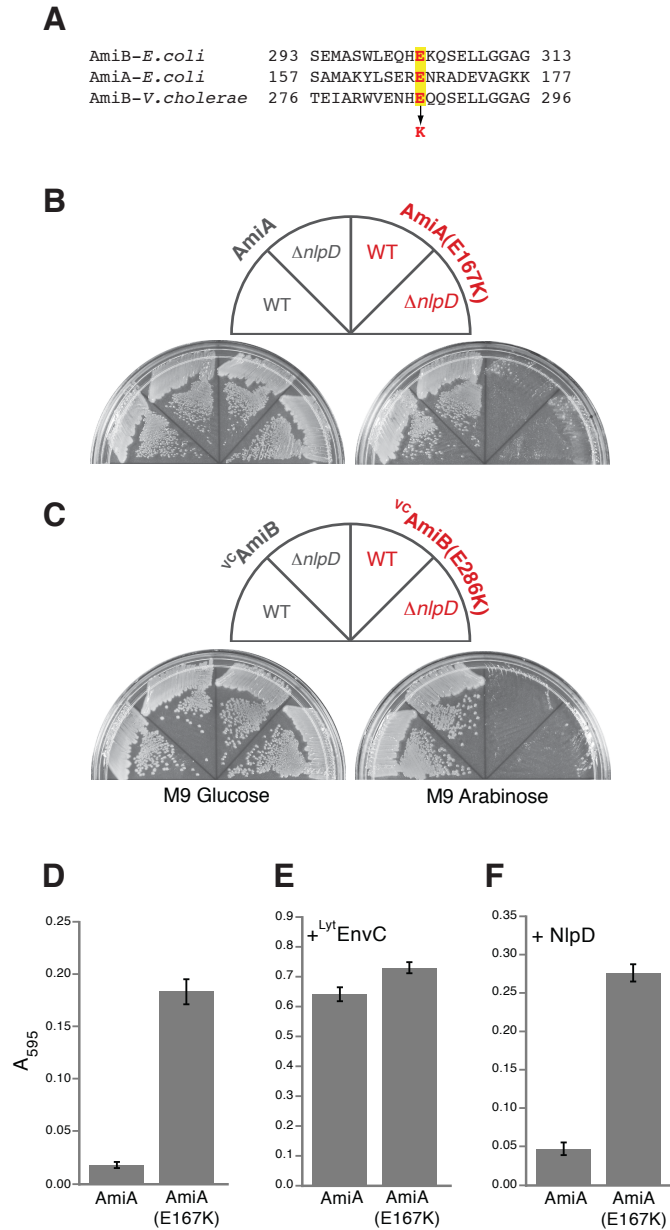
Figure 3.11. Lytic and PG hydrolase activities of other amidases with substitutions in their regulatory domains. (**A**) Sequence alignment of a portion of the regulatory domains of *E. coli* AmiB, *E. coli* AmiA, and *V. cholerae* AmiB (VCAmiB). The highlighted glutamatic acid (E) residues in red were changed to lysines (K) in AmiA and VCAmiB to yield AmiA(E167K) and VCAmiB(E286K), respectively. (**B-C**) As indicated, TB28 [WT] or TB145 [Δ*nlpD*] cells carrying AmiA, AmiA(E167K), VCAmiB, or VCAmiB(E286K) were struck out on M9-CAA-Cm[10] agar containing either 0.2% glucose or 0.2% arabinose. Plates were incubated overnight at 37°C and photographed. (**D**) Dye-release assay measuring basal PG hydrolase activity for AmiA (E167K) relative to AmiA (WT). Assays were performed as described in Figure 3.8 except that reactions contained 1 μM amidase with or without an additional 1 μM of purified LytM factor.

125

LytM factors exert their regulatory control by allosterically activating the amidases.

Using a genetic enrichment strategy we isolated a number of lytic *amiB* mutants and the amino acid changes in these [Lyt]AmiB variants resulted in increased basal PG hydrolase activity *in vitro* and induced lysis when expressed in cells. Interestingly, almost all of the mutations mapped to a region of *amiB* found only in cell separation amidases and structurally corresponds to an alpha-helix that obstructs the amidase active site, effectively serving as an autoinhibitory domain. We predict that the [Lyt]AmiB lesions have a destabilizing effect on this active site cleft-helix interaction and in accordance with this prediction purified [Lyt]AmiB variants have increased basal PG hydrolase activity *in vitro* compared to AmiB(WT). Additionally, follow-up experiments suggest that the interaction strength of the alpha-helix and active site cleft influences the specificity between each LytM activator-amidase pair.

Taken together, these results suggest that the LytM factors activate the amidases by stimulating the displacement of this regulatory helix to allow for amidase activity. This mechanism of conformational regulation appears to be conserved in other cell separation amidases as analogous amino acid substitutions in AmiA from *E. coli* or AmiB from *Vibrio cholerae* ([VC]AmiB), result in lytic variants and elevated PG hydrolase activity *in vitro*. In total, the findings presented here support a model where the LytM activators allosterically activate the amidases by inducing a conformational change that displaces a regulatory alpha-helix domain that occludes the active site cleft (Figure 3.12). These exciting results most likely represent a general control mechanism used to regulate PG hydrolase activity during important cellular processes that require modifications to PG.

Because of their potentially lethal activity, strict control mechanisms governing the activity of cellular PG hydrolases have long been postulated. Most of the regulatory strategies that have been characterized thus far function at the level of gene expression to control the amounts of PG hydrolases produced and/or the production of PG hydrolase inhibitors. For example, the transcriptional regulation of lytic PG hydrolases critical for spore-formation and germination are controlled by sporulation-specific sigma factors that restrict the production of these enzymes to a specific subcellular location and developmental stage during the sporulation process (22, 23). Additionally, the two component-system WalRK is an important transcriptional regulator for cell wall homeostasis in Gram-positive bacteria, which activates expression of genes encoding cell separation PG hydrolases and represses the expression of their inhibitors (14, 24-34).

However, additional post-translational mechanisms must be in place to regulate the activity of these enzymes once they are produced and although a few general regulatory strategies have been described, the mechanistic details are not well defined. For example, it has been postulated that in the cell, multi-enzyme complexes, containing PG synthases and PG hydrolaes, function to coordinate the activities of these enzymes (35, 36). Detection of PG synthase-PG hydrolase interactions have been reported in both Gram-positive and Gram-negative bacteria (37-40), but the functional consequence of such associations are still indeterminate.

Although the role that multi-enzyme complexes have on regulating PG hydrolases remains unclear, it has been demonstrated that some PG hydrolases are produced in an inactive form and must be proteolytically processed for activation (41-45), such as the lysostaphin-type metalloendopeptidases (42). A similar mechanism of activation has been proposed for RipA, an
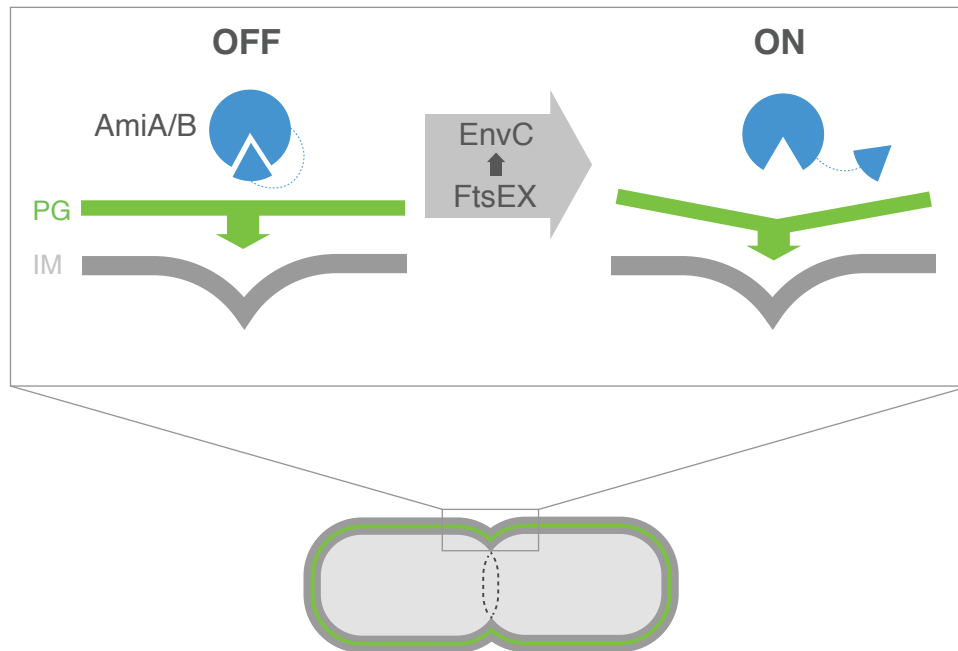
Figure 3.12. Conformational control of amidase activity during cell division. Shown is a schematic of a dividing cell with an assembled divisome apparatus (dotted circle). The box depicts a model for amidase activation during the division process. Prior to the initiation of septal PG splitting, AmiA and AmiB are held in an inactive conformation by an auto-regulatory domain that occludes the active site cleft (blue wedge). The initiation of septal PG splitting appears to be controlled by the FtsEX ABC system. Conformational changes brought about by FtsE-mediated ATP hydrolysis in the cytoplasm are thought to be communicated to EnvC via FtsX. These changes are in-turn thought to be transmitted to the amidases to ultimately displace the auto-regulatory domain from the amidase active site and promote PG cleavage. The process is thought to be discrete and cyclical such that a fixed number of PG cleavage events are activated per ATP hydrolyzed by FtsE. The mechanisms by which the putative conformational changes are transmitted between FtsX and EnvC or EnvC and the amidases remain to be determined. For simplicity, the outer membrane was omitted from the diagram. IM, inner membrane; PG, peptidoglycan.

endopeptidase from *Mycobacterium tuberculosis*, although there is some controversy as to whether cleavage of the N-terminal segment which occludes the active site is necessary for RipA activity (44, 46). However, what is apparent based on the crystal structures of RipA is that the N-terminal segment must be displaced, either by proteolytic processing or a conformational change, in order to allow for substrate binding (44, 46).

The idea of conformational regulation offers an attractive and potentially robust mechanism for controlling PG hydrolase activity. Nevertheless, up until now supporting experimental evidence to demonstrate this mode of control has been limited and ambiguous (i.e. RipA activation). By isolating unregulated AmiB variants we were able to identify a regulatory domain found only in cell separation amidases. A portion of this regulatory domain consists of an alpha-helix that occludes the amidase active site, essentially leading to an inactive enzyme. However, this autoinhibition can be relieved and the data presented here support a model where the LytM factors act by inducing a conformational change that displaces the regulatory domain and results in amidase activation. Such conformationally-based regulation is particularly appealing for a number of different reasons: (1) it would provide a direct and specific mechanism for control over PG hydrolase activity, (2) such a system can be made responsive to signals that can couple PG hydrolysis with other activities in the cell (see below), and (3) this mode of regulation provides another "fail-safe" to prevent unbridled PG hydrolysis since the default state of these enzymes is to be inactive.

These findings demonstrate that bacteria implement many layers of control over PG hydrolase activity. We recently discovered that the LytM activator EnvC is directly recruited to the division site by FtsEX, an ABC-transporter like complex and known divisome component

(7). In addition to recruiting EnvC to the septal ring, we believe that FtsEX is conformationally

regulating the ability of EnvC to activate its cognate amidases (7). Put into the context of our

work here, we propose a model where FtsEX directly regulates EnvC-activation of the amidases;

in turn, EnvC regulates the amidases by inducing a conformational change which displaces a

regulatory domain that occludes the active site, thus allowing amidase activity. Intriguingly, a

FtsE-FtsZ interaction has been reported (47), therefore this model could potentially provide a

mechanism for directly coupling the activities of the divisome apparatus with septal PG splitting

in the periplasm. Moreover, it appears that this system is likely to be more broadly conserved in

both Gram-negative and Gram-positive bacteria since an analogous connection was described in

S. pneumoniae, where FtsEX in this organism directly interacts with the essential cell separation

factor PcsB (13, 14).

Although we are beginning to dissect the mechanistic control necessary to keep these

potentially lethal enzymes in check there are still many unanswered questions that have yet to be

addressed. In the case of the *E. coli* LytC-type amidases, which are critical for cell division, we

lack molecular mechanistic insight underlying amidase activation by the LytM factors. How the

LytM factors promote the conformational change in the amidases that allows them to be active is

currently unclear. Therefore, characterizing the exact interface of a LytM-amidase complex will

be paramount to determining a detailed mechanism of activation. Additionally, our findings

suggest that the affinity between the active site cleft and regulatory alpha-helix domain may play

a role in dictating the specificity of cognate LytM-amidase pairs. However, follow-up

experiments will be required to fully elucidate these determinants and the efforts described

above, to define where the LytM factors and amidases interact and bind, will likely illuminate how this specificity is achieved.

In addition to EnvC, *E. coli* possesses another LytM factor important for cell division NlpD, the regulation of which is poorly understood (6, 12). Unlike EnvC which is a periplasmic protein associated with the inner membrane via its interaction with FtsEX, NlpD is an outer membrane lipoprotein which suggests that its mode of regulation is distinct from that of EnvC. Efforts are currently ongoing to determine how NlpD is regulated and what recruits it to the divisome. Along these lines, we are also actively investigating what factors recruit the amidases (AmiB and AmiC) to the septal ring. Uncovering these recruitment factors and how NlpD is controlled will be a vital component to understanding how septal PG splitting is coordinated with other activities carried out by the divisome.

PG hydrolases have the power to destroy bacterial cells as illustrated by phage lysins which lyse host cells in order to release newly-made virions. Nevertheless, further investigation into the strategies bacteria use to control these potentially lethal enzymes during the process of cell division and other cellular activities will undoubtably reveal new and exciting mechanisms of regulation. Because PG is an essential and unique component to bacteria, its biogenesis has been an important antimicrobial target. Indeed, some of our most effective antibiotics, like the β-lactams, specifically inhibit PG synthesis. Nonetheless, efforts to harness the potential power of PG hydrolases as a new source of antibacterial agents has yet to be realized. Interestingly, the human innate immune system utilizes lysozyme to help prevent bacterial infections. This poses the question of whether we can also exploit PG hydrolase biology in the effort to find new antibiotics. It may be feasible to identify small molecules that disrupt the mechanisms that

control PG hydrolase activity to induce cell lysis. Therefore, continued efforts to understand the mechanistic regulation of PG hydrolases will be paramount in transforming them into novel antimicrobial therapeutics.

Section 3.5: Material and methods

Media, bacterial strains and plasmids

Cells were grown in LB [1% tryptone, 0.5% yeast extract, 0.5% NaCl] or minimal M9 medium (48) supplemented with 0.2% casamino acids and 0.2% sugar (glucose, arabinose or maltose as indicated). Unless otherwise indicated, antibiotics were used at 10 (chloramphenicol; Cam), 15 (ampicillin; Amp) or 20 (kanamycin; Kan) μg/ml.

The bacterial strains are listed in Table 3.3. All *E. coli* strains used in the reported experiments are derivatives of MG1655. Plasmids used in this study are listed in Table 3.4. Vectors with R6K origins are all derivatives of the CRIM plasmids developed by Wanner and co-workers (49). They were either maintained in the cloning strain DH5α(*λpir*) where they replicate as plasmids, or they were integrated into the λ phage attachment site using the helper vector pInt-ts (49) as described previously (49).

Mutagenesis and plasmid release enrichment

Two independent mutant libraries were constructed by specifically mutagenizing the *amiB* gene encoded in pDY187 (P$_{ara}$::*amiB*) using the GeneMorph II EZClone Domain Mutagenesis Kit (Agilent Technologies). The forward 5'-AAAATCTAGAGCCGGTTAACCTTTGAAAGGTGGC-3' and reverse 5'-

GTCAAAGCTTGACCTGAATTGGCATCAATCGTCC-3' primers were used to amplify *amiB*

from pDY187 using error-prone Mutazyme II DNA polymerase. The resulting PCR products

were purified using the Qiaquick PCR purification kit (Qiagen) and subsequently used as

"megaprimers" that are denatured and annealed to the original donor plasmid (pDY187) to

amplify the vector backbone using the high fidelity EZClone enzyme mix. The completed

reactions were then subjected to DpnI-digestion to eliminate any remaining, non-mutagenized

donor plasmid DNA (pDY187) leaving intact plasmids carrying mutations in the *amiB* gene.

Both libraries where then transformed into NEB 5-alpha electrocompetent cells, plated on LB

plates supplemented with 10 μg/ml chloramphenicol (Cm^{10}) and glucose and allowed to incubate

overnight at 30°C. The following day the colonies were scraped up into LB broth and the

plasmid DNA was isolated using the Qiaprep miniprep kit (Qiagen). Again, both libraries were

then transformed into electrocompetent TB28 cells, plated on LB plates supplemented with 10

μg/ml chloramphenicol (Cm^{10}) and glucose and allowed to incubate overnight at 30°C. The

following day the colonies were scraped up and re-suspended to an OD_{600} of 0.04 in LB broth

supplemented with 10 μg/ml chloramphenicol (Cm^{10}) and grown at 37°C. Once the cultures

reached an OD_{600} of ~0.3 arabinose was added for a final concentration of 0.2% and growth was

continued for an additional 3 hours at 37°C. The cultures (5 ml each) were then iced for 5

minutes and centrifuged at 4°C for 10 minutes at 4000 x *g* to remove unlysed cells and debris.

The supernatants were then passed through 0.2 μm syringe filters before 5x (25 ml) PB buffer

was added (Qiagen). Each mixture was then passed through a Qiaprep spin column (Qiagen)

using a vacuum manifold and washed with additional PB and PE buffers as described for a

standard miniprep protocol. The plasmid DNA was the eluted into TE buffer. Electrocompetent

TB28 cells were then transformed with the isolated plasmid DNA library and plated on LB plates supplemented with 10 μg/ml chloramphenicol (Cm[10]) and glucose and allowed to incubate overnight at 30°C. 116 isolates were then struck on M9 media with 10 μg/ml chloramphenicol (Cm[10]) supplemented with either glucose or arabinose and incubate overnight at 37°C.

Growth Curves

Please see figure legends for details about growth conditions and sample preparation methods used for specific experiments.

Protein purification

All proteins were overexpressed and purified with a 6xHis-SUMO (H-SUMO) tag fused to their N-termini (50, 51). The sequence of the affinity tag in all cases was MRGSHHHHHHMASG. The SUMO sequence was amplified from the *Saccharomyces cerevisiae* genome (gene Smt3) as described earlier (52). After purification of the H-SUMO fusion protein by metal-affinity chromatography, the H-SUMO tag was removed using 6xHis-tagged SUMO protease (H-SP) (52). Cleavage reactions were passed through Ni-NTA resin to remove free H-SUMO and H-SP, yielding a pure preparation of the desired protein. Except for [Lyt]EnvC which contained no non-native residues, all the remaining proteins had an additional dipeptide SA at their N-termini.

[Lyt]EnvC, NlpD, AmiA, AmiA(E167K), AmiB, AmiB(S293R), AmiB(E300K), AmiB (E303K) and AmiB(S293R, E300K, E303K) were purified from BL21(λDE3) containing pTU104, pTU119, pDY278, pDY277, pDY279, pDY242, pDY81, pDY245 and pDY276,

respectively. Overnight cultures were diluted 1:100 into 1 L of LB supplemented with ampicillin

(50 μg/ml) and glucose (0.04%) and cells were grown at 30°C for 3.5 hours to an OD600 of

~0.5-0.7. IPTG was then added to 1 mM, growth was continued for an additional 3.5 hours, and

the cells were harvested by centrifugation. Cell pellets were resuspended in 40 ml buffer A (50

mM Tris-HCl (8.0), 300 mM NaCl, 10% glycerol) with 20 mM imidazole, split into two 10 ml

aliquots, and stored at -80°C prior to use for protein purification. For purification, a 10 ml

aliquot (0.5 L of culture) was thawed, and the cells were disrupted by sonication. Cell debris and

membranes were pelleted by centrifugation at 100,000 x g for one hour at 4°C. H-SUMO

fusions were purified using 1 ml Ni-NTA agarose resin (Qiagen) according to the instructions.

Resin was equilibrated in buffer A with 20 mM imidazole, washed with buffer A containing 50

mM imidazole twice and then buffer A containing 100 mM twice. The fusion proteins were

eluted with buffer A containing 300 mM imidazole. The purified H-SUMO fusions were cleaved

using a 1:1000 of H-SP preparation (6) and dialyzed overnight in buffer A containing 20 mM

imidazole at 4°C. The following morning the protein preparation was then passed over 1 ml Ni-

NTA agarose resin (Qiagen). Isolated untagged proteins were dialyzed three times against and

stored in buffer A at -80°C, except NlpD which was stored in 50 mM Mops-NaOH (pH 7.1)

300mM NaCl, 10% glycerol.

Protein crystallization and X-ray structure determination

For structural characterization of the *N*-acetylmuramyl-L-alanine amidase catalytic

domain, a part of the *Bartonella Henselae str. Houston-1 amiB* gene encoding the C-terminal

[BH]AmiB from residues S179 to L409 was cloned into vector pMCSG19B, generating the

expression construct pAPC62366.1. The gene was overexpressed in *E. coli* BL21(λDE3) cells. The cells were grown at 37°C in seleno-methionine (SeMet) containing enriched M9 medium under conditions known to inhibit methionine biosynthesis (53). The SeMet-labeled [BH]AmiB protein was purified from the *E. coli* cells using Ni-affinity chromatography as described earlier (54). After the protein was concentrated in the buffer of 20 mM HEPES pH 8.0, 250 mM NaCl, and 2 mM dithiothreitol (DTT), it was screened for crystallization conditions using the sitting drop vapor diffusion technique. Diffraction quality crystals appeared under the condition of 0.1 M Bis-Tris propane, 1.8M sodium acetate pH 7.0 at 16°C. Prior to X-ray data collection, crystals were treated with cryoprotectant (25% glycerol) added to crystallization buffer and were flash-frozen directly in liquid nitrogen.

A set of single-wavelength anomalous diffraction (SAD) data was collected near selenium absorption peak at the temperature of 100 K from a single SeMet labeled crystal. The data were obtained at the 19ID beamline of the Structural Biology Center at the Advanced Photon Source at Argonne National Laboratory using the program SBCcollect. The [BH]AmiB catalytic domain crystallized in space group *C2* with cell dimensions $a=71.19$ Å, $b=53.51$ Å, $c=58.50$ Å, $\beta=90.46°$ and diffracted X-rays to 1.24 Å resolution. The reflection intensities were integrated and scaled with HKL3000 suite (Table 3.5) (55). One [BH]AmiB with two methionine residues were expected in one asymmetric unit. Three heavy atom sites were located using the program SHELXD (56) and they were used for phasing with the program MLPHARE (57). The three heavy atoms are two Se and one Zn atoms as identified later based on the protein structure and an X-ray fluorescent spectrum of the crystal sample. The spectrum was measured with the primary beam energy of 12.659 keV and indicated the presence of Zn inside the crystal. After density

modification (DM) (57), a partial model of 197 residues (86% of [BH]AmiB catalytic domain) with 138 side chains was built in 5 cycles of Resolve model building (58). All of the above programs are integrated within the program suite HKL3000. Further model buildings to complete the structure were performed manually using the program COOT (59). The structural model was therefore refined using the program Phenix.refine (Table 3.5) (60). In the final model, six residues, E303SLELT, are missing due to the lack of electron densities. The crystal structure was deposited in Protein Data Bank (PDB:3NE8).

Preparation of sacculi labelled with RBB

Sacculi were prepared from strain TU163 (Δlpp) as described by Uehara *et al* (12). Isolated sacculi were treated with 200 μg/ml amylase (Sigma, St Louis, MO) at 37°C for 2 h in 1x PBS and washed with water. The amylase-treated sacculi were then incubated with 20 mM RBB (Sigma) in 0.25 M NaOH overnight at 37°C. The preparation was neutralized with HCl, and RBB-labelled sacculi were pelleted by centrifugation (21000 x *g*, 20 min, room temperature). The sacculi were then repeatedly resuspended in water and pelleted by centrifugation until the supernatant was clear. The final pellet was resuspended in water containing 0.02% azide and stored at 4°C.

Dye-release assay for PG hydrolysis

A measure of 10 μl of RBB-labelled sacculi were incubated at 37°C for 30 min with purified amidases and/or LytM factors in 100 μl of PBS buffer (10 mM Na_2HPO_4, 2 mM KH_2PO_4, 137 mM NaCl and 2.7 mM KCl, pH 7.4). Final protein concentrations are indicated in

Figure 3.8 and Figure 3.11. Reactions were terminated by incubating them at 95°C for 5 min.

Following termination, all reactions were centrifuged at 21000 x g, 20 min at room temperature.

Supernatants were removed and their absorbance was measured at 595 nm.

Table 3.3. Bacterial strains used in this study.

Strain	Genotype[a]	Source/Reference[b]
C6706	*Vibrio cholerae* O1 El Tor isolate from Peru	(61)
DH5α	F– *hsdR*17 *deoR recA*1 *endA*1 *phoA supE*44 *thi*-1 *gyrA*96 *relA*1 Δ(*lacZYA-argF*)U169 ϕ80d*lacZ*ΔM15	NEB
BL21(λDE3)	*ompT* rB– mB– (P$_{lac}$UV5::T7*gene1*)	Novagen
MG1655	*rph*1 *ilvG rfb*-50	(62)
TB28	*rph*1 *ilvG rfb*-50 Δ*lacIZYA*::*frt*	(63)
TB140	TB28 Δ*envC*::*frt*	(12)
TB145	TB28 Δ*nlpD747*::*frt*	(12)
TB170	TB28 Δ*amiB*::Kan^R	(6)
DY29	TB28 Δ*nlpD747*::*frt* Δ*amiB*::Kan^R	P1(TB170) x TB145

[a] The Kan^R cassette is flanked by *frt* sites for removal by FLP recombinase. An *frt* scar remains following removal of the cassette using FLP expressed from pCP20.

[b] Strain constructions by P1 transduction are described using the shorthand: P1(donor) x recipient. In all cases transductants were selected on LB Kan plates.

Table 3.4. Plasmids used in this study.

Plasmid	Genotype[a]	ori	Reference/source
pBAD33	*cat* P_{ara}::*mcs*	p15A	(64)
pInt-ts	*bla cI*857 *repA*(ts) P_R::*int$^\lambda$*	pSC101	(49)
pTU119	*bla lacIq* P_{T7}::*h-sumo-nlpD*	pBR/colE1	(6)
pTU104	*bla lacIq* P_{T7}::*h-sumo-^{lyt}envC*	pBR/colE1	(6)
pAPC62366.1	*bla lacI* P_{T7}::*h -^{BH}amiB*	pBR/colE1	This Study
pDY81	*bla lacIq* P_{T7}::*h-sumo-amiB(E300K)*	pBR/colE1	This Study
pDY187	*cat* P_{ara}::*amiB*	p15A*	This Study
pDY219	*cat* P_{ara}::*amiB(H302P)*	p15A*	This Study
pDY220	*cat* P_{ara}::*amiB(S306P)*	p15A*	This Study
pDY221	*cat* P_{ara}::*amiB(D314V)*	p15A*	This Study
pDY222	*cat* P_{ara}::*amiB(A405V)*	p15A*	This Study
pDY229	*cat* P_{ara}::*amiB(E303K)*	p15A*	This Study
pDY230	*cat* P_{ara}::*amiB(S293I)*	p15A*	This Study
pDY231	*cat* P_{ara}::*amiB(S306P)†*	p15A*	This Study
pDY232	*cat* P_{ara}::*amiB(S293R)*	p15A*	This Study
pDY233	*cat* P_{ara}::*amiB(A296V)*	p15A*	This Study
pDY234	*cat* P_{ara}::*amiB(E300K)*	p15A*	This Study
pDY235	*cat* P_{ara}::*amiB(R372C)*	p15A*	This Study
pDY236	*cat* P_{ara}::*amiB(S306L)*	p15A*	This Study
pDY237	*cat* P_{ara}::*amiB(H302P, A405V)*	p15A*	This Study
pDY238	*cat* P_{ara}::*amiB(Q333L)*	p15A*	This Study
pDY239	*cat* P_{ara}::*amiB(M295I)*	p15A*	This Study
pDY242	*bla lacIq* P_{T7}::*h-sumo-amiB(S293R)*	pBR/colE1	This Study
pDY245	*bla lacIq* P_{T7}::*h-sumo-amiB(E303K)*	pBR/colE1	This Study
pDY250	*cat* P_{ara}::*amiB(E215A)*	p15A*	This Study
pDY255	*cat* P_{ara}::*^{VC}amiB*	p15A*	This Study
pDY256	*bla lacIq* P_{T7}::*h-sumo-^{VC}amiB*	pBR/colE1	This Study
pDY260	*cat* P_{ara}::*^{VC}amiB(E286K)*	p15A*	This Study

Table 3.4 continued.

Plasmid	Genotype[a]	ori	Reference/source
pDY264	*attλ cat* P$_{ara}$::*^{ss}dsbA-amiA*	R6K	This Study
pDY266	*attλ cat* P$_{ara}$::*^{ss}dsbA-amiA(E167K)*	R6K	This Study
pDY268	*bla lacIq* P$_{T7}$::*h-sumo-^{VC}amiB(E286K)*	pBR/colE1	This Study
pDY272	*cat* P$_{ara}$::*amiB(S293R, E300K, E303K)*	p15A*	This Study
pDY276	*bla lacIq* P$_{T7}$::*h-sumo-amiB(S293R, E300K, E303K)*	pBR/colE1	This Study
pDY277	*bla lacIq* P$_{T7}$::*h-sumo-amiA(E167K)*	pBR/colE1	This Study
pDY278	*bla lacIq* P$_{T7}$::*h-sumo-amiA*	pBR/colE1	This Study
pDY279	*bla lacIq* P$_{T7}$::*h-sumo-amiB*	pBR/colE1	This Study

[a] A 6xHis tag for purification is indicated by the letter *h*. *^{ss}dsbA* corresponds to the first 24 codons of *dsbA* encoding its export signal. P$_{T7}$, P$_R$, and P$_{ara}$ indicate the phage T7, λR and arabinose promoters, respectively. Numbers in parenthesis indicate the codons included in the relevant clones.

[VC] *Vibrio cholerae*, C6706 strain {Thelin:1996we}, ^{VC}*amiB* - VC0344

p15A* is a derivative of p15A* with a mild increase in copy number (see Methods and Materials).

[†] Contains original premature stop codon

Table 3.5. Crystallographic Statistics.

Data Collection	
Space group	*C2*
Unit Cell (Å, °)	*a*=71.19,*b*=53.51, *c*=58.50, β=90.46
MW Da (residue)	25769 (231) [1]
Mol (AU)	1
SeMet (AU)	2
Wavelength (Å)	0.9793 (peak)
Resolution (Å)	29.3-1.24
Number of unique reflections	61785 [2]
Redundancy	3.5 (3.2) [3]
Completeness (%)	99.3 (90.7) [3]
R_{merge} (%)	7.0 (55.4) [3]
I/s (I)	27.8 (1.5) [3]

Phasing	
R_{Cullis} (anomalous) (%)	*67*
Figure of merit (%)	34.5 [4]

Refinement	
Resolution	29.3-1.24
Reflections (work/test)	58025/2934
$R_{crystal}/R_{free}$ (%)	16.1/17.4
Rms deviation from ideal geometry Bond length (Å)/angle (°)	0.005/0.985
No. of atoms (Protein/HETATM)	1877/306
Mean B-value (Å²) (mainchain/sidechain)	14.2/19.3
Ramachandran plot statistic (%) Residues in most favored regions, in additional allowed regions, in generously allowed regions, in disallowed region	95.1 4.4 0.5 0.0

[1] Not including cloning artifact; [2] Including Bijvoet pairs; [3] (Last resolution bin, 1.24-1.26Å);

[4] Before density modification

Section 3.6: References

1. Vollmer W, Seligman SJ (2010) Architecture of peptidoglycan: more data and more models. *Trends in Microbiology* 18:59–66.

2. Vollmer W, Blanot D, de Pedro MA (2008) Peptidoglycan structure and architecture. *FEMS Microbiol Rev* 32:149–167.

3. Typas A, Banzhaf M, Gross CA, Vollmer W (2011) From the regulation of peptidoglycan synthesis to bacterial growth and morphology. *Nature Publishing Group* 10:123–136.

4. Vollmer W, Joris B, Charlier P, Foster S (2008) Bacterial peptidoglycan (murein) hydrolases. *FEMS Microbiol Rev* 32:259–286.

5. Uehara T, Bernhardt TG (2011) More than just lysins: peptidoglycan hydrolases tailor the cell wall. *Curr Opin Microbiol*:1–6.

6. Uehara T, Parzych KR, Dinh T, Bernhardt TG (2010) Daughter cell separation is controlled by cytokinetic ring-activated cell wall hydrolysis. *EMBO J* 29:1412–1422.

7. Yang DC et al. (2011) An ATP-binding cassette transporter-like complex governs cell-wall hydrolysis at the bacterial cytokinetic ring. *Proc Natl Acad Sci USA* 108:E1052–60.

8. Bi EF, Lutkenhaus J (1991) FtsZ ring structure associated with division in Escherichia coli. *Nature* 354:161–164.

9. de Boer PA (2010) Advances in understanding E. coli cell fission. *Current Opin Microbiol* 13:730–737.

10. Heidrich C et al. (2001) Involvement of N-acetylmuramyl-L-alanine amidases in cell separation and antibiotic-induced autolysis of Escherichia coli. *Mol Microbiol* 41:167–178.

11. Priyadarshini R, de Pedro MA, Young KD (2007) Role of peptidoglycan amidases in the development and morphology of the division septum in Escherichia coli. *J Bacteriol* 189:5334–5347.

12. Uehara T, Dinh T, Bernhardt TG (2009) LytM-domain factors are required for daughter cell separation and rapid ampicillin-induced lysis in Escherichia coli. *J Bacteriol* 191:5094–5107.

13. Sham L-T, Barendt SM, Kopecky KE, Winkler ME (2011) Essential PcsB putative peptidoglycan hydrolase interacts with the essential FtsXSpn cell division protein in Streptococcus pneumoniae D39. *Proc Natl Acad Sci USA* 108:E1061–9.

14. Ng W-L, Kazmierczak KM, Winkler ME (2004) Defective cell wall synthesis in Streptococcus pneumoniae R6 depleted for the essential PcsB putative murein hydrolase or the VicR (YycF) response regulator. *Mol Microbiol* 53:1161–1175.

15. Delisle AL, Barcak GJ, Guo M (2006) Isolation and expression of the lysis genes of Actinomyces naeslundii phage Av-1. *Appl Environ Microbiol* 72:1110–1117.

16. Finn RD et al. (2008) The Pfam protein families database. *Nucleic Acids Res* 36:D281–8.

17. Korndörfer IP et al. (2006) The crystal structure of the bacteriophage PSA endolysin reveals a unique fold responsible for specific recognition of Listeria cell walls. *J Mol Biol* 364:678–689.

18. Smith TJ, Foster SJ (1995) Characterization of the involvement of two compensatory autolysins in mother cell lysis during sporulation of Bacillus subtilis 168. *J Bacteriol* 177:3855–3862.

19. Mayer MJ, Garefalaki V, Spoerl R, Narbad A, Meijers R (2011) Structure-Based Modification of a Clostridium difficile-Targeting Endolysin Affects Activity and Host Range. *J Bacteriol* 193:5477–5486.

20. Shida T, Hattori H, Ise F, Sekiguchi J (2001) Mutational analysis of catalytic sites of the cell wall lytic N-acetylmuramoyl-L-alanine amidases CwlC and CwlV. *J Biol Chem* 276:28140–28146.

21. Heidrich C, Ursinus A, Berger J, Schwarz H, Höltje J-V (2002) Effects of multiple deletions of murein hydrolases on viability, septum cleavage, and sensitivity to large toxic molecules in Escherichia coli. *J Bacteriol* 184:6093–6099.

22. Losick R, Stragier P (1992) Crisscross regulation of cell-type-specific gene expression during development in B. subtilis. *Nature* 355:601–604.

23. Errington J (1993) Bacillus subtilis sporulation: regulation of gene expression and control of morphogenesis. *Microbiol Rev* 57:1–33.

24. Dubrac S, Bisicchia P, Devine KM, Msadek T (2008) A matter of life and death: cell wall homeostasis and the WalKR (YycGF) essential signal transduction pathway. *Mol Microbiol* 70:1307–1322.

25. Ng W-L et al. (2003) Constitutive expression of PcsB suppresses the requirement for the essential VicR (YycF) response regulator in Streptococcus pneumoniae R6. *Mol Microbiol* 50:1647–1663.

26. Fabret C, Hoch JA (1998) A two-component signal transduction system essential for growth of Bacillus subtilis: implications for anti-infective therapy. *J Bacteriol* 180:6375–6383.

27. Dubrac S, Boneca IG, Poupel O, Msadek T (2007) New insights into the WalK/WalR (YycG/YycF) essential signal transduction pathway reveal a major role in controlling cell wall metabolism and biofilm formation in Staphylococcus aureus. *J Bacteriol* 189:8257–8269.

28. Dubrac S, Msadek T (2004) Identification of genes controlled by the essential YycG/YycF two-component system of Staphylococcus aureus. *J Bacteriol* 186:1175–1181.

29. Martin PK, Li T, Sun D, Biek DP, Schmid MB (1999) Role in cell permeability of an essential two-component system in Staphylococcus aureus. *J Bacteriol* 181:3666–3673.

30. Senadheera MD et al. (2005) A VicRK signal transduction system in Streptococcus mutans affects gtfBCD, gbpB, and ftf expression, biofilm formation, and genetic competence development. *J Bacteriol* 187:4064–4076.

31. Fukuchi K et al. (2000) The essential two-component regulatory system encoded by yycF and yycG modulates expression of the ftsAZ operon in Bacillus subtilis. *Microbiology (Reading, Engl)* 146 (Pt 7):1573–1583.

32. Hancock LE, Perego M (2004) Systematic inactivation and phenotypic characterization of two-component signal transduction systems of Enterococcus faecalis V583. *J Bacteriol* 186:7951–7958.

33. Kallipolitis BH, Ingmer H (2001) Listeria monocytogenes response regulators important for stress tolerance and pathogenesis. *FEMS Microbiol Lett* 204:111–115.

34. Lange R et al. (1999) Domain organization and molecular characterization of 13 two-component systems identified by genome sequencing of Streptococcus pneumoniae. *Gene* 237:223–234.

35. Koch AL (1990) Additional arguments for the key role of "smart" autolysins in the enlargement of the wall of gram-negative bacteria. *Res Microbiol* 141:529–541.

36. Höltje JV (1998) Growth of the stress-bearing and shape-maintaining murein sacculus of Escherichia coli. *Microbiol Mol Biol Rev* 62:181–203.

37. Rechenberg von M, Ursinus A, Höltje JV (1996) Affinity chromatography as a means to study multienzyme complexes involved in murein synthesis. *Microb Drug Resist* 2:155–157.

38. Romeis T, Höltje JV (1994) Specific interaction of penicillin-binding proteins 3 and 7/8 with soluble lytic transglycosylase in Escherichia coli. *J Biol Chem* 269:21603–21607.

39. Carballido-López R et al. (2006) Actin homolog MreBH governs cell morphogenesis by localization of the cell wall hydrolase LytE. *Dev Cell* 11:399–409.

40. Hett EC, Chao MC, Rubin EJ (2010) Interaction and modulation of two antagonistic cell wall enzymes of mycobacteria. *PLoS Pathog* 6:e1001020.

41. Odintsov SG, Sabala I, Marcyjaniak M, Bochtler M (2004) Latent LytM at 1.3A resolution. *J Mol Biol* 335:775–785.

42. Firczuk M, Mucha A, Bochtler M (2005) Crystal structures of active LytM. *J Mol Biol* 354:578–590.

43. Schlag M et al. (2010) Role of staphylococcal wall teichoic acid in targeting the major autolysin Atl. *Mol Microbiol* 75:864–873.

44. Ruggiero A et al. (2010) Structure and functional regulation of RipA, a mycobacterial enzyme essential for daughter cell separation. *Structure* 18:1184–1190.

45. Bublitz M et al. (2009) Structural basis for autoinhibition and activation of Auto, a virulence-associated peptidoglycan hydrolase of Listeria monocytogenes. *Mol Microbiol* 71:1509–1522.

46. Böth D, Schneider G, Schnell R (2011) Peptidoglycan Remodeling in Mycobacterium tuberculosis: Comparison of Structures and Catalytic Activities of RipA and RipB. *J Mol Biol* 413:247–260.

47. Corbin BD, Wang Y, Beuria TK, Margolin W (2007) Interaction between cell division proteins FtsE and FtsZ. *J Bacteriol* 189:3026–3035.

48. Miller JH (1972) *Experiments in Molecular Genetics* (Cold Spring Harbor Laboratory, Cold Spring Harbor, New York).

49. Haldimann A, Wanner BL (2001) Conditional-replication, integration, excision, and retrieval plasmid-host systems for gene structure-function studies of bacteria. *J Bacteriol* 183:6384–6393.

50. Mossessova E, Lima CD (2000) Ulp1-SUMO crystal structure and genetic analysis reveal conserved interactions and a regulatory element essential for cell growth in yeast. *Mol Cell* 5:865–876.

51. Marblestone JG et al. (2006) Comparison of SUMO fusion technology with traditional gene fusion systems: enhanced expression and solubility with SUMO. *Protein Sci* 15:182–189.

52. Bendezú FO, Hale CA, Bernhardt TG, de Boer PAJ (2009) RodZ (YfgA) is required for proper assembly of the MreB actin cytoskeleton and cell shape in E. coli. *EMBO J* 28:193–204.

53. Van Duyne GD, Standaert RF, Karplus PA, Schreiber SL, Clardy J (1993) Atomic structures of the human immunophilin FKBP-12 complexes with FK506 and rapamycin. *J Mol Biol* 229:105–124.

54. Kim Y et al. (2004) Automation of protein purification for structural genomics. *J Struct Funct Genomics* 5:111–118.

55. Minor W, Cymborowski M, Otwinowski Z, Chruszcz M (2006) HKL-3000: the integration of data reduction and structure solution - from diffraction images to an initial model in minutes. *Acta Cryst* 62:859–866.

56. Schneider TR, Sheldrick GM (2002) Substructure solution with SHELXD. *Acta Crystallogr D Biol Crystallogr* 58:1772–1779.

57. Collaborative Computational Project N4 (1994) The CCP4 suite: programs for protein crystallography. *Acta Cryst* 50:760–763.

58. Terwilliger TC (2002) Automated main-chain model building by template matching and iterative fragment extension. *Acta Cryst* 59:38–44.

59. Emsley P, Cowtan K (2004) Coot: model-building tools for molecular graphics. *Acta Cryst* 60:2126–2132.

60. Murshudov GN, Vagin AA, Dodson EJ (1997) Refinement of Macromolecular Structures by the Maximum-Likelihood Method. *Acta Cryst* 53:240–255.

61. Thelin KH, Taylor RK (1996) Toxin-coregulated pilus, but not mannose-sensitive hemagglutinin, is required for colonization by Vibrio cholerae O1 El Tor biotype and O139 strains. *Infect Immun* 64:2853–2856.

62. Guyer MS, Reed RR, Steitz JA, Low KB (1981) Identification of a sex-factor-affinity site in E. coli as gamma delta. *Cold Spring Harb. Symp. Quant. Biol*. 45:135–140.

63. Bernhardt TG, de Boer PAJ (2004) Screening for synthetic lethal mutants in Escherichia coli and identification of EnvC (YibP) as a periplasmic septal ring factor with murein hydrolase activity. *Mol Microbiol* 52:1255–1269.

64. Guzman LM, Belin D, Carson MJ, Beckwith J (1995) Tight regulation, modulation, and high-level expression by vectors containing the arabinose PBAD promoter. *J Bacteriol* 177:4121–4130.

Chapter 4

Discussion

Chapter 4: Discussion

Section 4.1: Summary of results

The ability to synthesize, remodel and degrade PG are important activities for all cell-wall containing bacteria that grow and divide. The enzymes responsible for cleaving the bonds that make up PG are known as PG hydrolases or autolysins (1). These enzymes have a diverse range of biological functions, ranging from outright cell wall destruction (e.g. lysozyme) to delicate remodeling processes necessary for growth and development (1). Harnessing PG hydrolases for this latter purpose demands precise control over their activity since inappropriate activation of these enzymes can form lesions in the cell wall resulting in death by lysis (1).

As discussed in Chapter 1, little is actually known as to how the activity of the PG hydrolases is regulated *in vivo*. Consequently, to begin understanding the mechanistic control that governs these enzymes, I have been studying how the PG hydrolases are controlled during the process of cell division in *E. coli*. In this organism the LytC-type *N*-acetylmuramyl-L-alanine amidases (AmiA, AmiB and AmiC) are required for cell division along with the LytM factors, EnvC and NlpD, that activate them (2-6). To begin investigating how the amidases are controlled, I set out to isolate unregulated AmiB variants that do not require EnvC for activation. Identification of such mutants would support a model where the LytM factors (*i.e.* EnvC) allosterically activate the amidases (*i.e.* AmiB) in order to degrade PG. Using a genetic enrichment strategy (adapted from 7), I isolated a number of mutations within *amiB* that produced lytic AmiB variants ([Lyt]AmiB). These mutations all mapped to a region of AmiB found only in cell separation amidases. Structural analysis of AmiB from *Bartonella henselae* ([BH]AmiB), an *E. coli* AmiB ortholog, showed that this region corresponds to an alpha-helical

domain that blocks the amidase active site. The [Lyt]AmiB variants have amino acid substitutions

that most likely disrupt the interactions responsible for keeping this regulatory region in place

and preventing inappropriate PG cleavage. Therefore, amidase activation by the LytM factors in

all likelihood proceeds via a conformational change that dislodges the regulatory helix from the

amidase active site.

In an effort to elucidate how the LytM factors are specifically recruited to and regulated

at the septal ring, I discovered that FtsEX is an important regulator of septal PG hydrolysis

during cell division (8). In *E. coli*, FtsE and FtsX form an ABC-transporter-like complex. It was

identified as an important divisome component a number of years ago (9), but its precise role in

cytokinesis has remained mysterious (10). ABC transporters are ubiquitous membrane protein

complexes that use ATP-induced conformational changes to move substrates across membranes

(11). They are composed of two transmembrane domains (TMDs) that act as the substrate

conduit and two nucleotide-binding domains (NBDs) which bind and hydrolyze ATP to power

transport. I found that FtsEX directly recruits EnvC to the division site via a protein-protein

interaction between the coiled-coil domain of EnvC and a large periplasmic loop of FtsX (8).

Importantly, FtsEX variants predicted to be ATPase defective still recruit EnvC to the septum but

fail to promote cell separation (8). Overall, my results support a model where conformational

changes induced by the ATPase activity of FtsE in the cytoplasm are transmitted to the amidases

in the periplasm via FtsX and EnvC. This model is attractive because it provides a mechanism

for converting the potentially dangerous activity of PG hydrolysis at the septal ring into a safe

and discrete process that can be cycled "on" and "off" in coordination with the other important

functions of the division apparatus (Figure 4.1). Furthermore, FtsE has been show to interact
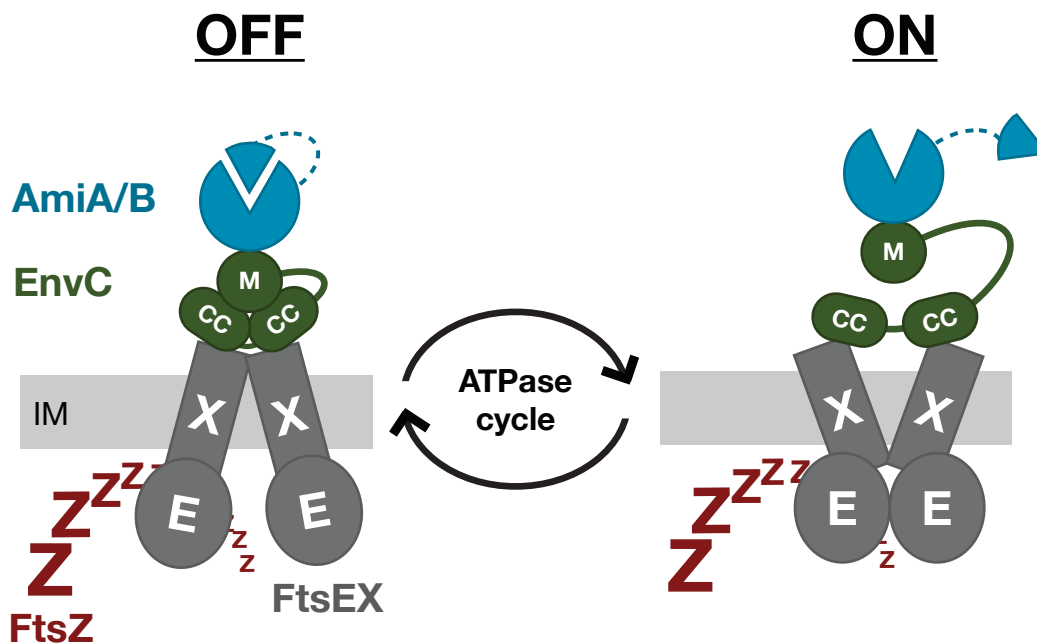
Figure 4.1. A model for the regulation of PG hydrolase activity at the division site. Shown here is a schematic diagram of a putative "on" versus "off" FtsEX-EnvC-AmiA/B complex at the Z-ring. I propose that conformational changes in FtsEX induced by FtsE-mediated ATP hydrolysis are transmitted to EnvC to control its ability to activate the amidases. EnvC exerts it regulatory control over AmiA/B by allosterically activating the amidases via a conformational change which displaces a regulatory domain that normally occludes the amidase active site (represented by the blue wedge). Removal of this domain allows substrate accessibility and enables the amidases to cleave septal PG (not depicted here). Adapted from (8).

with FtsZ (12), suggesting that the ATPase activity of FtsE may be sensitive to the dynamics of the Z-ring and provide a system for transmitting information about the status of the Z-ring to the septal PG splitting enzymes in the periplasm.

Section 4.2: Future directions

We are just beginning to dissect the mechanisms that keep cellular PG hydrolase activity in check. Many questions remain to be addressed, both with respect to amidase regulation and the control of PG hydrolases involved in other important physiological processes. Several of the most important questions and potential avenues for addressing them are discussed below.

What is the mechanism of amidase activation by the LytM factors?

The findings presented in this dissertation provide strong support for the idea that the LytM factors allosterically activate their cognate amidase(s). They likely do so by inducing a conformational change which displaces the regulatory helix that occludes the amidase active site. How the LytM factors promote this conformational change in the amidases is currently unclear, but I envision at least two possibilities. (1) The LytM factors possess affinity for the regulatory alpha-helical domain and essentially compete with the amidase active site for binding to this regulatory region. In this case, I envision that when the amidase transiently visits the open and active state, the LytM factor would bind the exposed regulatory helix and stabilize the active conformation. (2) The LytM factors bind the amidases in a region other than the regulatory helix to bring about the conformational change necessary to displace the helix from the active site. Follow-up experiments will be required to conclusively differentiate between these two

possibilities. An attractive approach would be the isolation of amidase variants that fail to be

activated by the LytM factors because the location(s) of amino acid substitutions, resulting in this

phenotype, would likely identify residues/domains within the amidase important for LytM factor

binding and/or activation. For example, mutations in *amiB* that disrupt the ability of EnvC to

bind AmiB may indicate possible interaction regions. Additionally, efforts to generate co-

crystals of a LytM-amidase complex are currently ongoing and, if successful, should provide us

with a high resolution picture of the activation mechanism.

What determines the specificity of cognate LytM-amidase pairs?

Along with determining the mechanism of amidase activation it is also unclear why EnvC

only activates AmiA and AmiB while NlpD only activates AmiC (6). Interestingly, amino acid

substitutions in the [Lyt]AmiB variants, described in Chapter 3, not only enhanced the basal activity

of AmiB, they also allowed the variants to be aberrantly activated by NlpD. Almost all of these

substitutions occur within the regulatory helix region of AmiB and are predicted to destabilize its

interaction with the amidase active site. This implies that LytM-amidase specificity is in part

determined by the strength of the interaction between the regulatory helix of the amidases and

the active site. These observations are consistent with an activation mechanism involving a

competition between the LytM factor and the amidase active site for association with the

regulatory helix. If the helix-active site interaction is weakened by an amino acid substitution,

then a non-cognate LytM factor with lower affinity for the helix region may gain the ability to

compete with the active site for binding of this region and thus promote amidase activation.

Alternatively, the LytM-amidase specificity may be determined by the binding affinity of a LytM

factor for a site on the amidase distinct from the regulatory helix. In this case, substitutions weakening the regulatory helix-active site interaction may somehow allow the relatively low affinity binding of a non-cognate LytM factor to promote the release of the amidase regulatory helix from the active site. A better understanding of the amidase activation mechanism is clearly required in order to define the determinants underlying the specificity of amidase activation by the LytM factors.

What regulates NlpD activity?

In Chapter 2, I described the identification of FtsEX as an upstream regulator of EnvC activity (8). Much less is known about the regulation of the analogous NlpD-AmiC pathway for septal PG splitting (6). Since NlpD is an outer membrane lipoprotein, it is likely to be regulated by a distinct mechanism relative to EnvC, which is a periplasmic protein regulated by the inner membrane protein complex FtsEX (8). One interesting possibility is that NlpD activity may be regulated based on changes in its proximity to PG. Prior to cell constriction, NlpD may be unable to "reach" the PG layer from the outer membrane in order to stimulate PG hydrolysis by AmiC. However, once cell division is initiated and the outer membrane begins to constrict, NlpD may be brought closer to the PG layer to stimulate AmiC activity. This activation may be achieved by changes in the physical proximity of NlpD and PG alone or the process may require additional protein cofactors. In either case, this model is attractive because it would provide a mechanism for directly coupling outer membrane invagination with septal PG splitting. Experiments to test this hypothesis are currently being performed by other members of the lab.

Identifying the factors that recruit AmiB, AmiC and NlpD to the divisome

In Chapter 2, I described the identification of FtsEX as the septal ring component directly responsible for recruiting EnvC to the division site (8). The factor(s) directly responsible for the recruitment of the remaining components (NlpD, AmiB, and AmiC) of the septal PG splitting system to the divisome remain unknown. The identification of these factors may shed additional light on the control mechanisms governing septal PG splitting. So far, we know that the amidases are recruited to the division site independently of their cognate LytM factor and that NlpD, AmiB, and AmiC all require FtsN for septal localization (13). Interestingly, NlpD and EnvC localize to the divisome normally when septal PG synthesis is inhibited with the PBP3 inhibitor cephalexin (13). AmiB and AmiC, on the other hand, fail to be recruited under these conditions (13). This phenomenon appears to be a part of a fail-safe mechanism that prevents the concentration of the amidases at the division site unless septal PG is actively being synthesized (13). An attractive hypothesis is that the N-terminal targeting domains of AmiB and AmiC directly recognize septal PG as the localization signal. That being said, it is presently unclear how the targeting domains might differentiate septal PG from the rest of the PG matrix. However, we cannot rule out the possibility of a protein-protein interaction mediating amidase localization. Like EnvC, our working hypothesis is that NlpD is recruited to the septal ring via a direct protein-protein interaction with another septal ring factor. We are currently attempting to identify this factor and determine whether or not it plays a role in the regulation of NlpD activity.

How is septal PG splitting coordinated with other functions of the divisome?

The divisome performs a number of important functions in addition to septal PG splitting. These include: invagination of the inner membrane, synthesis of the septal PG layer, and invagination of the outer membrane. A major challenge going forward will be to determine how all of these functions are coordinated, especially the processes of septal PG synthesis and splitting. A key player in this coordination is likely to be FtsEX. Since this complex spans the inner membrane, it is in prime position to interact with both cytoplasmic and membrane components of the septal ring as well as EnvC in the periplasm. The observed interaction between FtsE and FtsZ (12), may provide a mechanism to coordinate the contraction of the Z-ring with septal PG splitting. Additionally, the PBPs and many of the other essential septal ring constituents are integral membrane components. Thus, another attractive possibility is that interactions between the PBPs and FtsEX could help coordinate amidase activation with septal PG synthesis. As mentioned above, the outer membrane localization of NlpD may position it to help couple the PG splitting process with outer membrane invagination. Therefore, the need to coordinate septal PG splitting with the invagination of two different membranes may explain why *E. coli* utilizes two partially redundant septal PG splitting systems with distinct membrane localization patterns.

How are the peptidoglycan hydrolases regulated in other systems - i.e. the elongation complex

Finally, in addition to facilitating cell division, PG hydrolases are also important for numerous other processes in bacteria (refer to Section 1.2: Peptidoglycan hydrolases and their physiologic functions), including lateral cell wall growth by the elongation/rod complex. PG

bonds must be cleaved in order for this system to insert new material into the existing PG matrix. The elongation complex must therefore contain PG hydrolases and somehow coordinate their activity with the PG synthases. This idea is supported by the observation that in *B. subtilis* the PG hydrolase LytE interacts with the actin-like cytoskeletal element MreBH, which is involved in lateral cell wall growth (14). Moreover, inactivation of LytE and another PG hydrolase, CwlO, causes a block in cell elongation (15). The PG hydrolases involved in *E. coli* cell elongation have not been identified, but a similar mechanism of elongation is presumably occurring. In addition to identifying these elongation hydrolases, a major challenge will be to determine how they are controlled. I anticipate that conformational control mechanisms similar to those used for governing amidase activity will be employed. Understanding the diverse roles that PG hydrolases play during PG biogenesis and remodeling will undoubtedly reveal new and exciting mechanisms used to regulate and control their activity.

Section 4.3: Concluding remarks

As exemplified by phage lysins, which lyse host cells in order to release newly-made virions, PG hydrolases have the power to destroy bacterial cells. However, if properly controlled and regulated these enzymes facilitate important cellular processes that allow all cell wall-containing bacteria to grow and divide (1). Due to its essentiality and uniqueness to bacteria, PG biogenesis is a particularly powerful antimicrobial target. Many of our most potent antibiotics, like the β-lactam penicillin, specifically inhibit PG synthesis. However, attempts to harness the potentially lethal properties of PG hydrolases as a novel source of antimicrobials have yet to be fully tapped. The numerous biological examples of PG hydrolases being used to specifically

cause cell lysis (refer to Table 1.3) demonstrate that mother nature has already developed such an arsenal. This begs the question of whether we can also exploit PG hydrolase biology in the effort to find new antibiotics against the emerging threat of resistant bacterial pathogens. For example, it may be possible to identify small molecules that can inappropriately activate these enzymes to cause cell lysis. Therefore, understanding PG hydrolase regulation will not only help us define fundamental biological mechanisms, it will likely also provide us with the understanding necessary to disrupt the regulatory systems for the purposes of developing a new generation of lytic antibiotics.

Section 4.4: References

1. Vollmer W, Joris B, Charlier P, Foster S (2008) Bacterial peptidoglycan (murein) hydrolases. *FEMS Microbiol Rev* 32:259–286.

2. Heidrich C, Ursinus A, Berger J, Schwarz H, Höltje J-V (2002) Effects of multiple deletions of murein hydrolases on viability, septum cleavage, and sensitivity to large toxic molecules in Escherichia coli. *J Bacteriol* 184:6093–6099.

3. Heidrich C et al. (2001) Involvement of N-acetylmuramyl-L-alanine amidases in cell separation and antibiotic-induced autolysis of Escherichia coli. *Mol Microbiol* 41:167–178.

4. Priyadarshini R, de Pedro MA, Young KD (2007) Role of peptidoglycan amidases in the development and morphology of the division septum in Escherichia coli. *J Bacteriol* 189:5334–5347.

5. Uehara T, Dinh T, Bernhardt TG (2009) LytM-domain factors are required for daughter cell separation and rapid ampicillin-induced lysis in Escherichia coli. *J Bacteriol* 191:5094–5107.

6. Uehara T, Parzych KR, Dinh T, Bernhardt TG (2010) Daughter cell separation is controlled by cytokinetic ring-activated cell wall hydrolysis. *EMBO J* 29:1412–1422.

7. Delisle AL, Barcak GJ, Guo M (2006) Isolation and expression of the lysis genes of Actinomyces naeslundii phage Av-1. *Appl Environ Microbiol* 72:1110–1117.

8. Yang DC et al. (2011) An ATP-binding cassette transporter-like complex governs cell-wall hydrolysis at the bacterial cytokinetic ring. *Proc Natl Acad Sci USA* 108:E1052–60.

9. Ricard M, Hirota Y (1973) Process of cellular division in Escherichia coli: physiological study on thermosensitive mutants defective in cell division. *J Bacteriol* 116:314–322.

10. Schmidt KL et al. (2004) A predicted ABC transporter, FtsEX, is needed for cell division in Escherichia coli. *J Bacteriol* 186:785–793.

11. Rees DC, Johnson E, Lewinson O (2009) ABC transporters: the power to change. *Nat Rev Mol Cell Biol* 10:218–227.

12. Corbin BD, Wang Y, Beuria TK, Margolin W (2007) Interaction between cell division proteins FtsE and FtsZ. *J Bacteriol* 189:3026–3035.

13. Peters NT, Dinh T, Bernhardt TG (2011) A Fail-Safe Mechanism in the Septal Ring Assembly Pathway Generated by the Sequential Recruitment of Cell Separation Amidases and Their Activators. *J Bacteriol* 193:4973–4983.

14. Carballido-López R et al. (2006) Actin homolog MreBH governs cell morphogenesis by localization of the cell wall hydrolase LytE. *Dev Cell* 11:399–409.

15. Bisicchia P et al. (2007) The essential YycFG two-component system controls cell wall metabolism in Bacillus subtilis. *Mol Microbiol* 65:180–200.